ABSTRACT

Title of Document: AN INTEGRATED MICROSYSTEM FOR BACTERIAL
BIOFILM DETECTION AND TREATMENT

Young Wook Kim, Doctor of Philosophy, 2014

Directed By: Professor Reza Ghodssi
Department of Electrical and Computer Engineering
The Institute for Systems Research

Bacterial biofilms cause severe infections in clinical fields and contamination problems in environmental facilities. Due to the unique complex structure of biofilms that comprise diverse polysaccharides and bacteria, traditional antibiotic therapies require a thousand times higher concentration compared to non-biofilm associated infections. The early detection of biofilms, before their structures are fully established in a given host/environment, is critical in order to eradicate them effectively. Also, the development of a new innovative biofilm treatment method that can be utilized with a low dose of antibiotic would be extremely important to the medical community.

In this dissertation, a biofilm sensor and a new biofilm treatment method were independently developed to detect and treat biofilm communities, respectively. Furthermore, an integrated microsystem was demonstrated as a single platform of the sensor with the treatment method.

The sensor was based on the surface acoustic wave (SAW) detection mechanism, which is an extremely sensitive for biofilm monitoring (hundreds of bacterial population detection limit) and consumes very low power (~100 µW). A piezoelectric ZnO layer fabricated by a pulsed laser deposition process was a key material to induce

homogeneous acoustic waves. Reliable operation of the sensor was achieved using an Al$_2$O$_3$ film as a passivation layer over the sensor to protect ZnO degradation from the growth media. The sensor successfully demonstrated real-time monitoring of biofilm growth.

The new biofilm treatment was developed based on the principles of the bioelectric effect that introduces an electric field along with antibiotics to biofilms, demonstrating significant biofilm inhibition compared to antibiotic treatment alone. Specifically, the new bioelectric effect was implementedwith a superpositioned (SP) electric field of both alternating and direct current (AC and DC) and the antibiotic gentamicin (10 µg/mL). With the SP field treatment, significant biofilm reduction was demonstrated in total biomass (~ 71 %) as well as viable bacterial density (~ 400 times respected to the only antibiotic therapy) of the treated biofilms. This method was transferred to a microfluidic system using microfabricated planar electrodes. The microsystem-level implementation of the bioelectric effect also showed enhanced biofilm reduction (~ 140 % total biomass reduction improvement). The integrated system was based on the SAW sensor with the addition of coplanar thin electrodes to apply electric signals for the biofilm treatment.

The chip was tested with two bacterial biofilms (*Escherichia coli* and *Pseudomonas aeruginosa*) that are clinically relevant strains. In both biofilm experiments, the integrated system demonstrated successful real-time biofilm monitoring and effective biofilm inhibition. This systematic integration of a continuous monitoring method with a novel effective treatment technique has advanced the state of the art in the field of managing clinical and environmental biofilms.

AN INTEGRATED MICROSYSTEM FOR BACTERIAL BIOFILM DETECTION
AND TREATMENT

By

Young Wook Kim

Dissertation submitted to the Faculty of the Graduate School of the

University of Maryland, College Park, in partial fulfillment

of the requirements for the degree of

Doctor of Philosophy

2014

Dedication

to my wife "Ui Kyoung Park", daughter "Sue Kim", parents in South Korea for

everything. Without their support, this work would not be achieved.

Table of Contents

List of Tables

List of Figures

Figure 3.8: The total treatment efficacies of AC, DC and Superpositioned bioelectric effect. The treatment effects of gentamicin and electric field are evaluated in separate experiments. The synergistic effect is determined based on equation 13.

Figure 3.9: Schematic of set up of gentamicin gradient studies. 100 µl of the solution is sampled with by a pipette and quantified by the Coomassie blue.

Figure 3.10: The influence of the gentamicin concentration on the OD_{595nm} of the gentamicin solution quantified by Coomassie blue dye. Results demonstrate linearly in the range of concentrations.

Figure 3.11: Gentamicin was quantified by Coomassie blue dye. Normalized optical densities (OD_{595}) in the parallel electrode chamber were measured under the effect of either an AC, DC, or superpositioned (SP) electric field. OD_{595} values are normalized with respect to the measured value at the cathode over 8 experiments (N = 8). Statistical analysis was performed with respect to the normalized OD_{595} at the cathode (ANOVA, P = 0.014).

Figure 3.12: Schematic of the proposed mechanism for the SP-BE biofilm treatment. (A) In the SP electric field application with the antibiotic, the measured steady state antibiotic concentration gradient (Fig. 4C) results in increased local antibiotic concentration close to the biofilm. (B) Since the SP electric field includes both DC and AC components, the antibiotic permeability of biofilm is enhanced as the AC field induces local vibration of charged molecules. This results in increased antibiotic diffusion and electrophoresis through the biofilm (red arrows indicate them). We propose the combination of the elevated antibiotic concentration proximate surface of biofilm with the high antibiotic permeability of biofilm results in the strong synergistic biofilm treatment efficacy (T^*_{SP}) observed by the SP-BE.

Figure 3.13: A photo of the cuvette setup for electrolysis quantification. The electric field was applied for 24 hours continuously to the bacterial growth media (LB). Changes of pH were quantified by a pH indicator.

Figure 3.14: Demonstration of color changes of the pH indicator in known pH solutions using a phosphate buffer solution. The pH 8 color was referred to quantify electrolysis effects.

Figure 3.15: Representative OD_{616} spectrum between 500 nm and 700 nm by a spectrophotometer (Evolution 60, Thermo Scientific Inc.). Since the peak value from pH 8 buffer solution using a pH indicator was observed at 616 nm wavelength, OD_{616} was selected to quantify the electrolysis effect from different field applications. Only the 820 mV applied potential showed significantly higher OD compared to other fields.

Figure 3.16: OD_{616} values in each experiment. The AC electrical signal was 0.5 V amplitude of sinusoidal signal at 10 MHz and the DC was 0.5 V magnitude. The SP-field was combination of the AC and DC fields. A 0.82 V of DC was also applied separated as a control experiment of the electrolysis threshold to the media. The experiments were

repeated three times, the averages and standard deviations are presented. We conclude that SP field is not due to electrolysis of the growth media.

as well as low viable bacterial cell density (H). Seven fluorescence images were taken for each of the four treatment methods (N=7), with the images presented here representing regions of high biofilm density.

Figure 3.25: The percentage of viable biofilm bacteria with respect to total biomass after each treatment is calculated using image processing software (Image J 1.44). The results include the average of seven image analyses (N=7) for each of the four treatment methods. Viable cell percentages and standard deviations are obtained with respect to total fluorescent mass surface coverage using a binary image conversion (see the Methods). The density of non-viable cells in biofilms treated by the SP-BE is shown to increase 56% in comparison to treatments using antibiotics independently (P = 0.019).

Figure 4.1: Schematic of the device cross-section for electric field distribution analysis. The ZnO can affected by the voltage applied for the bioelectric effect during the biofilm treatment. The simulation was focused on the ZnO layer from X_2 to X_3 locations. $\square$ represents a dielectric constant of the each medium.

Figure 4.2: Schematic of the laminar flow on the SAW. The theoretical analysis was focused on the impact of the SAW speed changes due to the flow.

Figure 4.3: Schematic of the laminar flow at the microchannel. The velocity profile is related with the geometry of the channel (i.e. height).

Figure 4.4: Schematic of the integrated microsystem of the SAW sensor and electrodes for induction of the bioelectric effect. A microfluidic chamber is integrated over the system to introduce bacterial growth media and antibiotics.

Figure 4.5: Overall schematic process flow. (a) 60 nm PECVD SiO_2 deposition and interdigitated electrode pattern and deposition (Au) by an electron beam evaporation, (b) 500 nm ZnO deposition using pulsed laser deposition, (c) ZnO patterning using weak acid etchant (1:1:30 ratio of acetic acid: phosphoric acid: deionized water), (d) 100 nm thickness of ALD Al_2O_3 deposition at 150 C, (e) Electrode patterning and fabrication via Au evaporation (Cr/Au, 15 nm/200 nm) and (f) PDMS microchannel assemble. (g) Photo of assembled device with the PDMS reactor.

Figure 4.6: Optical microscopy image of the fabricated integrated microchip.

Figure 4.7: Flow chart of the switching setup. With this circuit integration, four sensors were tested at the same time for biofilm growth and treatment experiments.

Figure 4.8: Photo of the custom designed multiplexing testing electronic board. The counter controls switching rate of the multiplexer. The reset can initiate the switching from device 1.

Figure 4.9: Spring loaded electrodes for the contact with the chip.

Figure 4.22: Optical microscopy image of the ZnO layer after five times of consecutive biofilm growth experiments. ZnO layer was damaged due to the growth media exposure through the passivation layer (arrows indicate ZnO damages).

Figure 4.23: Profile of the ZnO damaged surface after five times consecutive uses of the device for biofilms. The depth of surface damaged points (arrows indicates damaged surface) are around 400 nm which is close to the ZnO thickness.

Chapter 1: Introduction

1.1 Background and Motivation

The number of medical devices for health care is expected to increase significantly over the next decades due to the increase in life expectancy resulting from biomedical technology advances. Medical deviceapplications include artificial joints, heart valves, and catheters as shown in figure 1.1[3]. One of the problems associated with medical implants is severe infection due to bacterial biofilms. Theseare complex communities of groups of bacteria with diverse extracellular materials. Once biofilms are established, traditional antibiotic treatments are often ineffective since biofilms are characterized by high antibiotic resistance and require significantly higher doses of drugs due to the extracellular matrix[2]. Thus, the early detection of biofilms is critical for effective management. Current diagnostic methods (i.e. blood tests, radiographic exams, multi-site biopsies, and cell culture) are not specific for detection of biofilms[1, 2] as well as selected time-point measurements. These methods often require external instruments, making in-patient treatment necessary and inconvenient for the patients. Furthermore, when biofilms are formed on the implants, the most effective way of biofilm treatment is surgery to remove the infected-implants. The treatments usually involve intravenous antibiotic administrationand replacement surgery[, 4]. Revisional surgery and care can cost over $500,000 per patient, amounting to more than $2 billion annually in the United States[1]. Therefore, developing a biomedical system that enables not only biofilm growth monitoring, but also its treatment[3], is desirable for clinical applications.

Biofilms are not simply a group of bacteria, but complex communities. Bacteria can adhere to surfaces, and by dividing, increase their population to form microcolonies[5].

When bacteria reach population threshold, they produce and secret cell communicating molecules, such as autoinducer-2 (AI-2), resulting in formation of extracellular matrix and toxins throughout the bacterial quorum sensing[3]. Figure 1.2 shows a summarized schematics of the biofilm growth.

(a)   **(b)**   **(c)**
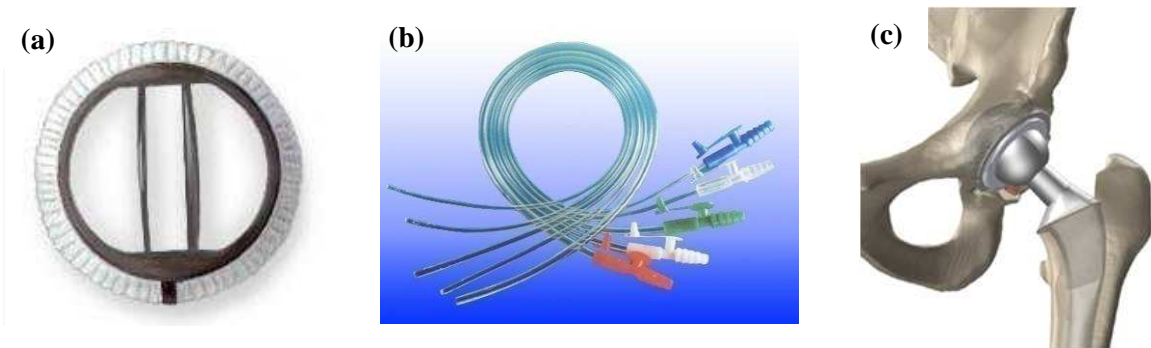
Figure.1.1: Examples of medical implants, (a) artificial heart valve (*ADAM Inc.*), (b) catheter (*NSC Inc.*), and (c) artificial hip joint (*Zimmer Inc.*)

Bacteria in biofilms can exchange genes, forming a heterogeneous bacterial composition which induces more resistance to antimicrobial agents than suspended bacteria[6, 7]. The extracellular matrix is composed of diverse polysaccharides and proteins, among other biological molecules[8]. The matrix maintains the mechanical structure of the biofilm and its physiological function as a protective layer against diffusion of antibiotics and recognition by the immune system[6]. Due to the complex structure and heterogeneous bacterial composition, not only can antibiotics not diffuse into biofilm, but biofilms also show high antibiotic resistance. As a result, the biofilms are much less susceptible to antibiotics than their nonattached individual planktonic bacteria.
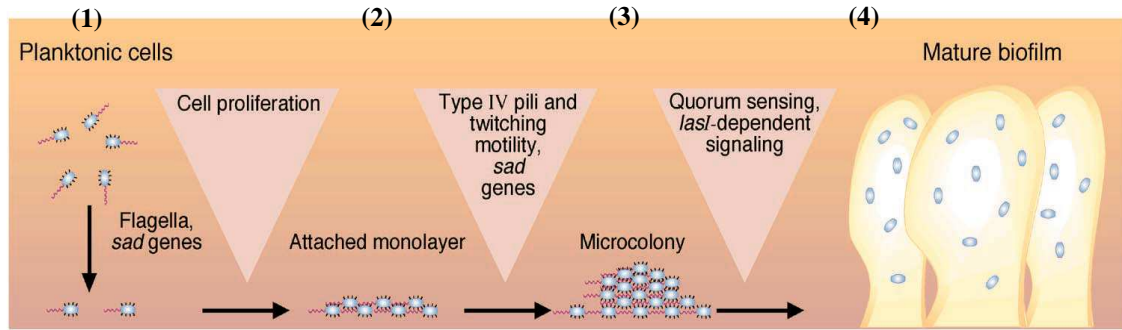
Figure 1.2: Schematic of biofilm growth progression[3]. (1) planktonic bacteria adhere on a surface, (2) form a monolayer of bacteria, (3) increase their population resulting in microcolonies, (4) and finally form a mature biofilm.

This fact is supported by studies indicating thatantibiotic concentration 500 – 5000 times higher is required to treat a biofilm as compared to a bacterial suspension[9].

Therefore, an early detection of biofilm is of great interest to alert the presence of the bacterial biofilms before establishing their structures. Furthermore, developing an alternative biofilm treatment utilizing low doses of antibiotics that cannot cause severe side effects due to the high concentration of drugs[10] is desired to reduce biofilms effectively andavoid invasive treatments.

1.2 Microsystems for Biological Applications

A microsystem in the form of a biomedical device has advantages for both in-vitro and in-vivo applications based on small dimensions, low electric power consumption, portability and small volume requirements of the system. A number of microscale

devices have been demonstrated for chemical and biological applications, such as personal medicine[11] and diagnostic methods[12].

Microsystems typically require micro/nano-liter volumes of the sample for analysis that is extremely small compared to the traditional macro-scale experimental setup[13]. Due to the low volume requirement, a high throughput microsystem is desired particularly when samples are limited. Lab-on-a-chip devices are examples of microsystemss for biological and clinical applications, such as sample preparation[14], biomolecular sensing[15] and platforms for drug discovery research[13]. These systems demonstrated high sensitivity and low detection limit[16] compared to traditional macro-scale setups due to the precise experimental condition control based on the unique physics of the microscale such as laminar flow[9].

In addition, an implantable microdevice has been demonstrated for in-vivo applications. Considering the challenges of implantable devices, microsystems have unique advantages. First of all, the materials used in typical microsystems, such as inert metals and silicon, can be fully biocompatible[17]. The size of the microscale device also is typically small enough to be implanted in the body[18]. Due to the low power consumption of the system (less than micro-watt[19]), the entire device can be designed as a passive system which does not require a battery to operateperiodically[20]. Finally, a high sensitivity of the microsensor allows for reliable operation of the device in an in-vivo environment[21]. Microfabrication technologies enable designing and producing of sophisticated structures, devices, and systems on the scale of micrometers with biocompatible materials beyond those used in integrated circuit (IC) fabrication technologies.

Highly sensitive biocompatible devices based on fabrication technologies have been demonstrated for biomedical applications, such as glucose sensors, blood pressure sensors, and explosive gas sensors[22]. An implantable blood pressure sensor as shown in figure 1.3 (a), has been applied for real-time monitoring of blood pressure for heart failure patients[23]. The capability of integration with other systems (i.e. wireless communication, CMOS electronics, microfluidic devices and energy storage systems) in a micro-scale device provides a unique advantage for real-time monitoring[24]. For example, a wireless and non-invasive glucose sensor for diabetes patients has been developed by integrating the sensor with a radio frequency (RF) circuit and antenna as shown in figure 1.3 (b)[25].
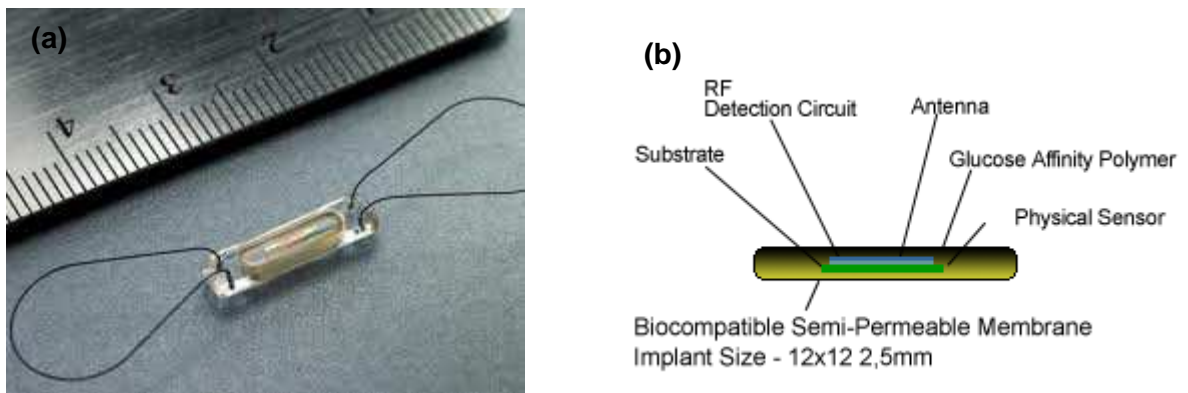
Figure 1.3: Examples of the implantable devices. (a) an implantable blood pressure sensor for heart failure patients(*www.cardioMEMS.com*), (b) schematic of an implantable glucose sensor for diabetes patients (*www.cybersensors.com*).

The robustness of fabrication technologies with biocompatible materials also allows development of a complex system which can be used in a harsh environment, such as space environments[26].

Based on these advantages of microfabricated devices, development of a microsystem for biofilm growth monitoring and enhanced treatment can be used for

biofilm associated infection challenges in biomedical fields including clinical and environmental applications, such as biofilm infections[27] and water contamination due to biofilm growth in the facilities[28].

1.3   Summary of Thesis Accomplishments and Impact

This thesis work accomplished (1) design, fabrication and test of a biofilm sensor, (2) development a new effective biofilm treatment with low doses of antibiotics and (3) integration of the sensor with the effective treatment as an integrated microsystem. The sensor successfully monitored biofilm growth in real-time and was reusable based on a novel passivation film. The newly developed biofilm treatment method was utilized by combining a low intensity of electric field with antibiotics based on the principles of the bioelectric effect. Reduction of biofilm treated by the new method demonstrated significant enhancement of biofilm treatment compared to traditional antibiotic therapies. Finally, the integrated microsystem was successfully designed, fabricated and demonstrated continuous biofilm growth monitoring as well as effective biofilm inhibition. The integration of biofilm detection and treatment on a single chip was critical to alert presence of biofilms at the early stage of their growth as well as achieve an alternative treatment method instead of massive antibiotic therapies. Since the system consumes low electric power and has small dimensions with biocompatible materials, it can potentially be applied for both in-vitro and in-vivo biofilm management, such as on water pipe biofilm growth monitoring and on the surface of implants where there are high risks of biofilm-associated infections. The implanted system especially would improve patient care through the early detection of biofilms and the potential prevention of revisional surgery through treatment of biofilms with the less invasive microsystem.

1.3.1 Design and Fabrication of a Biofilm Sensor

When biofilms are established, it is extremely difficult to eradicate them without using significantly higher doses of antibiotics or invasive surgeries[1-3, 6]. Moreover, since biofilms can be established within 10 – 20 hours from initial infection, real-time monitoring of biofilms is desirable for clinical applications compared to end-point evaluation. Therefore, continuous monitoring of biofilms is critical. The sensing of biofilm in this thesis work was achieved by a Surface Acoustic Wave (SAW) sensor considering its advantages such as low electric power requirement, high sensitivity and biocompatibility[29]. In the design of the sensor, a passivation film to achieve reliable operationin both bacterial growth media and animal serum was investigated theoretically with supporting experiments[30]. The operation frequency of the sensor was designed based on the regulation from the Federal Communication Commission for future implantable applications. High quality crystalline zinc oxide (ZnO) to achieve high sensitivitywas used as the piezoelectric material. Due to the effective passivation and high quality ZnO, the sensor was reusable in consecutive experiments and demonstrated sensitive biofilm detection. The SAW sensor has also shown successful real-time growth monitoring of biofilms in an animal serum[27].

1.3.2 Development of an Effective Biofilm Treatment

The concentration of antibiotic to treat biofilms is 500 – 5000 times more than that in planktonic bacteria[6] which requires invasive surgery to treat biofilms. Such high doses of antibiotics typically induce severe side-effects. Thus, development of an

alternative treatment utilized by low doses of drug is essential to manage biofilm infections effectively. The enhanced treatment of biofilms can be implemented by imposing electric fields with antibiotics simultaneously known as the bioelectric effect. In literature, electric fields typically applied either only direct or alternative current (DC or AC) for the bioelectric effect. In this thesis work, the combination of DC and AC fields was used for the first time as a superpositioned bioelectric effect and showed significant improvement of biofilm reduction compared to the traditional antibiotic method[31]. Due to the strong improvement of the efficacy, concentration of antibiotics was only required 2-3 times of the dose for planktonic bacterial infection. In addition, since the intensity of the field was even less than the electrolysis threshold voltage of biological fluid, the electric field caused minimized media decomposition which was critical to apply the method for clinical biofilm treatment. The development was completed in a macro-scale traditional cuvette setup[29] and evaluated by microbiological methods including live cell culture and total biomass quantification.

1.3.3   Demonstration of the Treatment in a Microfluidic System

Based on the new biofilm treatment method demonstrated in a macro-scale setup[29], the superpositioned bioelectric effect (SP-BE) was further developed using a planar electrode on a microfluidic platform[32]. Scaling of the SP-BE to the micro-scale is a critical requirement for realizing clinical applications of the method due to the required small dimension of the system, such as for *in vivo* biofilm treatment. The microfluidic device was chosen for on-chip SP-BE demonstration based on the advantages of high

experimental throughput, decreased volume requirements, and precise environmental control within microfluidic growth environments[33]. The voltage requirement of the SP field in the microfluidic platform (0.25 V) was further reduced below the electrolysis potential of the media (0.82 V at pH 7 with 25 °C) by decreasing the electrode spacing distance (2 mm) compared to the conventional macro-scale cuvette setup (4 mm). Planar thin film electrodes (200 nm thickness gold) were utilized to induce the electric field in a microfluidic growth reactor. Detection of biofilm growth and treatment within the platform is achieved via the *in situ* measurement of biofilm optical density (OD), where the use of linearly arrayed photopixels enables spatiotemporal biofilm monitoring within the microchannel. Using the platform, the SP-BE demonstrated significantly improved biofilm treatment efficacy[30].

1.3.4   Systematic Integration of the Biofilm Sensor with the Treatment

Based on the demonstration of the SAW sensor for biofilm detection and the superpositioned bioelectric effect for biofilm reduction in a microfluidic platform, an integrated microsystem was designed, fabricated and tested as biofilms were established and treated on the chips. This integration of the sensor with the treatment was designed as a feedback system. At first, the sensing component of the system provides total amount of the biofilms. Based on the stage of their growth, the treatment part of integrated chip can trigger the effective biofilm reduction by simultaneously monitoring changes in biomass by the SAW sensor component. Due to the bi-directional communication realized through

the integration, a systematic and effective biofilm management for clinical and environmental applications is demonstrated compared to the traditional end-pointbiofilm measurements either only detection or treatment. The chip was successfully microfabricated and demonstrated its biofilm detection as well as treatment monitoring with different bacterial biofilms[34].
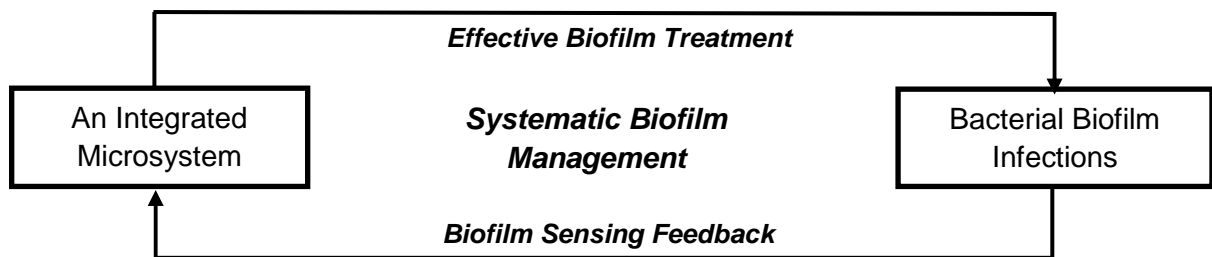
Figure 1.4: Concept of systematic biofilm management. By integrating a biofilm sensor with a treatment method as a microsystem, an effective biofilm infectious disease management can be achieved.

1.4 Literature Review

1.4.1 Macroscale Systems for Biofilms

The system developed in this work for the growth, treatment, and monitoring of bacterial biofilms represents a new method of conducting studies related to bacteria and their infections, including those studies aimed at drug screening and development. Currently, the majority of drug screening methods utilize macroscale devices and systems to perform assays that determine the effectiveness of prospective treatments on inhibiting or eradicating microbial growths. Advanced industry methods utilize primarily automated systems to perform common screening techniques, such as broth microdilution, antibiotic gradient, and disk diffusion studies on mature microbial cultures to determine the efficacy of various treatments as well as the minimal inhibitory concentration (MIC) of these drugs (Figure 1.5 and 1.6)[33].
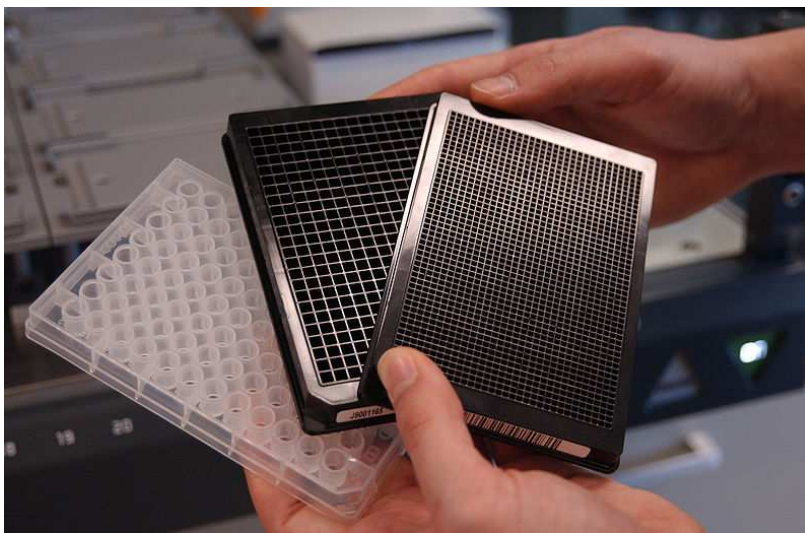
Figure 1.5: A broth microdilution susceptibility panel (microtiter plate) containing 98 reagent wells and a disposable tray inoculator[35]. Bacteria samples in suspension are treated with various concentrations of candidate drugs and each suspension tested using colony counting or spectroscopy to determine therapeutic efficacy.
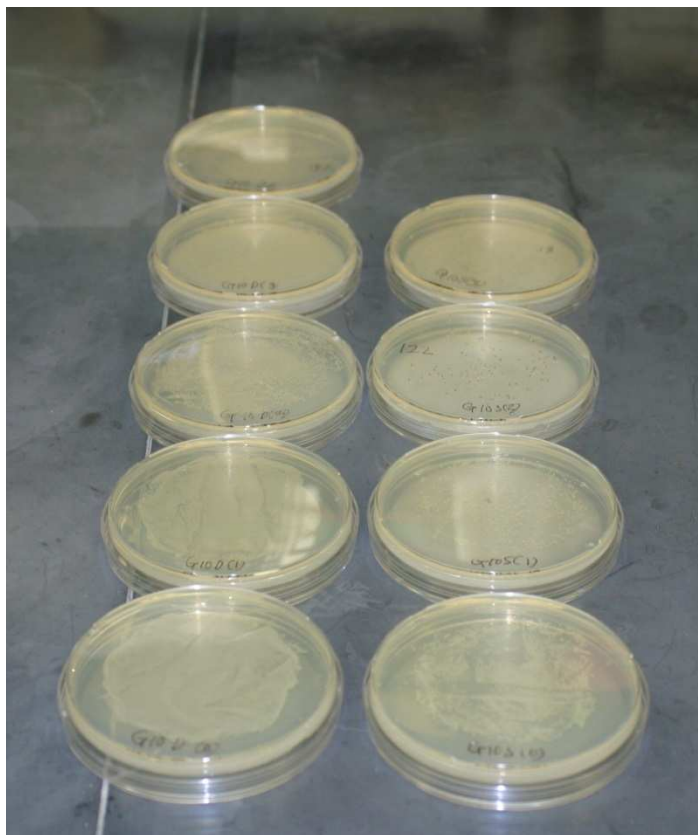
Figure 1.6: A colony forming unit (CFU) assay for evaluation of antibiotic biocidal effect in various concentration treatment. The number of CFU corresponds to the viable cell population in each treatment.

In addition to these microbiological methods, other immunoassays are frequently used to perform highly selective and sensitive studies by integrating methods such as ELISA, fluoroimmunoassay (FIA) and time-resolved fluoroimmunoassay (TRFIA) with large-scale capabilities, however, these methods are also limited in the types of molecules they can detect and therefore are not currently an all-encompassing method for antimicrobial drug screening.

The majority of previous biofilm studies have utilized macroscale methods to determine biofilm viability, biomass, and overall structure for various biomedical, industrial, and environmental applications. The majority of these studies were performed

13

using macroscale flow reactors to culture biofilm samples with integrated, external detection methods.

One of the most basic methods of biofilm quantification involves the counting of bacterial colonies, where bacteria are cultured on an agar plate and subsequently enumerated using microscopy and image analysis to determine their average density[36]. Polymerase chain reaction (PCR) techniques are another standard method, which uses the amplification of DNA segments to quantify the presence of target biological elements[37]. Fluorescence techniques provide an extremely accurate and simple method of biofilm detection by applying a fluorescent stain to a sample or, for greater precision, genetically engineering bacteria strains to selectively express a fluorescent protein[38]. Heyduk, et al.[39] demonstrated a representative fluorescent immunosensor technique shown in Figure 1.7, in which nanometer scale linkers modified with fluorochromes could participate in fluorescence resonance energy transfer (FRET) to increase sensitivity.
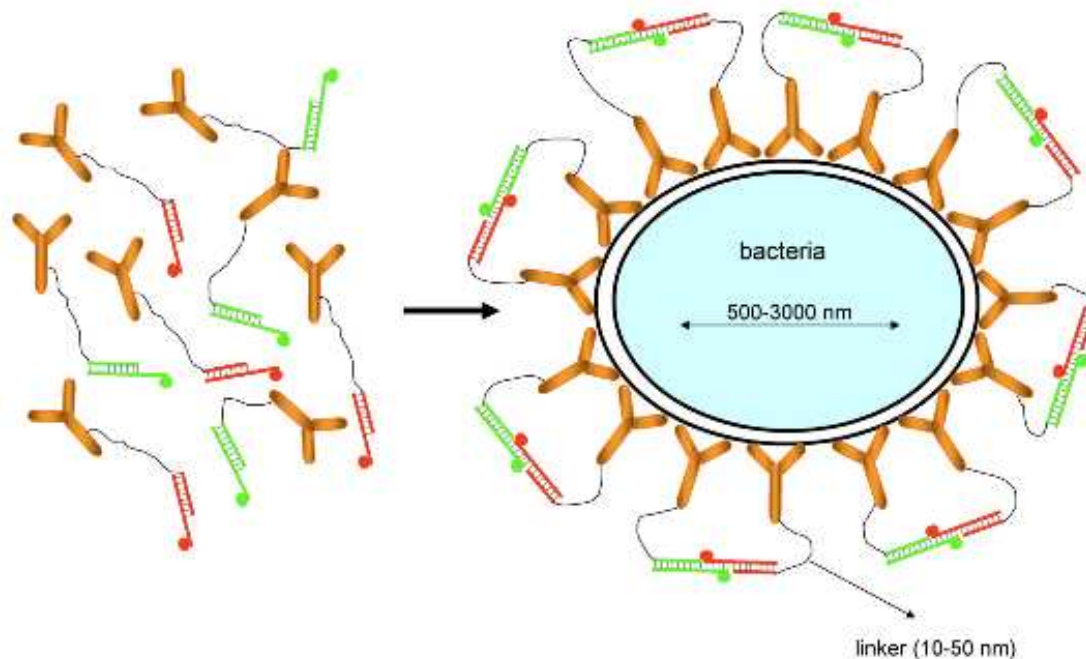
Figure 1.7 Design of homogeneous biological immunosensors for pathogenic bacteria detection[37].

Similar to the FRET approach, considerable research has been directed towards the use of the Enzyme-Linked Immunosorbent Assay (ELISA) in laboratories to perform detection analyses on mixed cultures[40]. ELISA utilizes the specific binding of particular antibodies and antigens in combination with a fluorescent label to enable a specific and highly sensitive method for quantitative measurement of target antibodies or analytes in solution. The method has seen vast use as a diagnostic tool in medical and other industrial fields and is also useful for chemical quality assurance due to its high sensitivity and selectivity. A typical procedure for performing an ELISA analysis in a laboratory setting is provided in Figure 1.8 below.

15
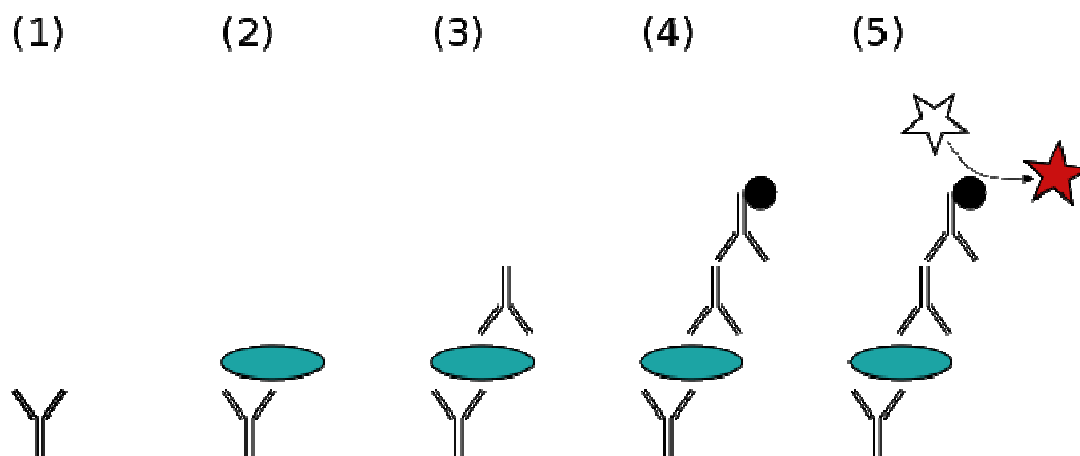
Figure 1.8: Typical ELISA procedure: (1) A plate is coated with a suitable capture antibody (2) as sample is added any matching antigen is captured by the antibody (3) a suitable biotin labeled detection antibody binds to the antigen (4) a second conjugate antibody binds to the biotin labeled detection antibody (5) add a fluorescent label and read out[41].

Despite the highly selective and precise results provided by ELISA, it is rather arduous to perform, often requiring up to a full week for analysis, and often difficult to perform in lab-on-a-chip devices. As a result, it has limited usefulness for high-throughput drug screening applications, lending to the development of new techniques for biofilm detection.

However, since this and similar approaches require a labeling method and external microscopy equipment such as a confocal or fluorescence microscope for biofilm detection, it does not represent a high throughput or cost effective method of sensing, thus presenting a barrier to drug screening applications. Moving forward, new methods of drug screening must utilize emerging technologies, such as the micro/nano methods

presented previously in order to take advantage of the benefits provided by devices at this scale.

1.4.2 Micro-Systems for Biofilms

Microsystems have significant advantages especially for bacterial biofilm studies due to the low sample volume requirement, high throughput system, and integration with other modules including sensing of biofilms. Microscale methods leverage the technologies available for larger systems while taking advantage of capabilities only available in microscale and microfabricated devices. Some of these methods enable on-chip biofilm detection that is not possible in macroscale systems, while others adapt existing macroscale technologies to smaller environments. By adapting macroscale technologies to microscale regimes, key advantages of micro/nano detection are leveraged including the use of small sample sizes, highly parallel throughput, tight control over environmental conditions, and inexpensive production through batch fabrication.

Recently, the development of small-scale devices and microsystems for drug screening applications has received attention. These 'lab-on-a-chip' devices typically rely upon optical methods such as surface Plasmon resonance (SPR) and fluorescence or electrochemical reactions on the sensor surface to detect microbial growth and treatment, which allows many measurements to be taken *in situ*. In addition, the relatively low cost of these devices enabled by batch fabrication allows for microsystems that are specific to particular assay types and applications.

Particularly, microfluidic platforms have been widely used for drug discovery research. Microfluidics provide laminar flow to the reactor and supply uniform nutrients

for biofilm growth. This is critical to have precisely controlled conditions for bacterial biofilm experiments since growth of biofilms is stochastic. In Meyer et al[144], a microfluidic based microdevice was developed and characterized as shown in figure 1.9.
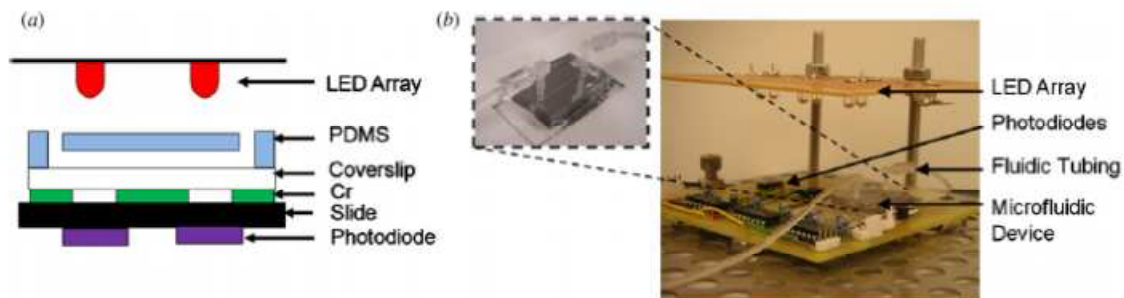
Figure 1.9: (a) Schematic of the microfluidic biofilm growth device, (b) Photo of the device setup[138].

The device was utilized to quantify the total biomass changes in various biofilm growth conditions including flow rate and different drug combinations[42]. The system utilized microfluidic growth reactors on glass coverslip substrates such as those utilized in fluorescence-based methods, with optical measurement performed by measuring changes in light transmittance through biofilms using COTS photodiodes. The measurement technique provides an *in situ* method of overall biomass quantification that does not require a permanent fixture on the external equipment used in confocal and fluorescence methods, thereby allowing for highly paralleled biofilm testing at reduced cost. The results showed successful continuous biofilm growth monitoring. In addition, microfluidic systems are used for antimicrobial efficacy evaluation. Compared to the traditional macro-scale experiments, it does not require large sample volumes that are

oftentimes difficult and/or expensive to synthesize particularly for new drug development[40].
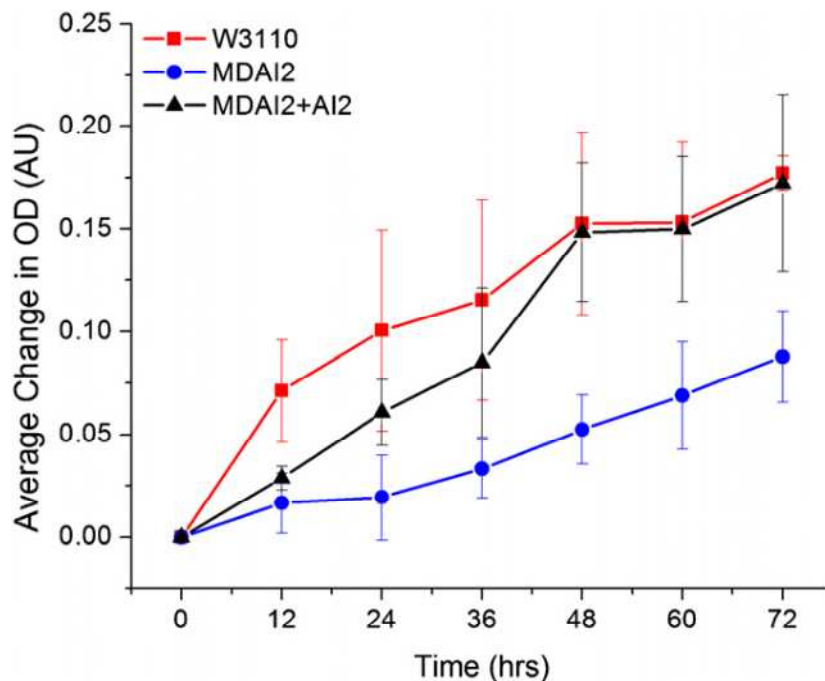
Figure 1.10: Measured optical density changes at the microfluidic platform. The results showed successful biofilm growth monitoring.[144]

Fluorescence imaging methods have been integrated with microfluidic systems in a number of cases, allowing for increased control over the growth conditions of bacterial biofilms while taking advantage of a highly accurate and easily implemented optical detection method[43]. Fluorescence microscopy systems of this type utilize fluorescent protein expression or cell staining methods to perform bacteria imaging and quantification of biofilm growth via cell colony counting or bacterial density. Similarly, laser confocal microscopy systems enable in-depth analysis of localized biofilm structures with respect to cell viability, surface roughness and morphology, and cell colony distribution within the polymeric ECM matrix.

19
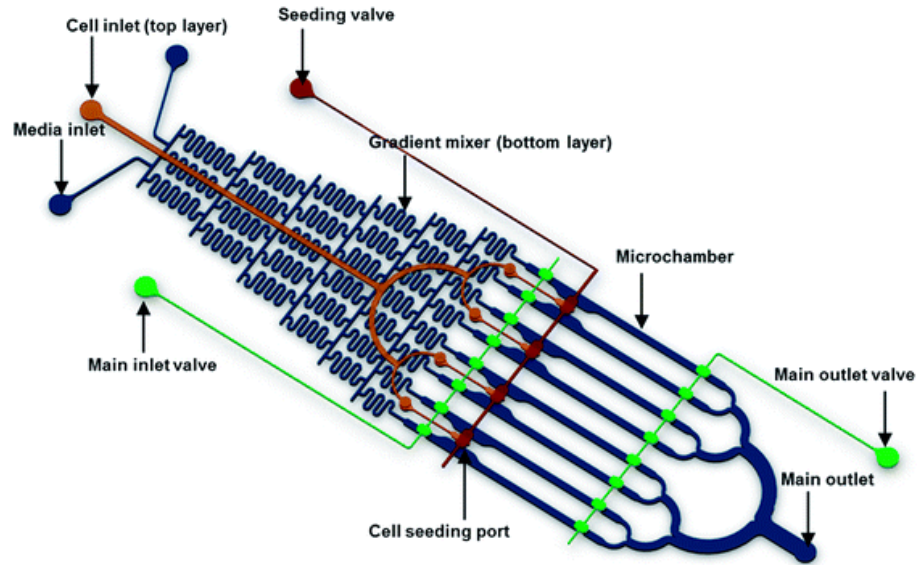
Figure 1.11: A microfluidic flow cell enabling gradient efficacy testing of eight concentrations of antibiotic simultaneously in a single device.[42]

The device produced by Kim et al [44] enables testing of different bacterial signal concentrations on biofilms formed in microchambers by integrating a gradient mixer into a microfluidic flow cell. The device produces results similar to those that could be obtained through traditional macroscale methods using lower reagent volumes and more parallel experimentation, with analysis of biofilm growth being performed via confocal microscopy at select points in time.

For extensive analysis and detection at the molecular level, microscopic systems have also been integrated with ELISA methods in order to utilize specific fluorescent labels to detect the presence of target antibodies within a solution, such as bacterial biofilm cells. While this and similar fluorescent microscopy-based methods are extremely accurate and provide precise information with regards to the development of bacterial biofilms, they require expensive and complex equipment for biofilm

measurement and, without a permanent fixture upon the microscope stage to perform continuous *in situ* measurement, are limited explicitly to end-point measurements [6].

In order to enable continuous measurement of bacterial biofilm development without the use of optical measurements, electrochemical sensors have been developed that are able to detect biofilm growth with respect to both time and position within a microfluidic reactor. Sensors of this type detect the presence of bacterial biofilms attaching to an exposed or passivated set of electrodes via changes in capacitance or impedance.

1.4.3   Biofilm Sensing

Biofilms are composed of a group of bacteria surrounded by an extracellular matrix with diverse proteins. Thus, the amount of total biomass is correlated to the growth of biofilms[45]. Biomass detection has been achieved based on capacitance[46], impedance[47], fluorescence[48], and acoustic wave[49] sensing techniques. These methods can be applied for either a macro-scale[50] or micro-scale device.

Colorimetric assays are traditional methods for total biomass quantification based on optical density changes in a specific wavelength. In the assay, typically a dye can bind with specific chemical functional groups. Sequentially, the dye is detached by a releasing solution and measured the optical density by a spectrophotometer. For instance, crystal violet assay is one of most frequently used for biofilm studies especially [51]. The dye can stain the cell wall and extracellular matrix of the biofilm resulting in quantitation of the total biomass. This colorimetric assay is typically utilized to investigate major changes of total biomass in biofilms at the end point of experiments[52].

Monitoring of electrical parameter changes as biofilms are established, such as capacitance and impedance, is demonstrated in microscale devices. A capacitance change based biomass detection sensor has been shown for biosensing applications[53, 54]. In Ghafar-Zadeh et al.[55], a dual channel microfluidic device, as shown in figure 1.12, based on a CMOS platform has been demonstrated for continuous bacterial growth monitoring. As bacteria grow in the channel, the dielectric constant of the bacterial suspension is changed. The changes of the dielectric constant affect the capacitance at the gate of the CMOS device. This capacitance-based biofilm monitoring system shows high sensitivity

22

(255 mV/fF ≈ 10^{-12} g), but it requires a continuous power supply and a signal converter from the capacitance to an electrical signal.
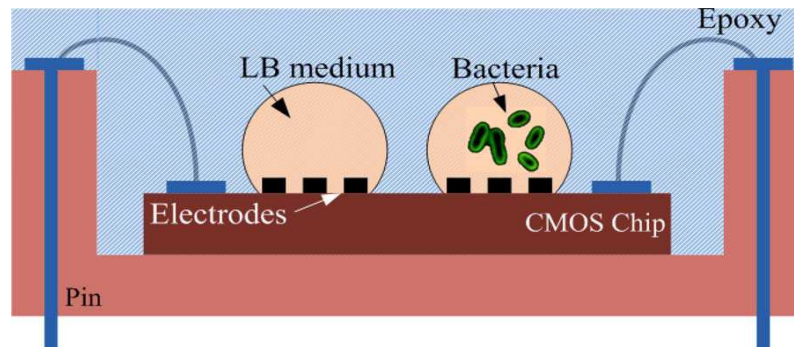
Figure 1.12: Schematic of differential bacteria growth monitoring using on-chip capacitive sensor[43]

The impedance measurement along biofilm growth has been investigated[56, 57]. The electric impedance of bacterial suspension is composed of resistance, capacitance, and inductance which can change during biofilm growth. In E. Spiller et al.[44], the group developed an arrayed impedance measurement platform for drug discovery studies.
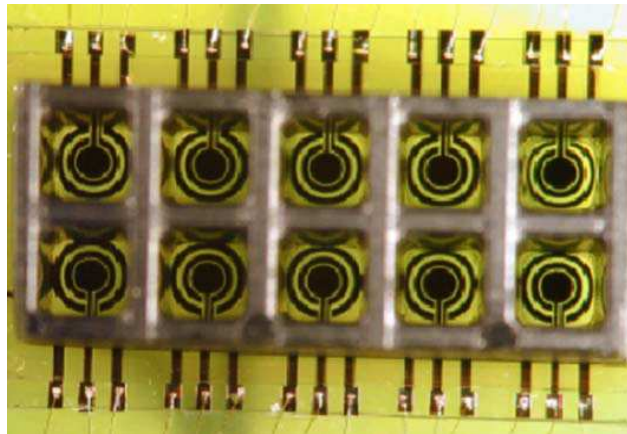
Figure 1.13: Top view of a 2 by 5-array of measurement chambers[44]

The 2 by 5 arrayed impedance measurement chamber is shown in figure 1.13. Each well has three electrodes, which are working, reference, and counter electrodes. The impedance is measured when a constant potential was applied between working and reference electrodes. Although this method showed a 10^5 CFU/mL $\approx$ (10^{-9} g) detection limit[44], a constant power source requirement for the continuous measurement can be a challenge for real-time long term biofilm detection including both in-vitro and in-vivo applications.

Biofilm labeling with fluorescence molecules is one of the well-established techniques for bacterial detection[58]. The procedure is not complex andthe sensitivity is very high. For instance, a fluorescent immunosensor for bacterial detection was demonstrated in Heyduk et al.[59]. Two samples of the antibody were prepared, each labeled with nanometer-sized flexible linkers with short complementary oligonucleotides modified with fluorochromes that could participate in fluorescence resonance energy

24

transfer (FRET) to increase the sensitivity. A fluorescent image showing the binding of the antibodies and bacteria is shown in figure 1.14.
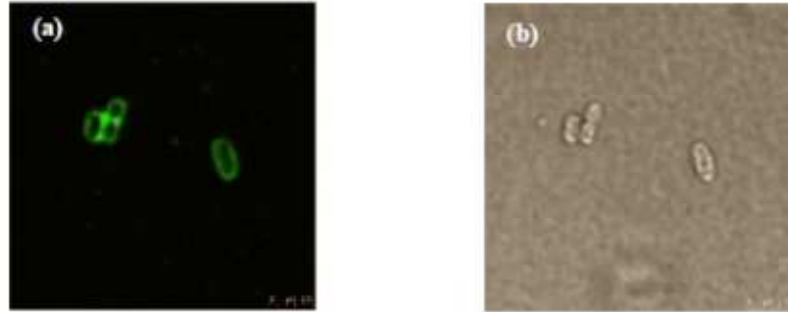
Figure 1.14: Fluorescence microscope image (a) fluorescent signal from the oligonucleotides proximity due to the bacteria binding, (b) light transmittance image in the same area Fluorescent biofilm quantification[47]

Based on the selective live/dead cell staining in biofilm, biofilm imaging work have demonstrated via fluorescence as an extremely sensitive method to visualize as well as quantify total biomass in a small scale device. Confocal microscopy is a representative method for biofilm visualization and has revealed details of biofilm composition. However, this biofilm imaging method requires bulk and expensive external equipment. In addition, the quantification area is relatively small due to the limited observation area of the microscope compared to other colorimetric assay and impedance monitoring platform.

The fluorescent biofilm quantification method is only an end-point measurement and also requires extra work for labeling which cannot be available in environmental and/or clinical biofilm monitoring systems such as water pipes and hospital infections. In

addition, due to the degradation of the fluorescence proteins, the labeling of the protein shows limited lifetime for measurements[60].

Surface Acoustic Wave (SAW) sensors have demonstrated a highly sensitive mass detection capability[61,62]. When an electric potential is applied at the interdigitated electrodes on a piezoelectric substrate, mechanical displacements are induced and propagated on the surface based on the reversible energy conversion between mechanical and electrical energy domains. The phase velocity of the waves is decreased when an additional mass is loaded[50]. The changes of velocity can be detected by monitoring the resonant frequency of the device[49, 50].

In M. Bisoffi et al.[63], viruses are detected by a SAW sensor. The surface of the SAW sensor was functionalized using a specific antibody for an interesting virus as shown in figure 1.8. As viruses bind to the antibody, the phase velocity of the SAW is decreased resulting in changes of the sensor operational frequency. The sensitivity of the sensor was~ 5000 RNA copies (corresponding to viral particles)[51].
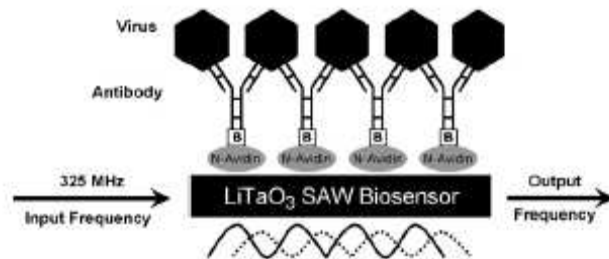
Figure 1.15: Schematic of the antibody-based virus surface acoustic wave biosensor. N-avidin protein is used as an intermediate layer for the antibody immobilization on the surface. The antibody is attached on the N-avidin protein. Virus has a specific structure to bind with the antibody[51].

In S. Krishnamoorthy et al.[64], a highly sensitive SAW sensor was demonstrated for an interlukin-6 detection which is one of the key molecules in the human immune system. A specific antibody was immobilized on the surface of the SAW sensor as shown in figure 1.16. The detection limit of the sensor was 10^{-18} g, which is the most sensitive method, using zinc oxide (ZnO) piezoelectric substrate.
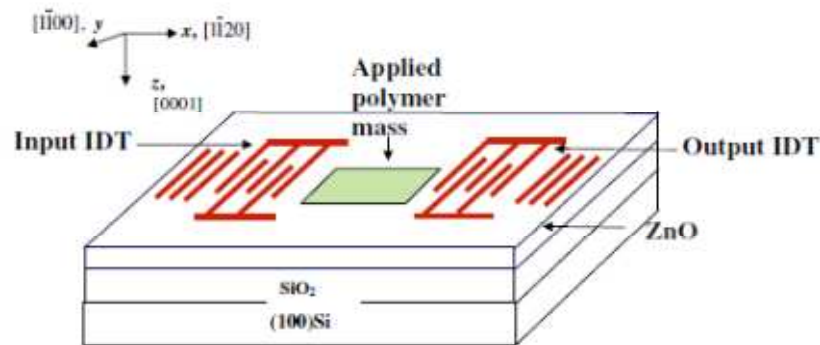
Figure 1.16: Schematic of the SAW sensor. A specific antibody for interlukin-6 was immobilized on the surface of the SAW sensor[52].

In table 1.1, the biomass sensing mechanisms are summarized. Since the SAW sensor is also a passive device, electric power to operate the sensor can be delivered by wireless coupling without a battery[65]. Based on that the SAW sensor requires an AC electric potential for operation and generates the AC electrical signal as the output, the sensor is compatible with a RF wireless communication system[66]. The wireless compatibility, battery-less operation and high sensitivity of the SAW sensor make it a unique tool for future non-invasive in-vitro and in-vivo biofilm monitoring applications.

	Capacitive Sensor	Impedance Sensor	Optical Sensor	Acoustic Wave Sensor
Input (excitation)	Electric signal	Electric signal	Optical source	Electric signal
Read out electronics	Yes	Yes	Yes	No
Structure	2D	2D	3D	2D
Detection limit or sensitivity	255 mV/fF $\approx (10^{-12}$ g) *(GHAFAR-ZADEH et al. / IEEE T BIO-MED ENG, 2010)*	10^5 cells/mL $\approx (10^{-9}$ g) *(E. Spiller et al. / Sensors and Actuators, 2006)*	4×10^3 cells/cm^2 $\approx (10^{-11}$ g) *(M. Fischer et al., Biosensors and Bioelectrionics, 2012)*	3 ag $(10^{-18}$g) *(S. Krishnamoorthy et. al / Biosensors and Bioelectronics, 2008)*

Table 1.1: Summary of the biomass detection methods

1.4.4 Biofilm Treatment

As previously discussed, biofilms are extremely difficult to treat once they are established. The concentration of antibiotics required to treat biofilms is 500 – 5000 times more than that in bacterial suspension[6, 67]. To increase the efficacy of antibiotic treatment, combination of different drugs or electric fields with antimicrobial agents has been investigated.

In Cottarel and Wierzbowski et al.[68], combinations of two or more antibiotics with adjuvants (cocktail therapy) were studied for bacterial infection treatment. The principles of bacterial treatment using antibiotics depend on the modes of the action of the agents, such as cell wall synthesis inhibition[69], and DNA transcription blocking[70]. A scheme of some modes of action of antibiotic agents is shown in figure 1.17.
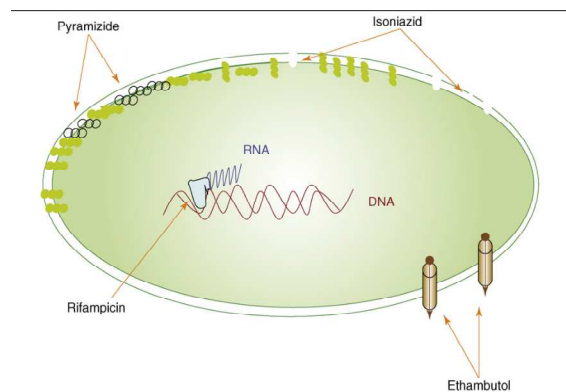
Figure 1.17: Schematic of the antibiotic mode of actions. Each antibiotic has a unique mechanism to treat bacteria[56]

For example, an aminoglycoside antibiotic blocks protein synthesis by ribosomes in bacterial cells. Hence, the antibiotic inhibits synthesis of essential enzymes resulting in cell death[71]. By combining two or more drugs, the treatment of bacterial infection can be enhanced based on multiple target attacks. However, combination of antibiotics can cause severe side effects due to unexpected interference between the antibiotics[56] and induce generation of more antibiotic resistive bacteria[72]. The combined antibiotic therapy often cannot be a universal method for bacterial treatment because of the severe side effects[56]. Furthermore, this method may be difficult to integrate with a microdevice due to the limited lifetime of drugs and delivery to specific locations especially considering in-vivo environments[73].

The efficacy of antibiotics for biofilm treatment can be radically enhanced if these agents are used under an electric field, known as the "bioelectric effect" [74, 75]. According to several studies, the treatment effect of antibiotics combined with direct or alternating current (DC or AC) electric field resultsin improved treatment since the DC or AC electrical signal can provide additional biocidal effects to biofilm, such as local pH difference[63] and biofilm permeability enhancement[62]. Costerton et al. reported the bioelectric effect for the first time[76]. In the paper, when antibiotics were combined with a DC electric field (5 V/cm), enhanced biofilm treatment efficacy compared to other treatments was demonstrated, as shown in figure 1.18.
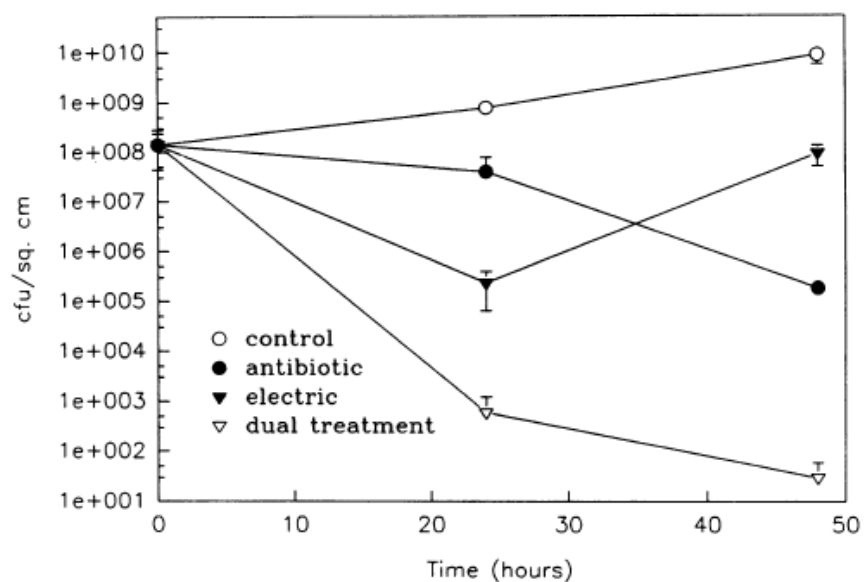
Figure 1.18: The treatment of biofilm in different treatment methods based on the cell viability studies (colony forming unit, CFU assay)[64].

In the results, when the antibiotic was combined with the electric field, the treatment efficacywas enhanced by approximately 6 orders of magnitude compared to the control (no treatment) and 3 orders of magnitude compared to antibiotic treatment only. However, the intensity of the electric field (5 V/cm) caused electrolysis of the media since the intensity is higher than the limiting potential of the electrolysis inbiological fluids[77].

In Del Pozo et al. (2009)[78], a comprehensive study of bioelectric effect using diverse antibiotics was reported. The testing set-up for the bioelectric effect investigation in different antibiotic treatments is shown in figure 1.19. It is composed of flow cells for growth media supply with electrodes to induce an electric field. Three biofilm strains are studied for the bioelectric effect: *Psudomonas aeruginosa, Staphylococcus aureus,* and *Staphylococcus epidermidis* biofilms. The electric current was applied for 20, 200, or 2000 microamperes of DC field with 11 different antibiotic additions in each experiment.

31
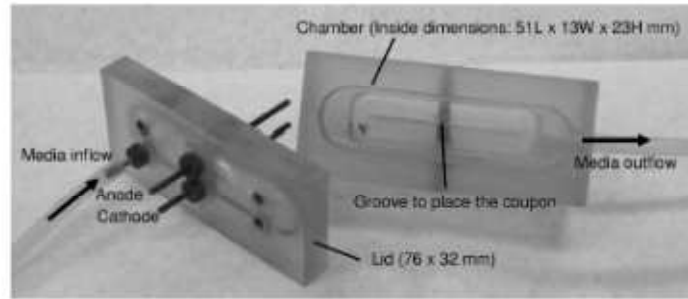
Figure 1.19: Polycarbonate chamber detail (internal volume $\approx 16\text{cm}^3$)[66].

The results of the study demonstrated improved biofilm treatments in all of tested bacterial strains. In addition, the study showed that the bioelectric effect is independent of the type of antibiotic as shown in the treatment results in figure 1.20.
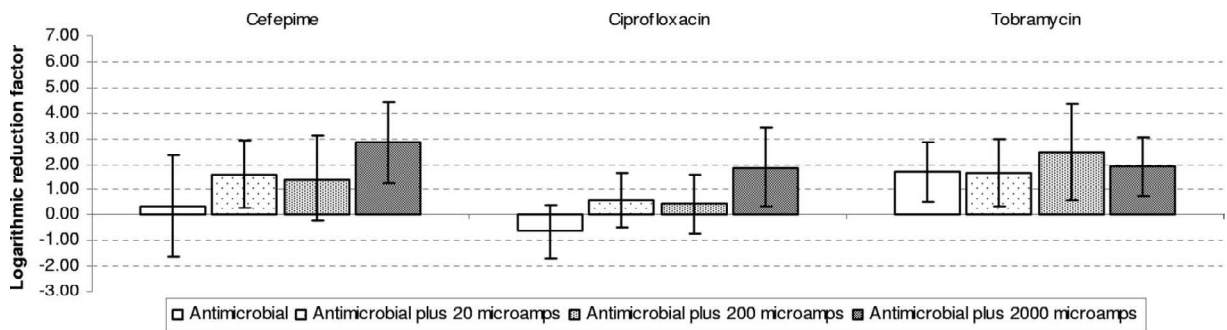
Figure 1.20: Averaged treatment efficacies with the standard deviations for Pseudomonas aeruginosa after exposure to four different treatments (i.e., antimicrobial agent alone, antimicrobial agent plus 20 µA, 200 µA, or 2000 µA of DC electric field)[66].

In Caubet et al. [79], an AC bioelectric effect implemented with a radio frequency electric field was demonstrated in a macro-scale set up (14 X 8 X 5 cm). The AC electric field is characterized to a 2 V/cm amplitude of sinusoidal signal at 10 MHz. The AC bioelectric effect also showed an enhanced biofilm treatment efficacy compared to only antibiotic treatment. Table 1.2 summarized the results of treatment in log-scale.

Expt	Mean LRF	SD
RFC alone	0.50	0.30
Gentamicin alone	2.11	0.05
Oxytetracycline alone	1.90	0.40
RFC + gentamicin	3.43	0.27
RFC + oxytetracycline	2.80	0.31

Table 1.2: Treatment results of only antibiotics (Gentamicin, or Oxytetracycline), only AC electric field, and AC bioelectric effect[67].

The treatment efficacy of the AC bioelectric effect was enhanced approximately by one order of magnitude compared to antibiotic treatment only. Even though the efficiency of the AC bioelectric effect is not in the same order of magnitude as the DC bioelectric effect, it still showed an improved treatment of biofilm.

Through the literature review, a DC or AC bioelectric effect has been demonstrated and characterized in a macro-scale experimental setup which requires high sample volume and is challenging to integrate within a single system for clinical applications as summarized in table 1.3. More importantly, intensities of the electric field

used for the bioelectric effect were high resulting in electrolysis of the surrounding media. The electrolysis of human serum can cause severe side effects due to the cell death[80].

	DC Bioelectric Effect	AC Bioelectric Effect
Intensity of Electric Field	5 V/cm *(J.W. Costerton et al. Antimicrobial Agents and Chemotherapy, 1994)*	2 V/cm at 10 MHz *(M. Giladi et al., Antimicrobial Agents and Chemotherapy, 2008)*
Treatment Efficacy	6 log	1-2 log
Set up (W X L X H)	Macro-scale (8 X 31 X 3 cm)	Macro-scale (8 X 14 X 5 cm)
Challenges	Electrolysis of media => Biocidal molecules generation	Electrolysis of media Relatively low enhancement

Table 1.3: Summary of parameters and challenges of DC and AC electric field bioelectric effect.

However, the bioelectric effect is not only a general effect to diverse bacterial strains as previously shown in literature[66], but also an independent method on the types of antibiotics[66]. Therefore, the bioelectric effect has an important advantage for biofilm treatment that can potentially be a general treatment method with different types of antibiotics. The development of a new bioelectric effect utilized with a low intensity electric field without causing significant electrolysis of human serum is required to apply the concept of the bioelectric effect for clinical applications.

1.5   Summary

Through the literature review focused on the biofilm detection and enhanced treatment aspects, both sensing and effective treatments are key required methods for biofilm associated problem management including clinical infectious diseases and environmental contamination challenges. As shown in the previous work, independent biofilm sensing and treatment methods are demonstrated with various approaches. However, integration of a sensor and an effective treatment has not yet been demonstrated which has significant impacts in terms of developing new technologies as well as practical applications contributing to overcome biofilm associated challenges especially infectious diseases.

In the rest of thesis, each component of the integrated system that include a newly developed biofilm SAW sensor and bioelectric effect biofilm treatment using superposition field of AC and DC signals is described in details of design, fabrication, testing and discussion of the results. Finally, a successfully integrated system with the sensor and treatment in a micro-scale device is presented.

Chapter 2: Biofilm Sensor

Based on the literature review, an integrated microsystem is an ideal solution for in-vivo and in-vitro biofilm monitoring and treatment. In this chapter, design, fabrication and testing reuslts of the biofilm sensing component of the system is presented based on the principles of the surface acoustic waves.

2.1 Principles of the SAW Sensor

Surface Acoustic Waves (SAWs) are generated on piezoelectric materials when an electric potential is applied to interdigitated electrode transducers (IDT). The IDT induces a uniform electric field on the piezoelectric material which generates mechanical displacements based on the piezoelectricity of the substrate. The induced mechanical displacements cause electric potential differences due to the reversible piezoelectricity from mechanical to electrical energies. Based on these energy conversions on the piezoelectric substrate, the mechanical displacement (surface acoustic wave) can propagate on the surface of the piezoelectric material. A high piezoelectric coefficient (coupling coefficient) material is critical to achieve a highly sensitive SAW sensor by minimizing energy loss of the conversion[81]. A diagram of energy conversion and a schematic of propagation in the substrate are shown in figure 2.1 and 2.2 respectively.

The wavelength of the SAW is related to the distance between the two electrodes in IDT; half of the SAW wavelength is equal to the distance of the two electrodes[34]. Since the input electrical signal is an alternating current (AC) signal, a standing mechanical displacement wave in each IDT electrode pair is formed at the specific frequency.
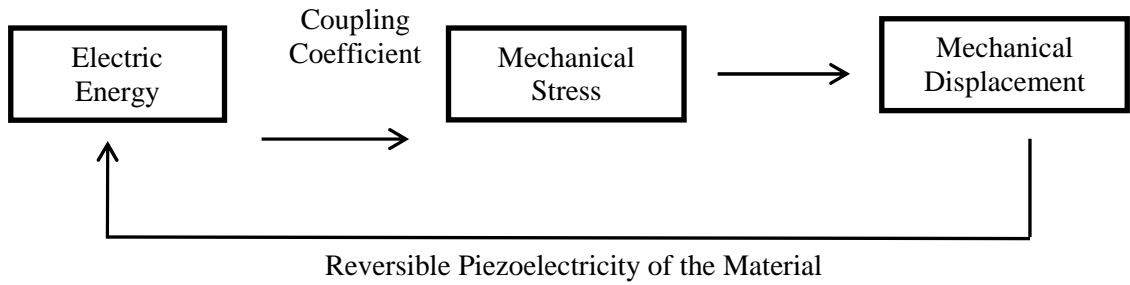
Figure 2.1: A diagram of energy conversion in the piezoelectric substrate to generate

SAWs

Propagation of the SAW
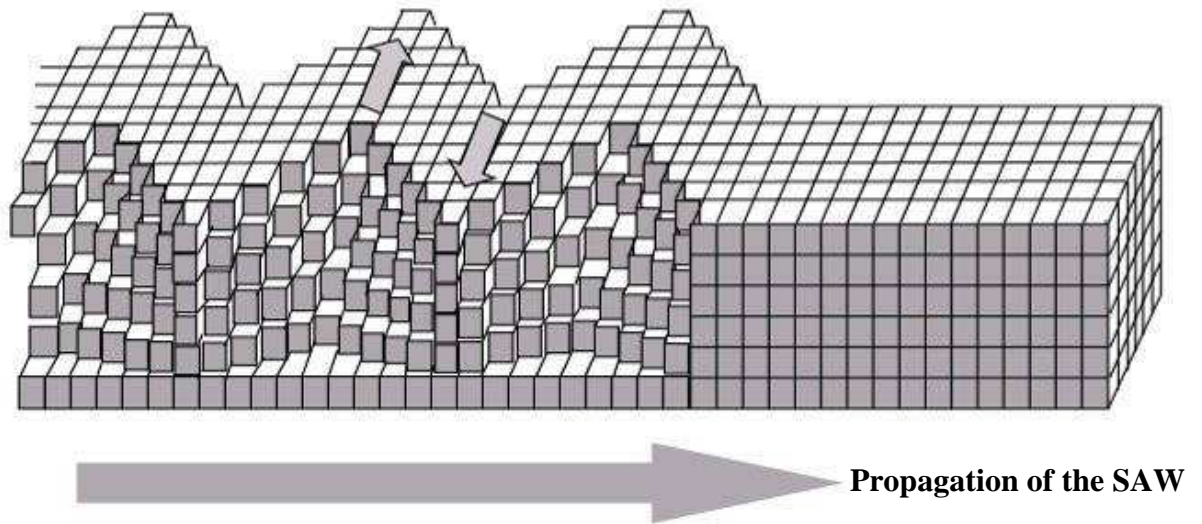
Figure 2.2: Schematic of SAW propagation on the piezoelectric substrate (Shear Horizontal mode)[82]

The standing wave is satisfied at the specific condition that the separation of the electrode

pair is equal to an integer times half of the SAW wavelength[83]. Theoretical relations

between the wavelength, speed of the wave and frequency are shown in equation (1), (2) and (3).

$$d = n\frac{\lambda}{2} \qquad (1)$$

$$v = f \cdot \lambda \qquad (2)$$

$$v = \sqrt{\frac{C}{\rho}} \qquad (3)$$

where d is the separation of the IDT electrode pair, λ is the wavelength of the SAW, n is an integer, v is the SAW speed, f is the operational frequency, C is the shear modulus of the substrate, and ρ is the density of the substrate. The velocity of the acoustic wave is inversely proportional to the square root of applied mass on the surface of the substrate as shown in equation 3. Thus, mass loading on the surface decreases the SAW velocity. The velocity of the SAW on the piezoelectric material is proportional to the resonant frequency because the wavelength is a constant set by the IDT. Therefore, the velocity change of the SAW due to mass loading can be monitored by measuring resonant frequency shifts. Since the speed of SAW is an intrinsic material property, the operational frequency of the sensor is designed based on the pattern of the IDT (electrode separation distance) and the selected piezoelectric material.

The sensitivity of the SAW sensor is extremely high since the speed of the wave is usually faster than other acoustic waves. For instance, a SAW propagates on a ZnO layer with approximately 4814.4m/s in S. Krishnamoorthy et al.[84]. Based on the relation between operational frequency and velocity of the wave, a 1 m/s change in speed, which

is equal to 100 pg of mass in S. Krishnamoorthy et al., induces approximately a 1 MHz frequency shift. Thus, SAW sensors have been used for extremely sensitive molecular sensing applications. In addition to the high sensitivity, the SAW sensor can be fabricated using biocompatible materials, such as gold, zinc oxide, and silicon allowing the sensor application to biomedical fields. Based on these advantages, the SAW sensor can be a sensitive transduction method for real-time biomass growth monitoring applications.

2.2 Love mode SAW

The standing mechanical wave, which is induced by the electric field at the IDT on the piezoelectric material, propagates on the surface based on the reversible piezoelectricity of the substrate[85]. Depending on the lattice structure of the substrate, two possible propagation modes of the SAW, which are called Rayleigh and Love modes, can be generated.

Lord Rayleigh discovered the vertical SAW mode of propagation and, in his classic paper, predicted the properties of these waves[86]. Named for their discoverer, Rayleigh waves have a longitudinal component and a vertical shear component as shown in figure 2.3. The Rayleigh SAW amplitude is typically about 10 Å and the wavelength ranges from 1 to 100 μm. This type of SAW sensor usually operates from 25 to 500 MHz[87].

Vertical and Shear Component

Propagation of the SAW
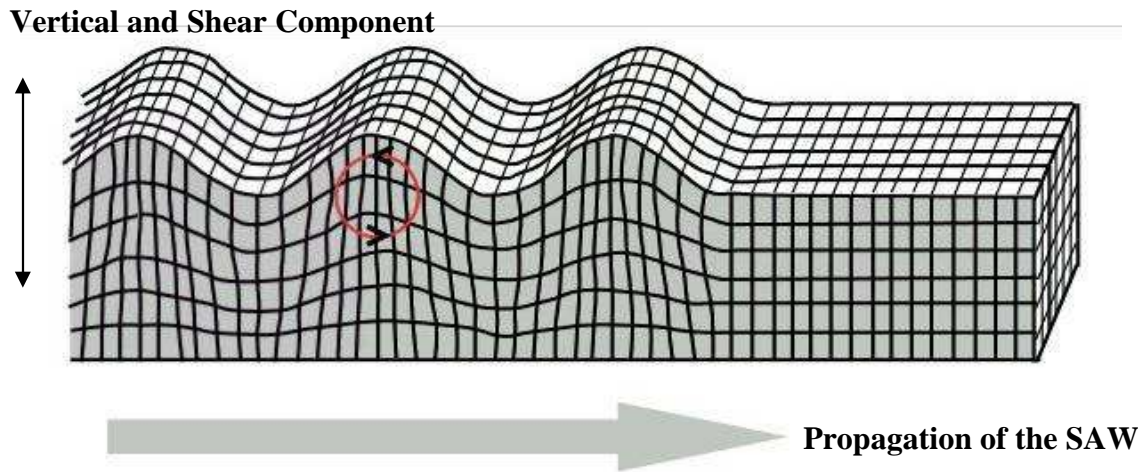
Figure 2.3: Schematic of Rayleigh mode SAW propagation[88]

This amplitude and frequency can couple with a medium placed in contact with the device's surface since Rayleigh waves have all their acoustic energy confined within one wavelength of the surface. Such coupling between the surface of the sensor and external media strongly affects not only the amplitude, but also the velocity of the wave. This feature enables SAW sensors to directly sense mass and mechanical properties of the contact media, such as shear modulus and thermal expansion coefficient. One of the disadvantages of the Rayleigh mode of SAW is that because the wave is a surface-normal wave, it makes the SAW device poorly suitable for liquid sensing application. When the Rayleigh mode SAW sensor is contacted by a liquid, compression waves are created, causing an excessive attenuation of the acoustic wave. As a result, Rayleigh mode SAW sensors are usually used for dry environmental sensing, such as temperature and pressure sensors[89].

On the other hand, if the cut of the piezoelectric crystal material is rotated appropriately, the wave propagation mode changes from a vertical shear SAW sensor to a shear-horizontal surface acoustic wave (SH-SAW) sensor[90], as shown in figure 2.4. Augustus Edward Hough Love predicted the existence of the SH-SAW wave mathematically in 1911. The lattice motion of a Love wave forms a horizontal line perpendicular to the direction of propagation (i.e. are transverse waves). Hence, it is critical to deposit a highly oriented c-axis piezoelectric material to generate a Love mode SAW[91]. When the SAW IDT is aligned perpendicular to the c-axis of the piezoelectric material, Love mode waves are predominantly generated. This Love mode SAW dramatically reduces the losses when liquids come in contact with the propagating medium, which allows Love mode SAW sensors to be used as biosensors[92].

Shear Horizontal Component

Propagation of the SAW
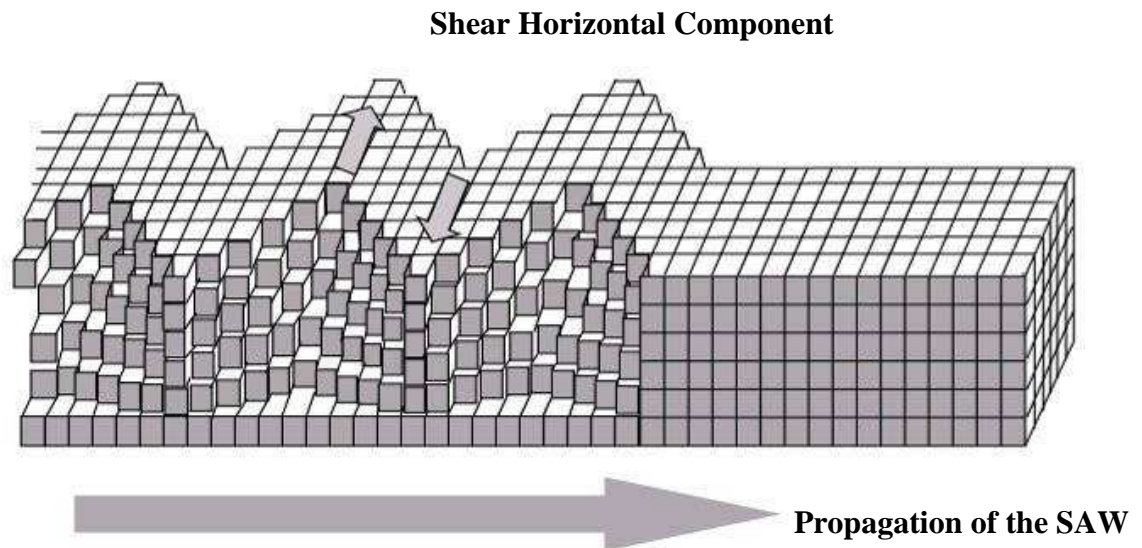
Figure 2.4: Love mode SAW propagation[64]

Love wave devices also offer the advantage of concentrating the acoustic energy in the guiding layer grown on an appropriate substrate, thus offering the opportunity of higher mass sensitivities. Several Love mode SAW sensors operating in both gaseous and liquid media have been demonstrated[93, 94].

2.3 Piezoelectric Material for the SAW Sensor

A SAW is generated on the piezoelectric material which operates at a high frequency oscillation governed by the design of the IDT. To obtain the maximum acoustic wave energy from the input electrical energy, the deposition of a high piezoelectric coefficient material as a substrate is the most important parameter of the SAW sensor as well as its high quality deposition method[95, 96]. The piezoelectric coefficient is defined as the ratio between mechanical energy and electrical energy[97] (equation (4)).

$$K^2 (piezoelectric\ coefficient) = \frac{acoustic\ energy}{electrical\ energy} \quad (4)$$

ZnO is a piezoelectric material with the highest piezoelectric efficiency along with Lithium Niobate (LiNbO3)[98]. Another advantage of ZnO is a biocompatibility of the material[99] that enable to apply for diverse biomedical devices[100]. Moreover, ZnO can be grown by thin film deposition methods, such as radio-frequency (RF) sputtering and pulsed laser deposition (PLD) with low limit of the substrate[101, 102]. A high quality ZnO thin film deposition process is well developed and compatible with traditional photolithography techniques. The PLD is one of the common ZnO deposition methods

for high quality film growth[103, 104]. PLD has several advantages and benefits over other growth techniques, including high control over growth parameters, precisely controlled growth rates, and low temperatures. Due to its relatively simple set-up and operation, it has been widely used in research. ZnO with a high piezoelectric coefficient is capable of generating very high frequency (GHz) SAW and when combined with a SiO_2/Si substrate it can be an excellent material choice for Love mode propagation[105]. Based on its piezoelectric properties, biocompatibility, and the high quality fabrication process, ZnO is the piezoelectric material for the biofilm sensor design.

2.4 Passivation of the Piezoelectric Layer

The ZnO film is soluble when in contact with a non-neutral pH liquid or after long term moisture exposure[106]. Zinc (Zn) has less ionization energy, which is the minimum required energy to become an ion respected to the energy of hydrogen (H). As a result, when non-ionized Zn and H atoms are in the same solution, Zn will be ionized in the solution due to the smaller ionization energy than H, resulting with generation of hydrogen gas. Because of this solubility of ZnO, a SAW sensor based on ZnO layer is challenging for biosensor applications[107, 108]. Specifically in this work, when the ZnO film was placed in the bacterial growth media without a passivation film, the ZnO layer was dissolved completely within three hours. Therefore, the ZnO film-based SAW sensor for biosensor applications is required to fabricate a passivation layer that can minimize loss of the sensitivity. Since the SAW propagates on the surface of the sensor, the

mechanical properties of the passivation film, such as shear modulus and density, are critical parameters to prevent significant sensitivity loss due to the mismatch in material properties. To study the sensitivity dependence in different passivation materials, a theoretical model for the biofilm SAW sensor was developed that is focused on the elastic modulus of the material, as shown the schematic of the cross sectional view of the model in figure 2.5.
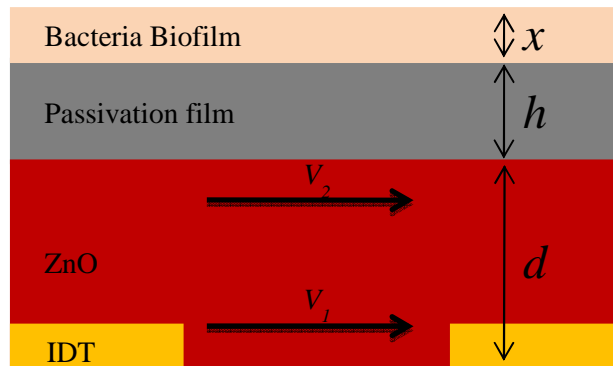
Figure 2.5: Schematic of passivation SAW sensor for biofilm detection[109]

where x is the biofilm thickness, h is the thickness of the passivation film, and d is the thickness of ZnO film. The bacterial growth over the sensor was assumed to be uniform, so that mass loading depends only on the thickness of the biofilm (x). In addition, the SAW velocities were assumed to be equal both in the bottom and top ZnO layers,

yielding $V_1 = V_2$ as indicated in figure 2.5 to simplify the model calculation (no dispersion). The mass sensitivity of the SAW sensor is given in equation (5)[72].

$$S_m^v = \lim_{\Delta m \to 0} \frac{1}{\Delta m}\left(\frac{\Delta v}{v_0}\right)$$

(5)

where S_m^v is the mass sensitivity of the SAW sensor, v_0 is the initial SAW velocity before mass loading, Δm is the amount of the mass loading, and Δv is the SAW velocity change due to the mass loading. Based on the uniform bacteria growth assumption and from equation (5), a one dimensional mass sensitivity for the SAW sensor can be derived as shown in equation (6).

$$S_m^v \propto \frac{dv}{dx}_{x \to 0}$$

(6)

where x is the bacterial biofilm thickness. The velocity of the SAW is derived in equation (7)[72, 110].

$$v = \sqrt{\frac{C}{\rho}}$$

(7)

where v is the SAW velocity, C is the shear modulus, and ρ is the density of the surface. The acoustic wave velocity in the passivated SAW sensor can be defined as a function of passivation film thickness (h), density (ρ), and biofilm thickness (x) for non-passivated and passivated SAW sensors by (8) and (9), respectively.

45

$$v = \sqrt{\frac{C_{ZnO}}{\rho_{ZnO} + \rho_{bac}}} = \sqrt{\frac{C_{ZnO}}{\rho_{ZnO}d}\left(\frac{1}{1 + \dfrac{\rho_{bac}x}{\rho_{ZnO}d}}\right)} \qquad (8)$$

$$v = \sqrt{\frac{C_{ZnO}}{\rho_{ZnO}d}\left(\frac{C_{film}}{C_{ZnO} + C_{film}}\right)\left(\frac{1}{1 + \dfrac{\rho_{film}h}{\rho_{ZnO}d} + \dfrac{\rho_{bac}x}{\rho_{ZnO}d}}\right)} \qquad (9)$$

where C_{film} is the shear modulus of the passivation film, h is the thickness of the film, and d is the thickness of the ZnO, as shown in figure 2.5. In the passivated SAW sensor calculation, the total shear modulus, including ZnO and passivation film, was calculated by the series mechanical spring model, since the mechanical displacement in the IDT is transferred from the ZnO film to the passivation film sequentially[97]. In equations (8) and (9), the key variable for the velocity is bacterial biofilm thickness (x), and the other parameters can be determined to investigate the sensitivity of the sensor. Some potential passivation materials, such as silicon nitride, aluminum oxide, and silicon dioxide, were selected based on the mechanical properties similarities to ZnO film and also water resistivity. The mechanical properties of the potential materials are summarized in table 2.1. Using these parameters and equation (9), the velocity function was defined

depending on the biofilm thickness. The normalized velocity in each material was plotted according to the biofilm film thickness change as shown in figure 2.6.

	Shear modulus (C_{film})	Poisson ratio	Density (ρ_{film})
ZnO	44.28 GPa	0.30	5.606 g/cm^3
Si$_3$N$_4$	80.60 GPa	0.24	3.290 g/cm^3
SiO$_2$	32.19 GPa	0.17	2.606 g/cm^3
Al$_2$O$_3$	124.0 GPa	0.21	3.950 g/cm^3
Teflon	0.005 GPa	0.46	2.199 g/cm^3

Table 2.1 Potential passivation film material properties[111, 112]
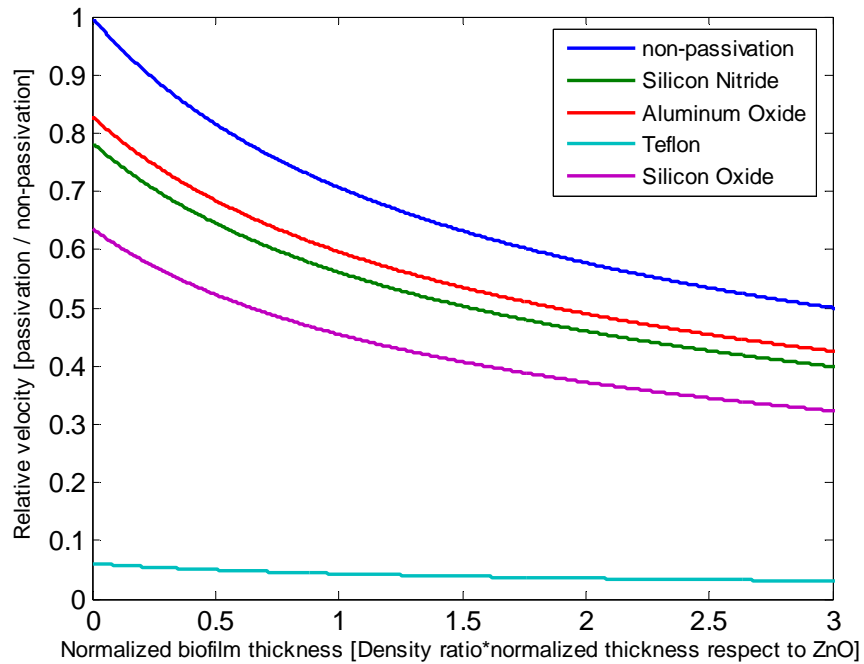
Figure 2.6: Relative SAW velocity from some candidate materials

Compared with a non-passivated SAW sensor, the velocity in the passivated SAW sensor was always more attenuated due to the passivation film mass loading and mismatch in mechanical properties as shown in figure 2.6.

The relative sensitivity of the passivated SAW sensor can be calculated by the fact that the sensitivity is proportional to the SAW velocity change during the biofilm growth which corresponds to the slope of the curve as shown in figure 2.6. The differentiated plot (relative sensitivity change) of figure 2.6 is shown in figure 2.7.
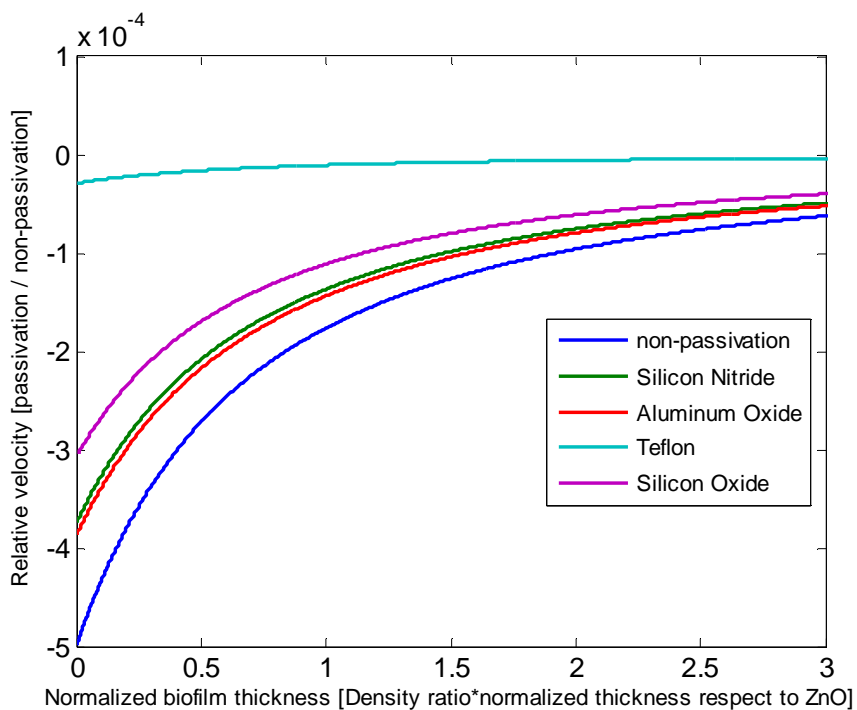
Figure 2.7: SAW sensor sensitivity from candidate materials

In figure 2.7, the normalized sensitivity for the potential passivation materials was the y axis intercept, since that is the point described in equation (6) where biofilm (x) approaches zero. The theoretical normalized sensitivity of SAW sensors passivated with different films (y axis intercepts in figure 2.7) are shown in figure 2.8.
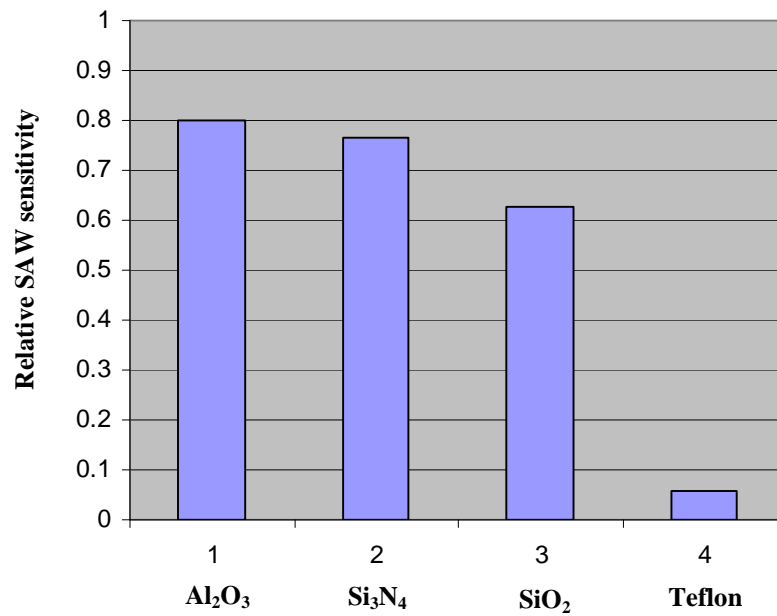
Figure 2.8: Normalized sensitivity from different passivation SAW sensors

Based on the numerical analysis, aluminum oxide passivated SAW sensor showed better sensitivity than other materials, and Teflon was the worst choice for this application, even though Teflon is one of the most common biocompatible materials for biomedical applications. Therefore, Al_2O_3 was chosen as a potential passivation film for the SAW sensor. The schematic of the passivated SAW sensor is shown in figure 2.9.
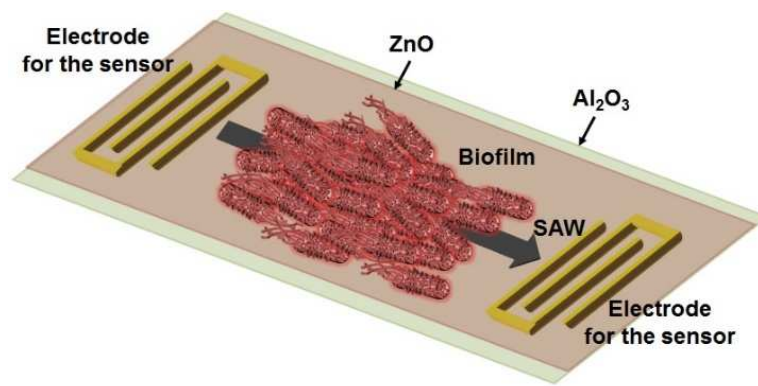
Figure 2.9: Schematic of the passivated SAW sensor

2.5 Design of the SAW Sensor

Based on the sensitivity studies of the passivated SAW sensor, the sensor was designed with considerations for future in-vivo biofilm monitoring applications. The resonant frequency of the SAW sensor was chosen based on the regulation for implantable medical devices set by the Federal Communication Commission. The SAW sensor was fabricated using biocompatible materials, such as gold, zinc oxide (ZnO), and silicon[113]. The SAW sensor is also a passive device. Thus, the required power for the

operation of the sensor can be delivered by RF inductive coupling[114, 115, 116] enabling a batteryless system which is significant to future applications.

The operational frequency of the SAW sensor is from 401 MHz to 406 MHz for Medical Device Radiocommunications Service (MedRadio). Based on the SAW velocity in our ZnO film (4812 m/s) and the fact that half of the SAW wavelength is equal to the separation of each electrode pair, the separation length of the IDT is designed to be 6 μm in order to achieve a 402 MHz operational frequency for the SAW sensor.

Material for the IDT is also crucial since the IDT can induce the energy insertion loss from the input electrical energy to the piezoelectric substrate. The energy insertion loss depends on the acoustic impedance and spacing distance of the IDT electrode width. Some potential materials for the IDT are compared based on the acoustic impedance matching theory and reflective coefficient equation[117], as shown in (10) and (11).

$$Z = \rho \cdot \upsilon = (density) \cdot (velocity) \qquad (10)$$

$$R = \frac{P_1}{P_0} = \left(\frac{Z_2 - Z_1}{Z_2 + Z_1} \right)^2 \qquad (11)$$
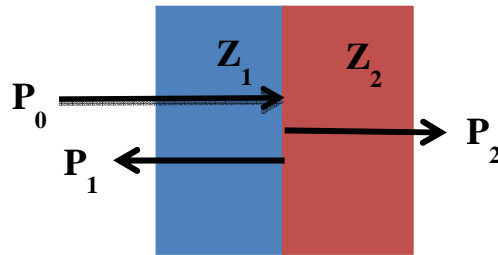
Figure 2.10: Schematic of the acoustic impedance match between two layers

where Z is the acoustic impedance, ρ is the density of the layer, v is the acoustic velocity of the material, R is the acoustic wave reflective coefficient, P_0 is the incident power, P_1 is the reflective power, P_2 is the transmission power, Z_1, and Z_2 are the acoustic impedance in each layer respectively. Aluminum and gold are selected as the IDT material and their properties were calculated based on equation (10) and (11). The results are shown in table 2.2. Lower value of reflective coefficient represents more energy supply to the piezoelectric substrate resulting in high sensitivity[105].

T R	Aluminum (Al)	Gold (Au)
a Acoustic Wave Reflective Coefficient	0.058	0.012

ble 2.2: Acoustic wave reflection coefficient calculation results

Based on the calculation results, gold (Au) was chosen as the material for the IDT. In addition to the acoustic impedance matching, the width of the electrode in the IDT also affects the energy insertion loss of the sensor[118]. Generally, the electric field in the piezoelectric material induced by the IDT is proportional to the gap distance between the electrodes indicating g in figure 2.11.
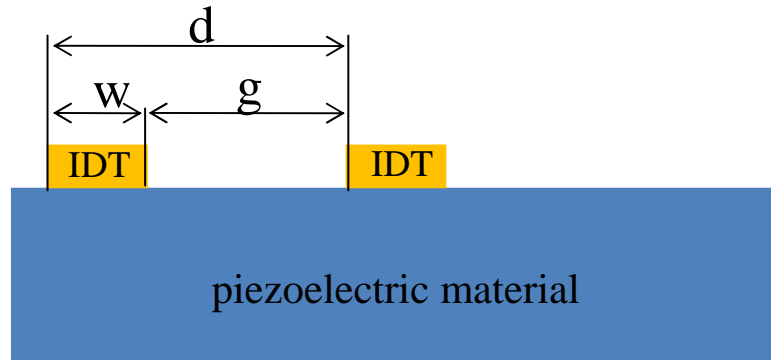
Figure 2.11: Cross sectional view of the IDT on the piezoelectric layer

where d is 6 μm in the design, w is the width of the electrode, and g is the gap between two electrodes. If the width of the electrode, w in figure 2.11, becomes narrower, more of the electric field affects the piezoelectric substrate, so the efficiency of the mechanical displacement is increased[105].

The PLD for ZnO deposition introduces a specific frequency pulsed laser to the Zn target, and the material is deposited on the chip in the oxygen chamber. Since limit area of the target is exposed by the pulsed laser, the PLD only allows a uniform film growth in a small chip level process, not for the wafer process[119]. Because of this limited uniformity of the PLD, prior to the ZnO deposition, a wafer process need to be completed. Considering minimum feature of electrodes (2 – 6 µm) for the IDT, the electrode fabrication designed before ZnO deposition to achieve the feature size of the IDT through the contact lithography that is compatible with a wafer process rather than diced chips. After electrode fabrication, the wafer was diced and followed by the PLD ZnO deposition. Hence, the final scheme of the SAW sensor is an inverted structure that the IDT is patterned under the piezoelectric film as shown in figure 2.12 (b) compared with the

traditional SAW structure in figure 2.12(a), where the IDT is patterned over the piezoelectric material.

Figure 2.12: Cross sectional views of (a) traditional SAW sensor and (b) inverted SAW sensor for PLD ZnO deposition

Even though the traditional SAW sensor can achieve higher sensitivity than the other design based an additional mass loading affects directly on the SAW propagation[120], there can be corrosion problems on the IDT, since the IDT exposed to the external environment directly. In the inverted SAW sensor design, the SAW, which is generated in the IDT, can disperse from the bottom to the top of the piezoelectric thin film area. As a result, the sensitivity of the sensor would be decreased based on the inverse relation between the sensitivity and SAW velocity dispersion ratio[121]. However, considering the total biomass of the biofilm is typically in hundreds nano-gram or a few micro-gram, this structure still can detect the mass based on the previously demonstrated detection limit (10^{-18}g). The sensitivity was characterized after the sensor was fabricated and shown appropriate detection limit (10^{-12}g) for biofilm applications. Another advantage of this revised structure includes the reduced possibility of IDT corrosion than the traditional SAW structure since the IDT is covered by ZnO film. Furthermore, this new structure is

compatible with the PLD for ZnO film deposition, which allows a high quality and specific lattice structure deposition.
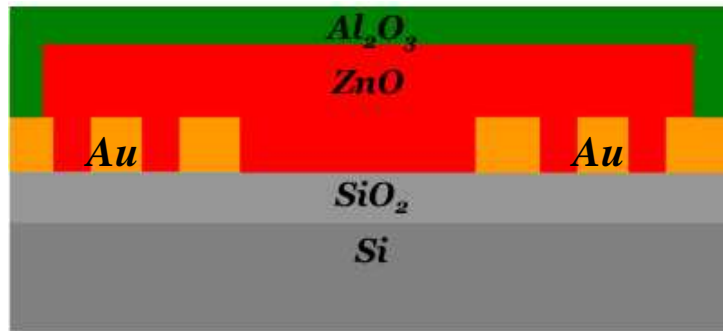
Figure 2.13: Schematic of cross sectional view of the inverted SAW sensor

The thickness and fabrication process of aluminum oxide were characterized by empirical studies. The major objectives of the experimental work were focused on characterizing the minimum required thickness of the film with an appropriate fabrication process to prevent significant sensitivity loss due to the thicker film deposition. The Al_2O_3 film was deposited in the thicknesses of 20 nm, 30 nm, 40 nm and 45 nm by atomic layer deposition (ALD) on the ZnO layer. The ALD was chosen based on highly dense thin film deposition capability.

The test chips were placed for two days in bacterial growth media, which is composed of diverse nutrient and electrolytes for bacterial growth. The optical microscopy images of the surface are shown in figure 2.14. All ZnO layers were damaged by the growth media except when passivated by 45 nm of Al_2O_3 film. Since a thicker

passivation film will cause more loss of sensitivity due to the higher initial mass loading and dispersion of the waves[122], an Al_2O_3 thickness of 45 nm is chosen for the passivation film.

The deposition of aluminum oxide film on a ZnO layer can be achieved by other fabrication techniques. Since the density and uniformity of a thin film highly depend on the deposition technique, the 45 nm Al_2O_3 film was also fabricated by electron beam evaporation, sputtering and ALD. The test devices were placed in the bacterial growth media for two days. The optical microscopy images are shown in figure 2.15. Interestingly, only Al_2O_3 deposited by ALD can protect the ZnO film from media due to the conformal and dense film fabrication capability of the technique.
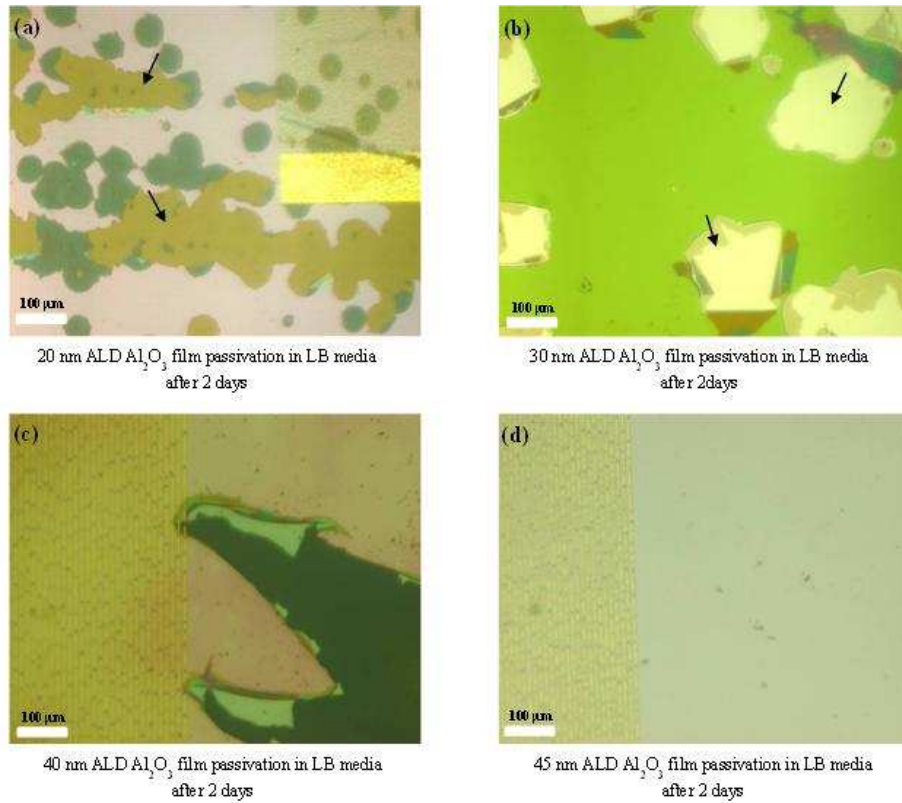
Figure 2.14: Optical microscopy images of the surface of four different (20nm, 30nm, 40nm and 45nm) thicknesses of Al_2O_3 film deposition on ZnO layer after two days in a bacterial growth media. The 45nm thickness of Al_2O_3 film successfully protected the ZnO layer from media diffusion.
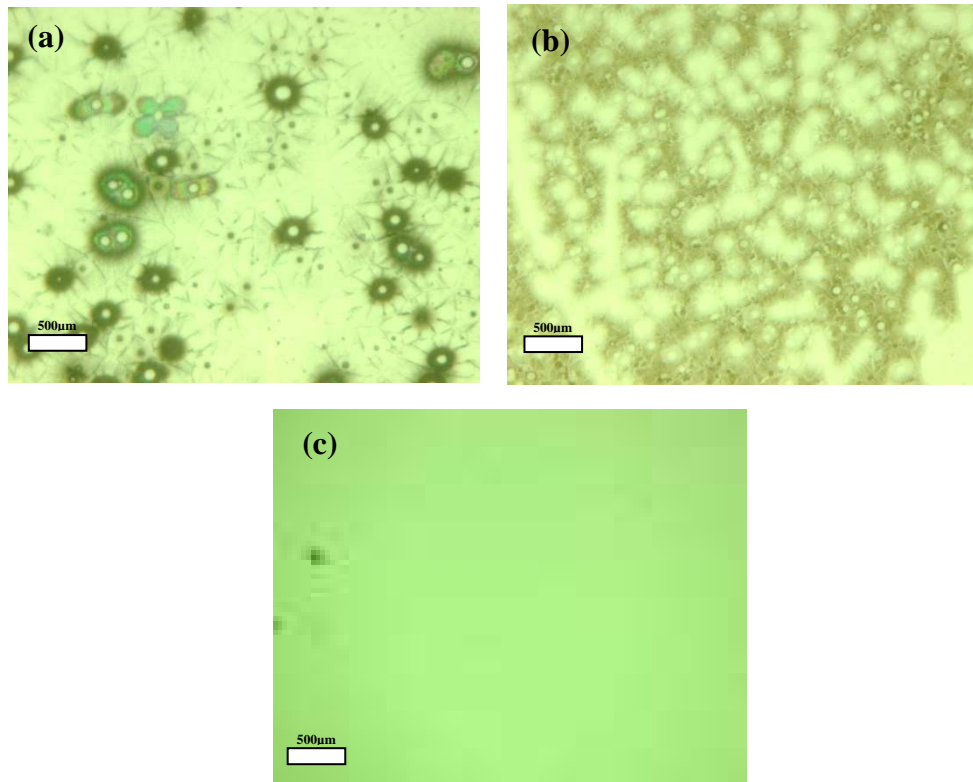
Figure 2.15: The optical surface images of the SAW sensor passivated by 45 nm Al_2O_3 film using (a) e-beam evaporation (black dot is ZnO), (b) RF sputtering (dark area is ZnO), and (c) ALD (no ZnO damage) in LB media with the bacterial solution after two days[28].

In addition to the passivation film characterization in a bacterial growth media, the 45 nm Al_2O_3 film passivated SAW sensors were tested in an animal serum (10% Fetal Bovine Serum). The FBS is composed of a number blood proteins and electrolytes simulating in-vivo conditions[123]. The device surfaces were inspected after two days incubation in the FBS by an optical microscope as shown in the images in figure 2.16.
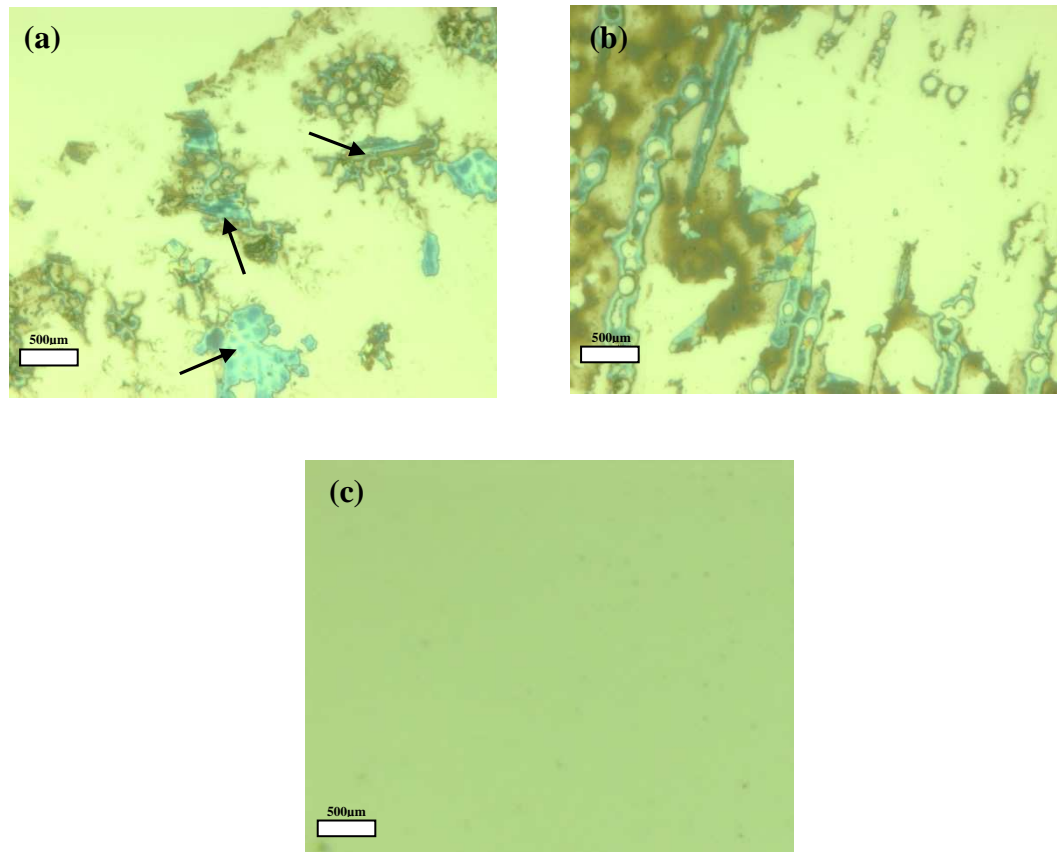
Figure 2.16: The optical surface images of the SAW sensor passivated by 45 nm Al_2O_3 film using (a) e-beam evaporation (arrows indicate ZnO residue), (b) RF sputtering (dark areas are is ZnO), and (c) ALD (no ZnO damage) in 10% FBS for two days[28].

As shown in the results, the ALD Al_2O_3 film only successfully protected the ZnO layer from the serum. Based on the thickness and fabrication process characterization studies, the 45 nm Al_2O_3 film deposited by ALD is used for the passivation film of the ZnO-based SAW sensor. Fabrication process specifications and design of the IDT of the SAW sensor are summarized in table 2.3 and table 2.4.

Material	Process	Characteristic
ZnO	Pulsed laser deposition, 500 – 600 nm	Piezoelectric film
Al_2O_3	Atomic layer deposition, 45 nm	Passivation layer for ZnO
Au	Evaporation, 200 nm	Electrodes for IDT
SiO_2	PECVD, 60 nm	Prevent SAW propagation to Silicon
Si	Substrate, 500 µm	Substrate

Table 2.3: Summary of the SAW sensor material specification

Design of the SAW	Description
Wavelength of the SAW	12 µm (λ) for 402 MHz resonant frequency
IDT electrodes	2 µm width and 4 µm distance (one pair takes 6 µm = $\lambda/2$)
Distance between two IDTs	$100\lambda = 1200$ µm
Thickness of ZnO	$\lambda/2 = 600$ nm

Table 2.4: Design description of the SAW sensor

2.6 Fabrication Process

2.6.1   Overall Process Flow

      The fabrication process of the SAW sensor has been developed in the previous work[27]. A 60 nm silicon dioxide (SiO_2) layer to prevent acoustic wave loss to silicon substrate was deposited on (100) Si substrates by low pressure chemical vapor deposition (LPCVD)[27]. The IDT was patterned using traditional photolithography before depositing the ZnO film. Cr/Au (15 nm / 200 nm) as the IDT material was deposited on the wafer by electron-beam evaporation, followed by lift-off (figure 2.17). The wafer was diced before ZnO deposition by pulsed laser deposition (PLD). Crystalline (001) orientation ZnO (c-axis oriented ZnO) films on SiO_2/(100)Si substrates were grown by PLD. The laser deposition system used a KrF excimer laser at a wavelength of 248 nm with pulse duration of 25 ns to ablate a high purity (99.99 %) ZnO ceramic target. The ZnO layer was grown at 300 $^{\circ}$C with an ambient oxygen partial pressure of ~1.0×10^{-4} Torr. After ZnO film deposition, the ZnO was patterned using a solution that consisted of phosphoric acid, acetic acid, and deionized water (1:1:30) with photoresist mask. The device was annealed at 800 °C for one hour to increase the resistivity of the ZnO[124]. Finally, the ZnO surface of the SAW sensor was coated by depositing an Al_2O_3 film using atomic layer deposition (ALD)[125]. The detailed process flow is presented in table 2.5.

Process Step	Process Description	Cross Sectional View
SiO$_2$ Deposition	LPCVD 60 nm at 150 °C	
Photolithography for IDT (AZ5214)	AZ 5214 image reversal pattern	
Cr/Au deposition	Cr/Au (15nm / 200 nm) E-beam evaporation deposition	
Lift off	Ultrasonication in acetone	
Dice wafer		
ZnO deposition (500 - 600 nm) by pulsed laser deposition	KrF excimer laser at a wavelength of 248 nm with pulse duration of 25 ns at 300 °C	
ZnO pattern	H$_3$PO$_4$ + Acetic acid + DI water for 40 seconds (1:1:30 dilution by volume)	
Annealing	800 °C for 1 hour (ramp up for 1 hour, cool down)	

Passivation film deposition (Al₂O₃ 45nm)	Al₂O₃ deposition at 150 °C using atomic layer deposition (ALD)	
Open electric pads	H₃PO₄ + Acetic acid + DI water (1:1:30 dilution by volume)	

Table 2.5: Overall fabrication process for the SAW sensor
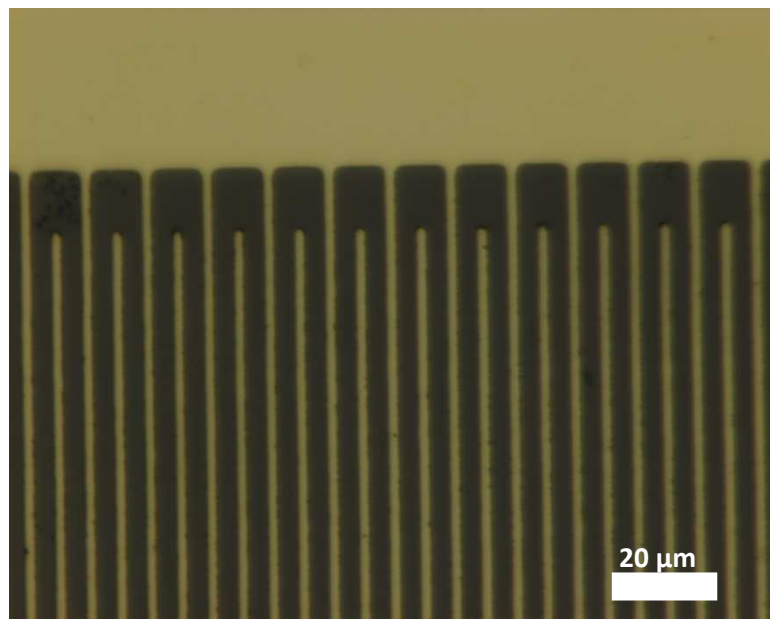
Figure 2.17: Microscopy image of the fabricated IDT electrode. The width of electrode is 2 μm with 4 μm distance.

2.6.2   Pulsed Laser Deposition

A single crystalline ZnO growth on the substrate is crucial to induce a shear horizontal mode of the acoustic wave (SH-SAW or Love wave) that is sufficient to use in a liquid environment without significant wave propagation loss. The induction of the wave is determined by the crystal orientation of the piezoelectric ZnO layer. A c-axis oriented (001) ZnO film is induced the Love wave. Since the wave propagates with a horizontal actuation of the amplitude, damping of the waves due to the water contact on the surface is significantly reduced. As a result, Love mode SAW was utilized to diverse biosensing applications in liquid environments[126].

The c-axis orientation of the ZnO can be grown by a RF sputtering, atomic layer deposition (ALD) and pulsed laser deposition (PLD). The sputtering provides advantages of wide uniform film deposition with high throughput, but the quality of ZnO is considered less than the other methods since concentration of impurities typically is higher than ALD and PLD[127]. The ALD is required expensive precursors as well as low throughput of the process. The PLD provides the highest quality of the ZnO with extremely low concentration of impurities. The process is relatively simple[138]. Furthermore, the orientation of the ZnO is well controlled due to the high stochastic correlation with the target material crystal structure[128]. Based on the high quality and single crystal ZnO film fabrication advantages, the PLD was chosen to deposit the piezoelectric ZnO film (600 nm) for this SAW sensor development. The schematic of the PLD setup is shown in figure 2.18.
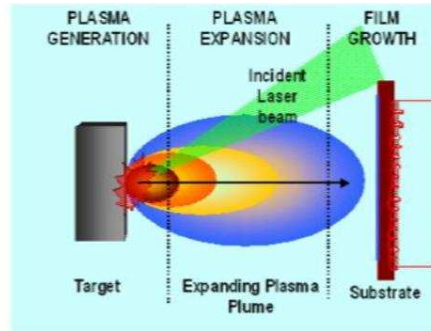
Figure 2.18: Schematic of the PLD.

An external optical source generates a pulsed laser signal (10 Hz, 248 nm of KrF excimer laser, 24 kV) that is aligned with the Zn target. The energy of the pulsed laser induces plasma condition on the target resulting in producing vapor phase Zn in the chamber. Oxygen reacts with the Zn vapor in the chamber and the film is grown on the substrate as the plasma is expanded toward the growth chuck. The critical parameters including the energy of laser, vacuum pressure, target quality, substrate temperature and alignment of the plasma plume to the substrate are crucial to have a consistent film growth rate. The thickness of the ZnO layer was aimed to be approximately 600 nm to maximize the sensitivity of the sensor based on the relation between the ZnO thickness and the wavelength of the SAW; 5% of the wavelength is the optimal thickness of the piezoelectric ZnO layer[52]. The grown ZnO layer was investigated purity via spectrum analysis (photoluminescence spectroscopy) and orientation via X-ray diffraction (XRD).

Photoluminescence spectroscopy (PL) is a process in which a substance absorbs photons (electromagnetic radiation) and then re-radiates photons. Quantum mechanically, this can be described as an excitation to a higher energy state and then a return to a lower energy state accompanied by the emission of a photon. Depending on the bandgap energy

of material, the emission wavelength is different. Based on the distribution of the observed wavelength peaks, the material composition can be investigated. After ZnO film deposition by the PLD, the surface of the film was inspected by PL (figure 2.19).
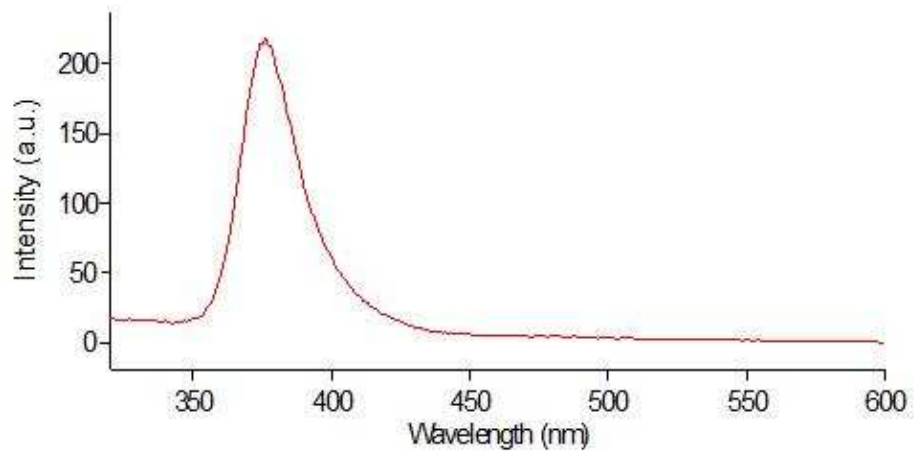
Figure 2.19: Photoluminescence spectrum of the ZnO layer, (380 nm wavelength is corresponding with the bandgap of the ZnO)

As shown in figure 3.4, the peak wavelength of the emission light was in 380 nm. The ZnO has 3.3 eV direct bandgap, and it corresponds to the 380 nm wavelength of the light based on the energy and wavelength relation. Therefore, this result represents the high quality of ZnO deposition since there was no other peaks in the PL spectrum[129].

In addition, the crystal orientation of ZnO was investigated by the XRD to determine what is the preferred lattice texturing of the deposited ZnO thin film. XRD is a method of determining the arrangement of atoms within a crystal, in which a beam of X-rays strikes a crystal and diffracts into many specific directions[130]. From the angles and intensities of

these diffracted beams, a crystallographer can produce a three-dimensional picture of the density of electrons within the crystal. From this electron density, the mean positions of the atoms in the crystal can be determined, as well as their chemical bonds, their disorder and other crystallographic, including preferred lattice orientation information. The XRD pattern of the ZnO thin film is shown in figure 2.20.
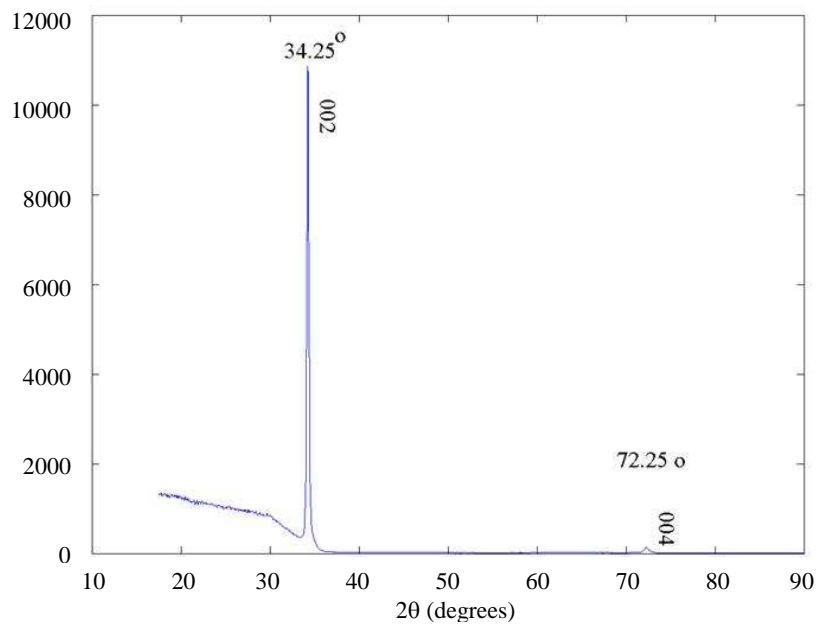
Figure 2.20: XRD pattern of the ZnO film deposited by PLD

To make sure that the Love mode SAW is generated, the ZnO film should be deposited in the c-axis direction (00L) so that the c-axis of its crystal lattice is perpendicular to the

substrate. As shown in figure 3.5, the diffraction angle of the X-rays at 34.25° and 72.25° (2θ) corresponding to the (002) and (004) lattice directions, were the most intensive reflections in the PLD-prepared ZnO film.

Based on these ZnO layer characterization results, it is concluded that low impurity c-axis oriented ZnO layer was successfully deposited by the PLD.

2.6.3   Atomic Layer Deposition

Atomic layer deposition (ALD) process contributed to the scaling down of electronic devices into the nano-meter regime due to its highly dense and conformal film coating capability. ALD can control the thickness of film from a single to thousand atomic layers of the material which is critical to fabricate precise and robust microelectronic systems at a low temperature (~ 150 ºC)[141]. This process has been widely used for diverse industry and research areas including CMOS, microfabricated devices and biochips[131]. The ALD was utilized in this thesis work for fabrication of a passivation layer for long term reliable operation of the SAW sensor. An ALD Al_2O_3 film was used for the sensor as a protecting layer of the ZnO from degradation due to long term exposure to biological fluids.

Aluminum oxide (Al_2O_3) is well known for its biocompatibility and stability[132]. Several methods of fabricating Al_2O_3 films are available, including RF sputtering, evaporation and ALD. RF sputtering and e-beam evaporation of Al_2O_3 targets as well as ALD Al_2O_3 were compared in terms of their ability to efficiently passivate the device in the liquid environment. The passivation performance of the Al_2O_3 films were investigated in bacterial growth media (Lysogeny Broth) and animal serum (10% Fetal Bovine Serum).

The Al$_2$O$_3$ film passivated devices were placed in the growth media for two days and the surface was inspected using optical microscopy.
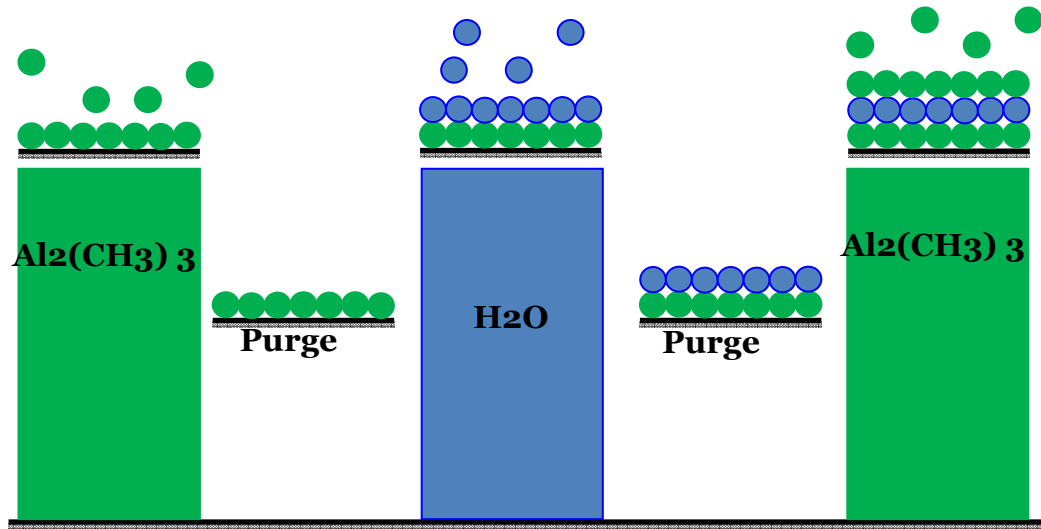
Figure 2.21: Schematic of the atomic layer deposition process of aluminum oxide. Trimethylaluminum (TMA) and water are used as liquid precursors at 150 ° C.

Figure 2.21 shows images of the passivated ZnO layer for each of the three deposition techniques. The thickness of the deposited Al$_2$O$_3$ film was 45 nm as optimized by parallel studies performed with films of varying thickness previously. It was observed that while sputtered and evaporated passivation layers gradually dissolved in both media, the films deposited using ALD can effectively passivate the device even after prolonged exposure. This is attributed to the conformity and thickness control of ALD, which result in the formation of highly dense nanometer thick films compared to physical vapor deposition techniques. These results demonstrate the suitability of ALD for the reliable passivation of biomedical ALD was an enabling technology for reliable biosensor developments.
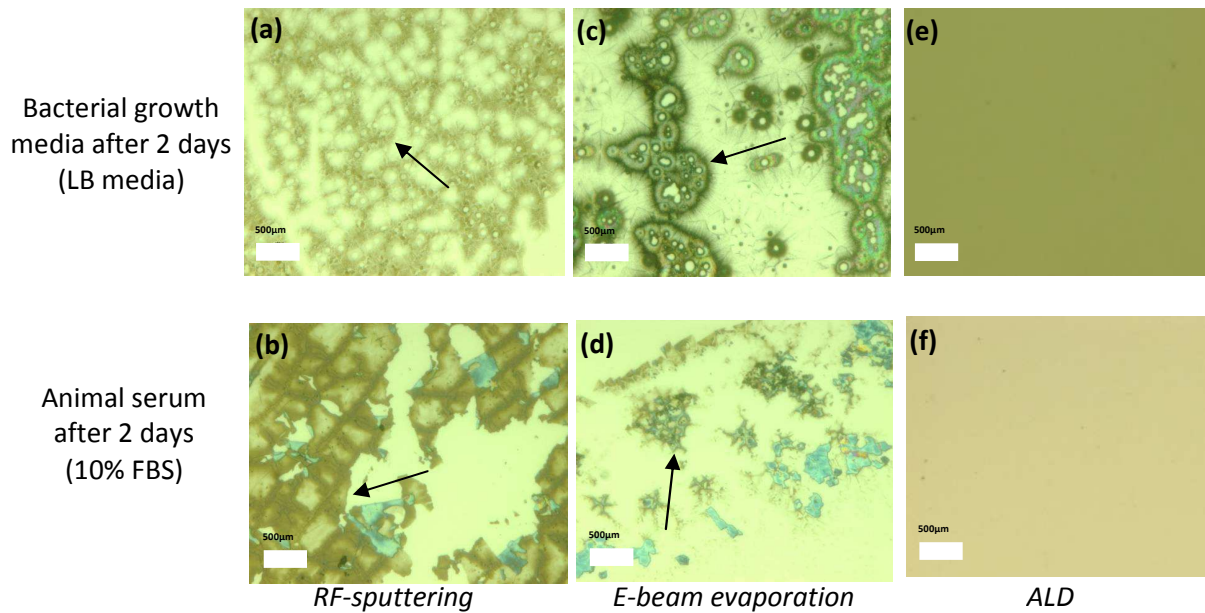
Figure 2.22: Optical microscopy images of the surface of the device in different 45 nm thickness Al_2O_3 film fabrication processes: (a) and (b) from RF-sputtering Al_2O_3 film (ZnO damage in both media), (c) and (d) E-beam evaporation Al_2O_3 film (ZnO damage in both media), (e) and (f) from ALD Al_2O_3 film (no ZnO damage), (arrows indicate ZnO damages)[28]

The Al_2O_3 ALD thin films were fabricated at 150 ℃ in a flow-through chamber system of the Beneq TFS-500. First, water vapor (H_2O) that was used as the oxygen source was absorbed on the substrate and formed a hydroxyl group. This was followed by the introduction of Trimethyl aluminum (TMA) liquid precursor into the ALD reactor. A covalent bond between the TMA and hydroxyl group is formed creating a single atomic layer deposition that decomposes into Al_2O_3. Each deposition cycle (500 ms) consisted of a pulse and purge of the precursors resulting in a consistent 0.09 nm/cycle of deposition rate.

2.7 Testing Setup and Experiments

The ALD aluminum oxide passivated SAW sensor was tested for biofilm growth monitoring. The resonant frequency of the SAW sensor was measured by a network analyzer (HP8510, Agilent Inc., USA). The network analyzer consists of the sweeper, the test set, the vector signal processor, and the display as shown the schematic in figure 2.23.
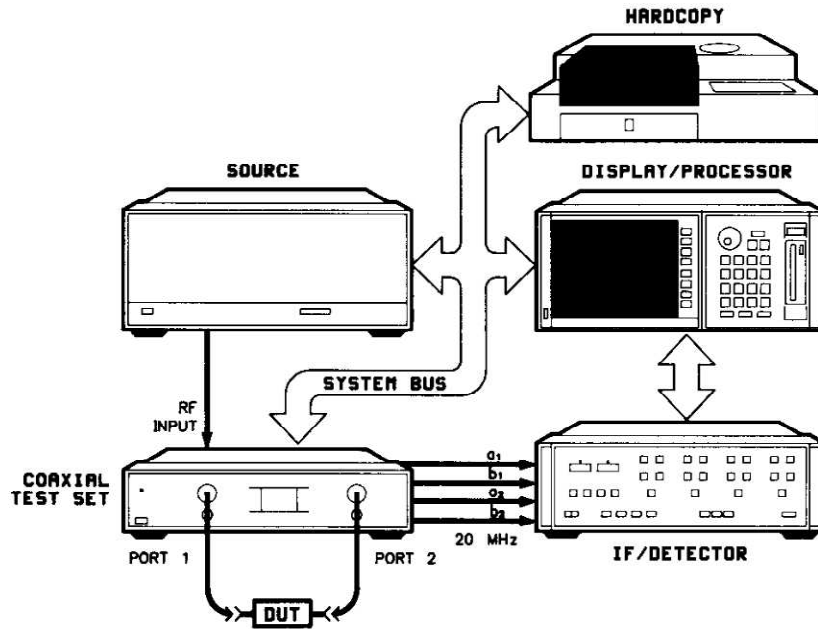
Figure 2.23: Schematic of the network analyzer [133]

The sweeper or synthesizer provides the RF stimulus to the test set from 10 MHz to 26.5 GHz. The test set supplies the RF signal for the device resonant frequency analysis. Together these comprise a complete stimulus / response test system which provides stimulus to the device under test and measures the signal transmitted through the device (S_{21}) or reflected from its input (S_{11}). The system then detects and processes the data to provide various displays showing the magnitude and phase of these responses. Accuracy

enhancement techniques permit measurement calibration at the interface to the device under test, minimizing the effect of systematic measurement errors. Many electrical properties of networks of components, such as inductors, capacitors, and resistors, may be expressed using S-parameters. For instance, the system gain, return loss, voltage standing wave ratio (VSWR), reflection coefficient, and amplifier stability can be measured by analyzing S-parameter values. The scattering refers to the way in which the traveling current and voltages in a transmission line are affected when they meet a discontinuity caused by the insertion of a network into the transmission line. This is equivalent to the wave meeting an impedance difference from the line's characteristic impedance. The schematic definition of the four S-parameters is shown in figure 2.24.

$$S_{11} = \frac{b_1}{a_1} \qquad S_{21} = \frac{b_2}{a_1} \qquad S_{12} = \frac{b_1}{a_2} \qquad S_{22} = \frac{b_2}{a_2}$$

Figure 2.24: Four S-parameters in the network analyzer, where a_1 is the forward reference which is provided by the synthesizer in wide frequency range RF stimulation, b_1 is the

reflected signal from the testing device, b_2 is the transmitted signal through the device, and a_2 is the reverse reference from the test set.

Based on these S-parameter definitions, a resonant frequency of testing system can be measured. The minimum value of S_{11} at a frequency means that the least RF energy reflection occurs at the frequency. Most RF energy transmits through the device because the impedance between the test device and energy source are matched demonstrating the resonant frequency of the tested system. In addition, the resonant frequency of the device can be monitored by the S_{21} maximum values. The S_{21} high peak at a frequency represents the transmission of the most RF energy at that frequency since the impedance is matched. Therefore, a resonant frequency of the test device can be measured by monitoring either the S_{11} low peak or the S_{21} high peak at the network analyzer.

The measured resonant frequency data was saved in the computer which communicates with the network analyzer by the GPIB. The GPIB communication and data saving program were designed using C++ language. Biofilm growth experiments typically span more than 48 hours, so the data sampling rate does not have to be fast, such as in 10 seconds rate per biofilm testing device. In addition, the only data needed to monitor the device's resonant frequency shift during bacterial growth are either the S_{11} low peak or S_{21} high peak reducing the amount of data saved as opposed to saving the entire waveform. Based on these considerations, the program was designed to save either the low peak of the S_{11} or high peak of S_{21} that it was possible to expand the experiment time without concern for the data capacity. In addition, the data sampling rate can be set by a user when the experiments are initiated. Typical data sampling rate for four parallel

experiments was 4 minutes for each device. The full C++ code is shown in the Appendix A.

The testing setup requires consideration of natural properties of biofilms including their growth variation, temperature and fresh media supply. A custom made device package for a stable electrical connection was developed and is shown in figure 2.25. The resonant frequency of the sensor during biofilm growth was monitored by a network analyzer (HP 8510B). *E. coli* K-12 W3110 was used as a bacterial model for the biofilm growth.
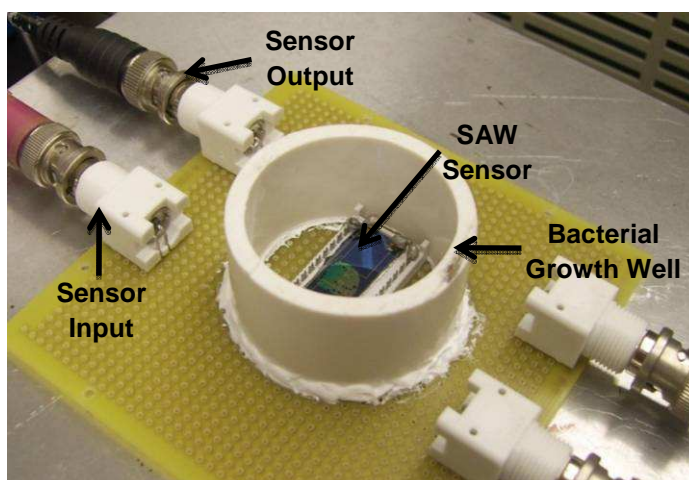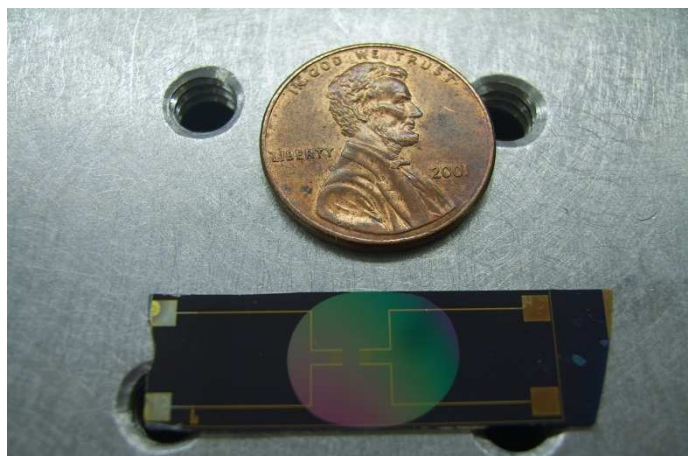
Figure 2.25: A custom made the SAW sensor package for bacterial biofilm growth experiments (The input and output of the sensor are connected with the network analyzer)[27].

In preparation of bacterial suspension, a 20 μl frozen culture of *Escherichia coli* K12 W3110 (wild type) was innoculated in a 5 mL of Luria Broth (LB) bacterial growth media in a cell culture tube. Then, the bacteria were cultured overnight in the 250 rpm shake incubator at 37 °C. The optical density (OD_{600}) was measured after the overnight culture growth by a spectrophotometer, and the OD_{600} was typically in 4.20 - 4.50 ranges.

An 1 mL of the overnight cultured bacteria was diluted 20 times by adding LB media to achieve the initial bacterial concentration to be $OD_{600} \approx 0.21 - 0.23$. The total volume of the bacterial growth well is approximately 20 mL. During the biofilm growth experiments, the well is placed on the hotplate set at 37 ℃ and sealed the surface by a paraffin film to prevent significant evaporation of the media.

2.8 Biofilm Detection of the SAW Sensor

An *E. coli* suspension ($OD_{600} \approx 0.25$) was placed in the bacterial growth well of the package with 10% FBS. The resonant frequency of the sensor was monitored for 48 hours. The negative frequency shift (decrease of the resonant frequency) of the sensor is correlated to the amount of biomass loaded on the sensor. A newly fabricated SAW sensor was used for three consecutively biofilm growth experiments. Between the experiments, the chip was cleaned by oxygen plasma for 30s at 150 W RF power. To confirm the sensitivity of the sensor, 10 µl of deionized (DI) water was loaded and the resonant frequency changes were measured by the network analyzer before each biofilm growth experiment. The negative frequency shift results of the SAW sensor in the consecutive biofilm growth experiments are shown in figure 2.26.
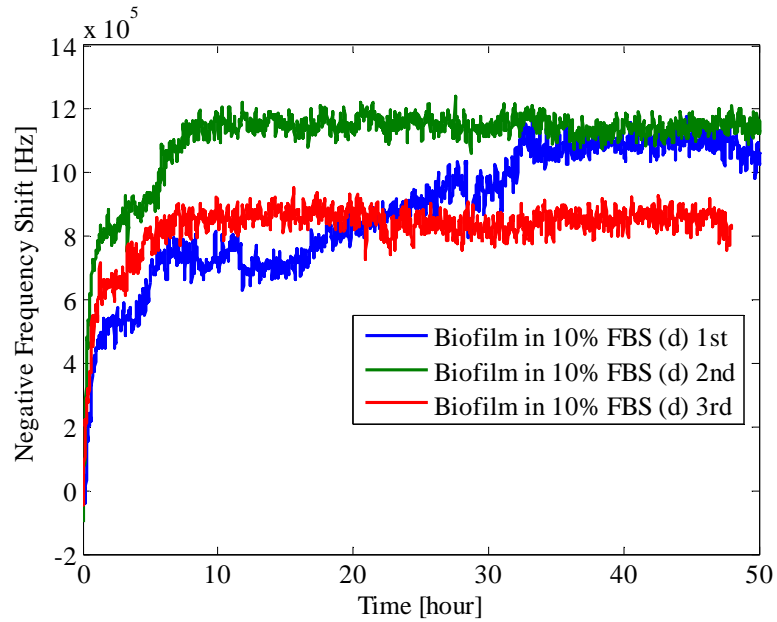
Figure 2.26: Resonant frequency shifts of the SAW sensor in three consecutive biofilm growth experiments. The growth media was 10% Fetal Bovine Serum to simulate an in-vivo condition for a future implantable environment. The results show repeatable responses of the sensor[27].

In figure 2.26, the SAW sensor showed repeatable biofilm monitoring results over three consecutive biofilm growth experiments. At the beginning of all three experiments, the response indicates exponential bacterial growth, corresponding to natural bacterial growth. After 24 hours, the stationary stage of biofilm growth was observed. Furthermore, the variation of the frequency changes in the stationary stage was only approximately 0.3 MHz, which indicates reliable operation of the SAW sensor in the animal serum. Growth of biofilms on the sensor was also confirmed by inspecting the surface of the sensor using an optical microscope. The images are shown in figure 2.27.

77
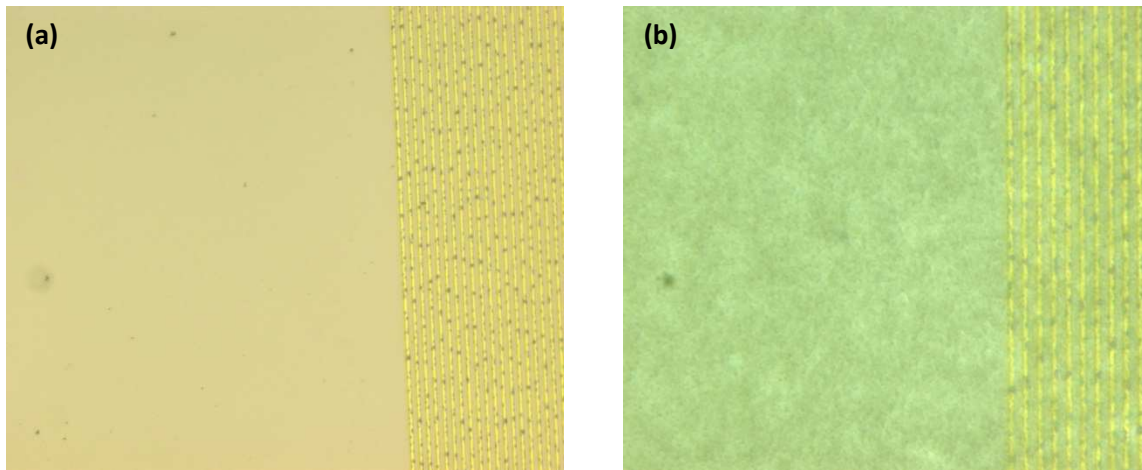
Figure 2.27: Optical microscopy images of the surface of the SAW sensor (a) before biofilm growth and (b) after biofilm growth[27].

The detection limits of the sensor using 10 µl of deionized (DI) water are summarized in table 2.5. The results show an excellent sensitivity recovery of the sensor. Based on the highly dense and conformal passivation of the ZnO layer using ALD, the performance of the sensor was not degraded in repeated uses.

	Before biofilm experiment	After 1st biofilm growth experiment	After 2nd biofilm growth experiment	After 3rd biofilm growth experiment
Frequency shift due to 10 µl DI water	185 KHz	157 KHz	141 KHz	143 KHz
Sensitivity	1.85×10^{10} Hz/g	1.57×10^{10} Hz/g	1.41×10^{10} Hz/g	1.43×10^{10} Hz/g
Detection limit	5.4 pg	6.4 pg	7.1 pg	7.0 pg

Table 2.6: Detection limit of the SAW sensor based on the frequency shift by 10 µl of DI water[27]

2.8 Summary

As shown in the results, the SAW sensor successfully demonstrated real-time biofilm growth detection. The sensor was fabricated using a c-axis oriented high quality ZnO deposited by PLD. To achieve reliable operation of the sensor in a biological solution, the ZnO layer was coated by 45 nm Al_2O_3 film fabricated by an atomic layer deposition. Based on the novel ALD Al_2O_3 film passivation, the SAW sensor can be used in multiple biofilm growth experiments without losing sensitivity. The detection limit of the SAW sensor studied by 10 µl DI water loading was approximately 5.3 pg. These results support further development of an integrated microsystem for biofilm monitoring and treatment applications.

Chapter 3: Biofilm Treatment

When bacteria are still in the pre-biofilm stage, antibiotic treatment can inhibit bacterial growth based on the minimum inhibitory concentration (MIC) of each antibiotic for the type of bacteria used[134]. However, once biofilms are formed, treatment requires 500 – 5000 times higher doses compared to the concentration needed to treat bacterial suspension. Therefore, developing an effective biofilm treatment is critical to avoid severe antibiotic side effects due to such high antibiotic concentration requirement. When an antibiotic and an electric field are introduced to biofilms simultaneously, the treatment efficacy of the antibiotic can be significantly improved in a phenomenon known as the bioelectric effect. In this chapter, a newly developed bioelectric effect using a superimposed electric signal is presented. The superimposed electric field method resulted in an improved biofilm inhibition.

3.1 Development of Bioelectric Effect Using a Macro-scale Setup

3.1.1 Superpositioned Electric Field

As discussed in the previous literature review, the bioelectric effect improves the biofilm treatment efficacy without depending on the strain of bacteria as well as types of antibiotics[29, 62, 63, 64, 66, 114]. The biocidal effects of electric fields have been investigated for several decades. The effects of biocidal and antimicrobial agents are enhanced when used under the influence of electric fields[135]. Costerton and colleagues demonstrated improved biofilm treatment through the application of either a direct or alternating current (DC or AC) electric field[111, 113]. Many hypotheses have been suggested to explain

the fundamental mechanisms underpinning the BE, including both an improvement of antibiotic binding efficiency to biofilms by an external electrostatic force[136] and increased membrane permeability due to local molecular vibrations induced by an AC field[137]. Oxidants generated by the imposed electrochemical conditions also affect the activities of antibiotics including byproducts of electrolysis of the medium[138]. However, previously demonstrated bioelectric effects were utilized using higher than 0.82 V resulting in electrolysis of the surrounding biological media[65]. Therefore, a new bioelectric effect with low intensity of electric field needs to be investigated particularly considering for in-vivo biofilm infection treatment.

Although studies have presented improved biofilm treatment through AC and DC field treatment independently, a combination of both AC and DC fields for the BE has not appeared. A superpositioned (SP) electrical signal that simultaneously imposes both an AC and DC electric force is applied for the matured biofilms. Based on the suggested biocidal mechanisms of AC and DC fields with antibiotics, the SP field is expected to induce an enhancement of the biofilm treatment efficacy. The AC field can induce permeability of extracellular matrix (ECM) in biofilms which have a lot of partial charges due to the molecular local vibration of the ECM[74, 79]. The molecular vibration results in increased porosity of the matrix that antibiotic can diffuse through the layer effectively. The DC field provides consistent a directional electrostatic force to the biofilm. This induces local electrolyte non-uniform distribution resulting in pH changes, oxygen depletion, and nutrient or drug gradient[112]. This imposed condition increases metabolic biocidal stress to bacteria in biofilms. Thus, when the AC and DC field are applied for biofilm concurrently, the biocidal effect of the antibiotics can be dramatically intensified.

The intensity of the SP electric field was characterized based on minimizing electrolysis of biological fluid. Since the electrolysis produces hazardous radicals, the lower voltage application for the SP field was significantly considered for the characterization. The required voltage was determined to be 0.5 V that is well below the threshold electrolysis voltage (0.82 V) for 4 mm distance of two electrodes creating an 1.25 V/cm of electric field. The intensity was applied for the amplitude of both AC and DC signals. Frequency of the AC component was chosen by 10 MHz based on the previous literature[139]. Thus, the SP field was characterized as 1.25 V/cm sinusoidal signal at 10 MHz (AC component) with 1.25 V/cm offset (DC component) as shown in figure 3.1.
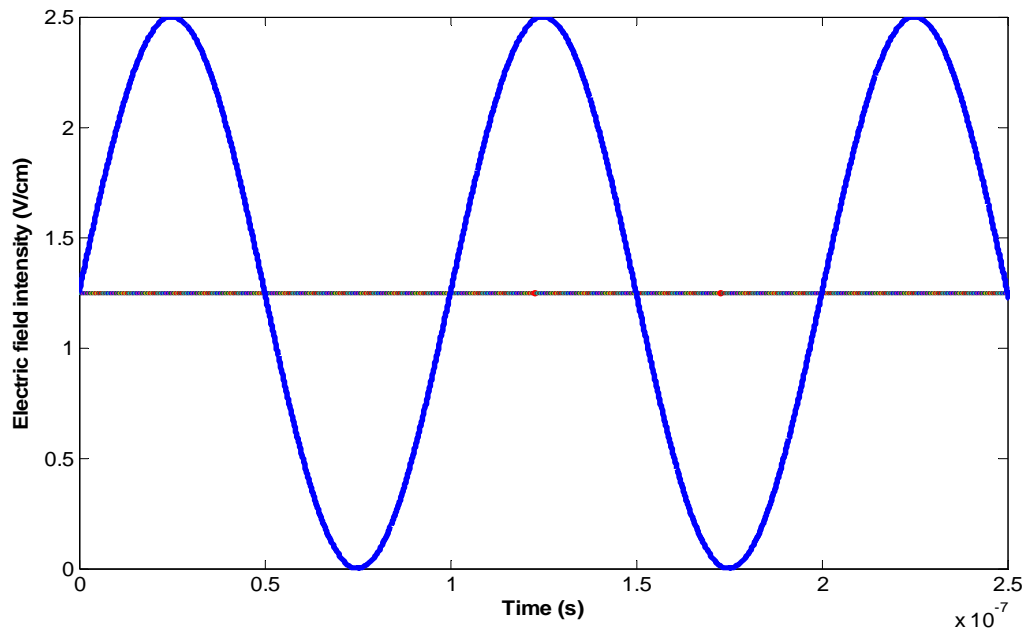
Figure 3.1: Signal form of the superimposed electric field for bioelectric effect[29]

3.1.2 Gentamicin (antibiotic)

The antibiotic selected for this work was gentamicin (Invitrogen Inc. USA). Gentamicin is one of the aminoglycoside antibiotics, which disrupt protein synthesis by ribosome in the cell, and is widely used for *E. coli* treatment. The chemical structure of gentamicin is shown in figure 3.2.
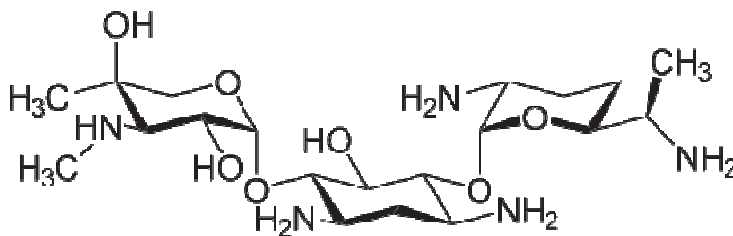
Figure 3.2: Chemical structure of the gentamicin[140]

Gentamicin has four amine groups and is known as a cationic (positively charged) antibiotic[141]. The minimum inhibitory concentration (MIC) of gentamicin for *E. coli* is approximately 2-5 µg/mL[142]. In the rest of the presented bioelectric effect studies, 10 µg/mL of gentamicin is applied to investigate the enhancement of the bioelectric effect treatment with a low antibiotic concentration.

3.1.3   Experimental Setup

To characterize the bioelectric effect with high throughput parallel experiments, a cuvette-based experimental setup was developed as shown in figure 3.3.

Cuvettes (Invitrogen Inc., USA) with parallel electrodes forming two of the walls were used to apply a uniform electric field to the media inside of the cuvette. The cuvette is a widely used for biological researches particularly to transform bacterial cells which requires applying a high intensity electric field for a short period to insert a DNA stand or a protein into bacterial cells[143]. The metal electrodes provide an electric field directly inside of the cuvettes since the electrodes are exposed both the inside and outside of the cuvette that are convenient for applying external electrical signals.
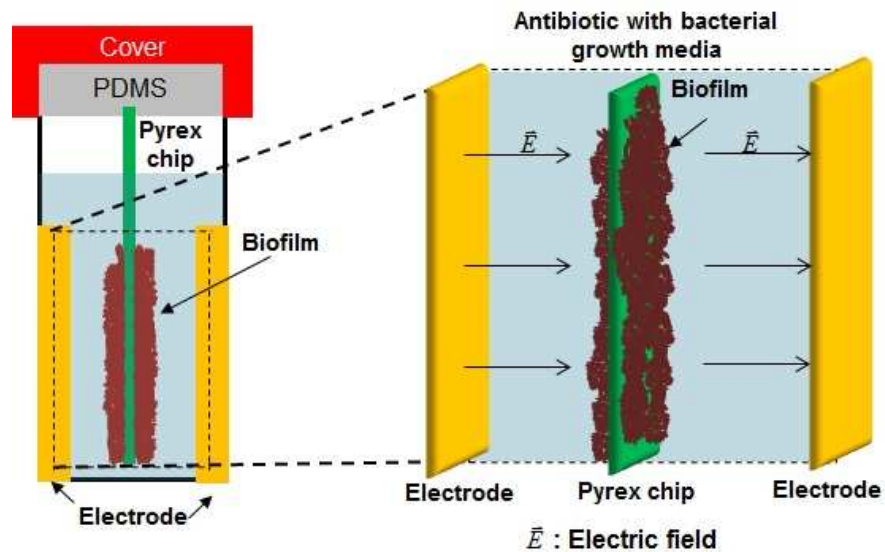
Figure 3.3: Schematic of the cuvette setup used for bioelectric effect experiments depicting suspension of the Pyrex[TM] chips for biofilm formation between the two electrodes (spacing 4 mm). *E. coli* W3110 biofilms were pre-formed on the Pyrex[TM] chip before treatments. PDMS is used to hold a Pyrex[TM] chip upright providing a constant surface area for biofilm growth. Antibiotic (10 µg/mL of gentamicin) and Luria Broth (LB) growth media were placed in the cuvette, across which an electric field was applied. The width of the Pyrex[TM] chip is smaller than the width of the cuvette, providing fluidic continuity between the two electrodes.

The setup for 6 parallel experiments was developed as shown in figure 3.4. A 500 µm thick Pyrex^{TM} wafer was diced into chips with dimensions 0.4 cm × 8.0 cm (width × length) and placed into cuvettes. A section of polydimethylsiloxane (PDMS) (prepared in a 10:1 ratio, base : curing agent) was placed into the cap of each cuvette, and was used to hold one Pyrex^{TM} chip upright between the two electrodes. Since the Pyrex is inert in biological solution and re-useable after biofilm cleaning via typically bleach, it was chosen to provide a constant area for biofilm growth. The Pyrex^{TM} chip was placed in the middle of the cuvette where the electric field is uniform. Biofilms were first grown on the Pyrex^{TM} chip in untreated bacterial growth media. The biofilm-coated Pyrex^{TM} chip was then transferred to a new cuvette with the same growth media but with an electric field of selected magnitude applied. The electrical signal was provided by a function generator (Agilent Inc., USA) with BNC cable connections to the electrical contact board (figure 3.4).
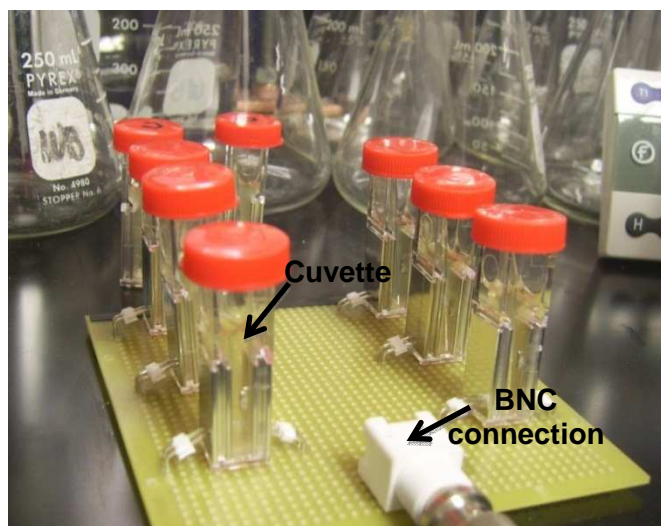
Figure 3.4: Photograph of 6 parallel experimental setup

3.1.4 Biofilm Experimental Procedures and Methods

The overall experimental procedures are described in figure 3.5. *E. coli* W3110 biofilms were formed on the Pyrex^{TM} chips for 24 hours in LB media at room temperature. The Pyrex^{TM} chips with matured biofilms were transferred to new sets of cuvettes containing 10 µg/mL of gentamicin in LB media. For bioelectric effect studies, electric fields were applied for 24 hours to the biofilm-containing cuvettes. Following treatments, both total biomass and viable cell densities of the remained biofilms on the chips were investigated.
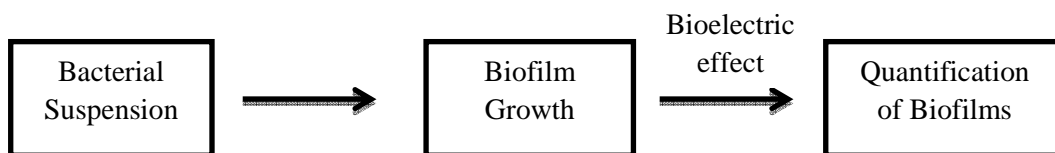
Figure 3.5: Overall experimental procedure for bioelectric effect studies

Quantification of remaining total biofilm on the chips was achieved by staining each chip for 15 minutes with 0.1 % crystal violet stain[144]. Each chip was gently immersed and rinsed sequentially in 4 prepared beakers of clean DI water to remove unbound crystal violet. After the chips were rinsed in DI water, the stained biofilms were resuspended in a 1 mL solution of 80% ethanol and 20 % acetone for 30 minutes. The optical density (OD$_{540}$) of the solution was measured by a spectrophotometer (Beckman Coulter Inc., USA). The final OD$_{540}$ of the crystal violet released from biofilms corresponds to the total biomass growth on the chip.

In addition to the measuring total biomass, the viability of cells within the treated biofilms is a parameter indicative of the health/integrity of the remaining structure. Densities of vaiable cells in biofilms after various treatment were investigated using the colony forming unit (CFU) assay. The Pyrex^{TM} chips after treatments were vortexed for 2-3 minutes in LB to remove and resuspend biofilms. Based on the OD_{600} of the solution, dilution ratios were selected for the assay. 20 µL of resuspended biofilm solution was plated on sterilized LB agar gel plates which were prepared with 25 g/L of LB and 15 g/L of agar. The plates were placed in an incubator overnight at 37 °C. The density of live bacteria (CFU/mL) on each plate was calculated based on the number of CFU, dilution ratio, and original volume (20 µL) of the biofilm solution. Each experiment was repeated 4 times (N = 4) and the results were averaged. The error in the results represents the standard deviation from the averaged live bacterial density. Three bioelectric effects are investigated. The AC bioelectric effect (AC-BE) is studied when 1.25 V/cm sinusoidal signal at 10 MHz is combined with 10 µg/mL of gentamicin. The DC bioelectric effect (DC-BE) is investigated by applying a 1.25 V/cm DC electric field with 10 µg/mL of gentamicin. The superpositioned bioelectric effect (SP-BE) is the combination of the superimposed electric field, consisting of the DC and AC signals, with 10 µg/mL of gentamicin.

3.1.5 Theoretical Representation of the Bioelectric Effect

To investigate components of the SP-BE, I have developed a model of the independent effects of antibiotics and electric fields ($T_{antibiotic}$ and $T_{electric\,field}$). The model was formulated based on an assumption that the total treatment efficacy (T_{total}) expressed log reduction of viable cell number, can be linearly decomposed into an antibiotic ($T_{antibiotic}$) component, an electric field ($T_{electric\,field}$) component, and a 'synergistic' effect (T^*) based on the combination of the electric field and the antibiotic. The enhanced bioelectric effect (BE) is hypothesized to result from combining many previously observed bacteriocidal mechanisms associated with electric fields and antibiotics. Thus, a linear model of the BE can be an effective approach to quantify and analyze the treatment efficacy of different BEs. All variables of the equation in the model are defined here as the logarithmic reduction of viable biofilm bacterial density after treatments with respect to that of untreated biofilms, resulting in positive dimensionless T values as shown in Eq.12.

$$T = \log_{10}\left(\frac{viable\ cell\ density\ of\ untreated\ biofilm}{viable\ cell\ density\ of\ treated\ biofilm}\right) \quad (12)$$

Therefore, the total BE (T_{total}) represents the sum of both the antibacterial agent ($T_{antibiotic}$) and electric field ($T_{electric\,field}$) effects alone, combined with the synergistic effect (T^*) of the electric field with the antibacterial agent (Eq. 13).

$$T_{total} = T_{antibiotic} + T_{electricfield} + T^* \tag{13}$$

Since the synergistic effect (T^*) represents the enhanced treatment efficacy due to the combination of the antibiotic with the electric field, additional insight can be provided by investigating how different types of electric fields (i.e. DC, AC, and SP) produce different synergistic effects (i.e. T^*_{DC}, T^*_{AC}, and T^*_{SP}). The treatment efficacies of antibiotics ($T_{antibiotic}$), applied electric field ($T_{electric\,field}$) and the total BE (T_{total}) were experimentally obtained using the CFU assay by quantifying the reduction of viable biofilm bacteria with respect to control experiments. Thus, three parameters in Eq. 13, T_{total}, $T_{antibiotic}$, and $T_{electric\,field}$, were experimentally obtained and the synergistic effect (T^*) was then calculated.

This proposed equation can be further used as a first order theoretical model for independently investigating each parameter of the BE ($T_{antibiotic}$, $T_{electric\,field}$ and T^*). These parameters may individually be functions of different variables. For instance, because the BE depends on the electrical energy provided by the externally applied field, higher electric fields supply more electrical energy resulting in stronger antibacterial effects. Thus, each component of the model can be studied as an independent function represented by different variables, such as the duration of treatment with antibiotics or electric fields, the concentration of antibiotics, different types of antibiotics, the intensity of the electric fields and various combinations of AC and DC currents. The work presented here, based on the suggested model, can provide a mathematical framework for optimizing the bioelectric effect, as well as for understanding the relationships between the various treatments and hypothesized mechanisms (e.g., temperature, pH, oxygen, etc).

Hence, although the intensity and frequency of the SP electric fields were chosen based on avoiding media elecrtrolysis, the mathematical methodology may be useful to fully expand the range of various physical and biochemical inputs for analyzing their bacteriocidal effects. That is, one may investigate the mechanistic basis for the synergistic effect quantification by examining different genetic backgrounds and other physiological measures that can be manipulated via biological means.

3.1.6 Experimental Results and Discussion

The SP electric field imposes both a constant electrostatic force by the DC component and alternating electrical force due to the AC component. The SP field also provides more electrical energy than only that of either the AC or DC field without causing significant medium electrolysis. Supplying higher electrical energy for the BE corresponds to increasing the treatment efficacy. Therefore, the superpositioned bioelectric effect (SP-BE) was expected to result in an intensified treatment based on the presence of both high electrical energy and the individual mechanisms underpinning the effects of AC and DC fields.

When a DC electric field is applied to a bacterial growth medium, however, there is a limit to the intensity of the applied potential (~ below 0.82 V) so as not to generate toxic byproducts through electrolysis of the media. To determine this limit, biomass quantification using crystal violet staining of biofilms was performed after application of different DC electric field intensities without gentamicin. The two electric field intensities investigated were 2 V/cm and 1.25 V/cm of DC electric field (corresponding 0.5 V and 0.8 V respectively). 1 mL of *E. coli* suspension (OD_{600} = 0.20 – 0.25) was placed in each of the cuvettes. Two different intensities of electric signal were applied to the suspension separately for 24 hours. After DC electric fields were applied for 24 hours, the total biomass were quantified by the crystal violet staining method. Hence, this study can provide efficacies of biofilm growth prevention without antibiotics even pre-biofilm status (i.e. bacterial suspension).
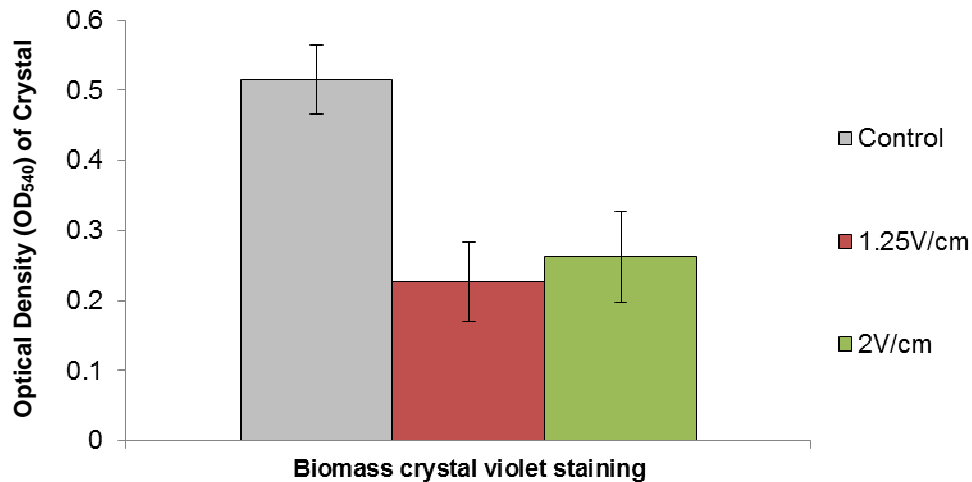
Figure 3.6: Biomass quantification using crystal violet staining. The OD_{540} of the dye is proportional to the biomass.

However, there was not an observed statistical difference in biomass growth between the two different electric field intensities (2 V/cm and 1.25 V/cm) as shown in the measured crystal violet OD_{540} (figure 3.6). Since the 2 V/cm intensity DC electric field (0.8 V over a 4 mm distance between two electrodes) induced electrolysis, 1.25 V/cm as the intensity of the DC electric field was selected to be used in later studies. The amplitude of the AC component of the SP electric field used in this work was the same as the intensity of the DC field. The frequency of the AC electric field was chosen based on the previous work[67]. Even though the intensity and frequency of the electric field were selected based on experimental results and literature, these parameters can be studied further to optimize the bioelectric effect with different combinations of the DC and AC electric fields.

With the selected intensities of the electric field, total biomass reduction in different bioelectric effect treatment of matured biofilms was investigated using the crystal violet

method. The total biomass of *E. coli* biofilms was investigated following no treatment (no antibiotic or electric fields), antibiotic treatment (10 μg/mL of gentamicin), or application of the electric fields with the antibiotic. After 24 hours of *E. coli* biofilm growth, the biofilms were treated by four different methods for an additional 24 hours: 1) antibiotic treatment, 2) AC field with the antibiotic (AC-BE), 3) DC field with the antibiotic (DC-BE) and 4) SP field with the antibiotic (SP-BE). In figure.3.7, the biofilm density (OD_{540} after crystal violet staining) is depicted after various treatments. Gentamicin treatment had minimal effect relative to the untreated controls. Each applied electric field (DC and AC) resulted in 50% loss of biofilm due to the AC-BE and 46% reduction by the DC-BE. Interestingly, the SP field resulted in yet another 50% reduction compared to either AC-BE or DC-BE and ~73% overall ($P < 0.05$) relative to the untreated control. This result demonstrates significant biomass reduction by the SP field treatment.
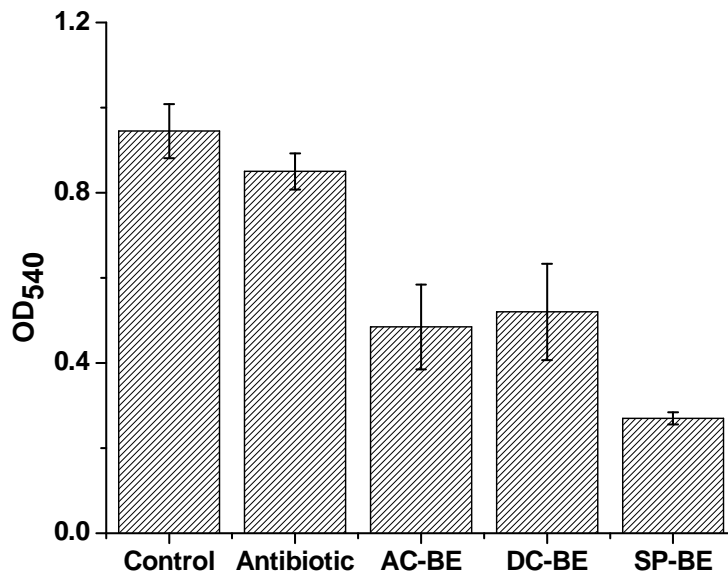
Figure 3.7: Total biomass quantification results using crystal violet staining after bioelectric effect (BE) treatment. In the superpositioned (SP) BE, the minimum total biomass was measured compared to other treatments. The OD_{540} at SP-BE shows a ~71% decrease with respect to that of control experiments (Analysis of Variance (ANOVA), P < 0.05). The data is presented as the average OD_{540} with standard deviation over 6 repeated experiments (N = 6 in each experiment).

In addition to the overall biomass reduction due to the SP-BE, the viability of cells within the treated biofilms is a critical parameter indicative of the health/integrity of the remaining structure. The total treatment efficacy of each bioelectric effect is evaluated by the log reduction of live bacterial density based on the CFU density after biofilm treatment. The total treatment efficacy (T_{total}) was evaluated with separate experiments by applying either only gentamicin $(T_{antibiotics})$ or only an electric field $(T_{electric\ field})$ as described the method in the previous section of this chapter (3.1.4).

As shown in table 3.1 and figure 3.8, the decrease in the number of viable cells within biofilms following application of the SP field in conjunction with gentamicin (T_{total} = 2.6 log reduction of viable bacteria) was 13 and 4.3 times greater than the reduction from the AC and DC fields with the same antibiotic (T_{total} = 0.2 and 0.6 reduction of logarithmic viable bacterial density, respectively). The synergistic treatment by the SP electric field (T^{*}_{SP} = 2.53) was shown to exhibit higher values than that of the AC (T^{*}_{AC} = 0.133) or DC (T^{*}_{DC} = 0.440) field treatments (19 and 5.6 times more reduction of viable cell density, respectively) as shown in Table 1C. By analyzing the effects of AC and DC fields, we found a synergy in reductions to biofilm viability beyond the sum of the effects of each field separately. The synergistic reduction of viable cells created by the SP field (T^{*}_{SP} = 2.53) was 4.4 times more than the sum of the effects of the AC and DC fields (T^{*}_{DC} + T^{*}_{AC} = 0.573). Therefore, the combination of the DC and AC components in the superimposed electric field with gentamicin was not simply sum of two mechanisms, but is a rather complex function which induced a stronger synergistic effect that was absent when only DC or AC electric fields were applied.

Samples	Viable biofilm cells (CFU/mL) (average ± stdev)	Log of viable biofilm cells (average ± stdev)	Log reduction of viable biofilm cells (respect to control)
Control	2.14×10^8	8.330	NA
Gentamicin	$(1.95 \pm 0.01) \times 10^8$	8.290 ± 0.004	0.040 ± 0.004
AC field	$(2.01 \pm 0.02) \times 10^8$	8.303 ± 0.008	0.027 ± 0.008
DC field	$(1.62 \pm 0.04) \times 10^8$	8.210 ± 0.021	0.120 ± 0.021
SP field	$(1.99 \pm 0.01) \times 10^8$	8.299 ± 0.004	0.031 ± 0.004
AC-BE	$(1.39 \pm 0.09) \times 10^8$	8.143 ± 0.056	0.20 ± 0.06
DC-BE	$(5.69 \pm 0.40) \times 10^7$	7.755 ± 0.061	0.60 ± 0.06
SP-BE	$(5.63 \pm 0.40) \times 10^5$	5.750 ± 0.062	2.60 ± 0.06

Table 3.1 (a): Averaged viable cell densities and logarithmic values in untreated (control) and treated biofilms (N = 4 in each treatment). The BE treatments applied were either the AC, DC, or SP fields with the gentamicin.

	No electric field	AC electric field	DC electric field	SP electric field
No gentamicin	N/A	0.027 ± 0.008	0.120 ± 0.021	0.031 ± 0.004
Gentamicin (10 µg/mL)	0.040 ± 0.004	0.20 ± 0.06	0.60 ± 0.06	2.60 ± 0.06

Table 3.1 (b): Resulting bioelectric effect parameters (T values) following different treatments using results in table 1A (log reduction of viable bacterial density with respect to no treated biofilms).

	AC electric field (T^{*}_{AC})	DC electric field (T^{*}_{DC})	SP electric field (T^{*}_{SP})
Synergistic effect	0.133	0.440	2.53

Table 3.1 (c): Synergistic effects in different BEs based on Eq. 2 and table 1(B) (log reduction of viable cells in biofilms).
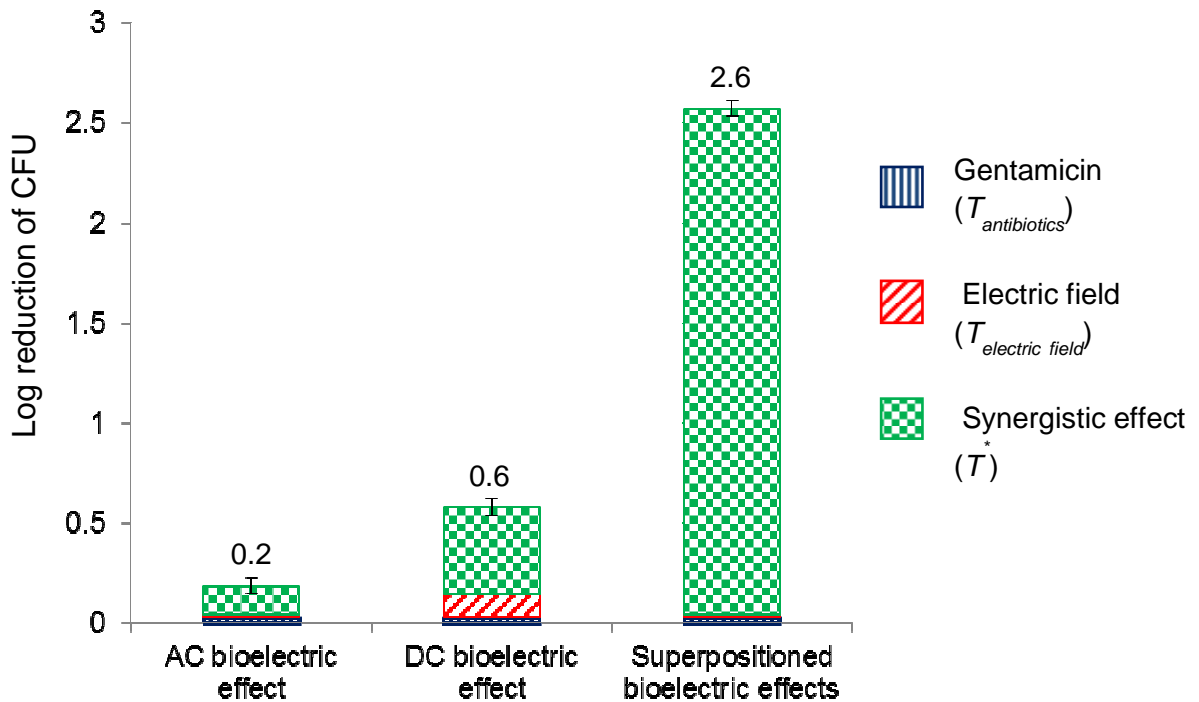
Figure 3.8: The total treatment efficacies of AC, DC and Superpositioned bioelectric effect. The treatment effects of gentamicin and electric field are evaluated in separate experiments. The synergistic effect is determined based on equation 13.

The significantly greater reduction in total biomass and viable biofilm bacteria seen with the SP electric field (figure 3.7 and 3.8) can be attributed in part to the combined effect created by the increased electrophoretic and diffusion efficiency of the antibiotics due to the DC electric field along with the extracellular matrix polarization of biofilms generated by the AC electric field. That is, by inducing a high antibiotic concentration close to the biofilm surface and a strong gradient between the bulk fluid and the biofilm, electrophoresis and diffusion of the antibiotics through the biofilm are enhanced. Since gentamicin is cationic due to its four amine groups present in the molecular structure of the antibiotic, its local concentration is expected to vary under the influence of electric fields. We hypothesize that this may lead to spatially varied antibiotic efficacy.

To test this hypothesis we created a macroscale electrode system for analysis of antibiotic distribution (figure 3.9).
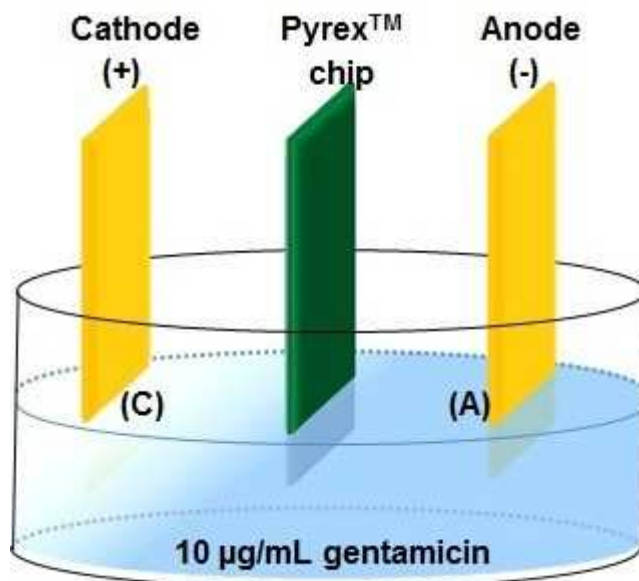
Figure 3.9: Schematic of set up of gentamicin gradient studies. 100 µl of the solution is sampled with by a pipette and quantified by the Coomassie blue.

Coomassie blue dye shifts the absorbance peak of the gentamicin solution towards 595 nm as the dye is reduced by the amine groups of gentamicin. Gentamicin was diluted with DI water to concentrations of 1, 10, 50, 100, and 1000 µg/ml for characterization of the reaction between Coomassie blue dye and gentamicin. 1 ml of Coomassie blue diluted ten times in DI water was added to 100 µl of gentamicin prepared in one of the three concentrations listed above. Following 5 minutes of incubation at room temperature, the OD_{595} of the solution was measured. The OD of the solution produced a linear relation from 1 to 50 µg/ml with the gentamicin concentration as shown in figure 3.10. The linearity of the OD changes with different concentrations of gentamicin confirms that Coomassie blue can be used for quantification of the gentamicin concentration. Additionally, compared to other antibiotic titrate methods, such as fluorescence[145] or radioactive molecule labeling[146] on antibiotics, this assay has advantages including a label-free system and direct correlation to the concentration of the agents. This newly developed assay can be used for the quantification of antibiotic concentrations especially in microbiology and pharmacology studies.
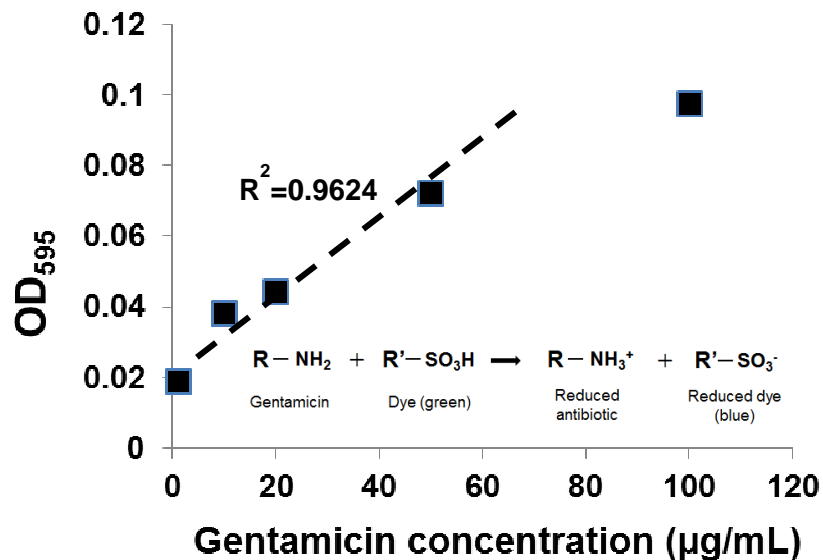
Figure 3.10: The influence of the gentamicin concentration on the OD_{595nm} of the gentamicin solution quantified by Coomassie blue dye. Results demonstrate linearly in the range of concentrations.

Figure 3.11: Gentamicin was quantified by Coomassie blue dye. Normalized optical densities (OD_{595}) in the parallel electrode chamber were measured under the effect of either an AC, DC, or superpositioned (SP) electric field. OD_{595} values are normalized with respect to the measured value at the cathode over 8 experiments (N = 8). Statistical analysis was performed with respect to the normalized OD_{595} at the cathode (ANOVA, P = 0.014).

Using this assay, the gentamicin distribution was measured under applied AC, DC, and SP electric fields for two hours. We evaluated gentamicin concentration at the indicated sample points (figure 3.11; C: cathode and A: anode). The OD_{595} at each location was normalized with respect to the OD_{595} at the cathode (C) as shown in figure 3.11 since gentamicin is cationic (*21*). The SP electric field created statistically higher gentamicin concentrations at surfaces of the electrode (anode: A) compared to the concentrations produced by the DC or AC electric fields alone; the average normalized concentration of gentamicin induced by the SP field was approximately 2.0 times that of the other fields at the anode ($P < 0.05$).

The local concentration of a charged molecule is affected by the energy density of the external electric field. The electrical energy densities of DC, AC, and superimposed electric fields are calculated by equation 13 [147],

$$W_{superpositioned} = W_{DC} + W_{AC} = \frac{1}{2T}\varepsilon \int_0^T (E_{DC}^2 + E_{AC}^2)dt \qquad (14)$$

where $W_{superpositioned}$ is the electrical energy density [J/cm^3] of the superpositioned electric field, ε is the dielectric constant of the bacterial growth media [C/(V·cm)], W_{DC} is the electrical energy density of the DC electric field, W_{AC} is the electrical energy density of the AC electric field, T is the period of the electric field [s], and E is the intensity of electric field [V/cm]. Based on equation 4, the energy densities of the AC, DC, and superpositioned electric fields were 0.39ε, 0.78ε, and 1.17ε respectively. The superpositioned electric field provides an energy density that is 3 and 1.5 times higher than densities of the AC and DC electric fields respectively. The ODs in different electric fields are shown in figure 3.11. The SP electric field demonstrated a higher overall gentamicin concentration gradient than that imposed by a DC or AC electric field alone.

Although the normalized concentration gradient of gentamicin due to the SP electric field is not on the same order of magnitude as the synergistic effect, this high concentration gradient of the gentamicin enhances diffusion and the electrophoretic force on gentamicin into the biofilm, likely contributing to the strong synergistic effect. These results suggest that the generated concentration gradient may be one of the mechanisms contributing to the stronger synergistic effect in the superpositioned electric field with gentamicin (figure 3.12)

Figure 3.12: Schematic of the proposed mechanism for the SP-BE biofilm treatment. (A) In the SP electric field application with the antibiotic, the measured steady state antibiotic concentration gradient (Fig. 4C) results in increased local antibiotic concentration close to the biofilm. (B) Since the SP electric field includes both DC and AC components, the antibiotic permeability of biofilm is enhanced as the AC field induces local vibration of charged molecules. This results in increased antibiotic diffusion and electrophoresis through the biofilm (red arrows indicate them). We propose the combination of the elevated antibiotic concentration proximate surface of biofilm with the high antibiotic permeability of biofilm results in the strong synergistic biofilm treatment efficacy (T^*_{SP}) observed by the SP-BE[148].

3.1.7 Summary

Significantly improved treatment of biofilms was demonstrated by employing a superpositioned (SP) electric field in conjunction with an antibiotic. The SP bioelectric effect (SP-BE) was greater than the sum of the bioelectric effects of the DC and AC fields independently. Thus, the SP field enables a synergistic effect that yields more bacteriocidal activity when both DC and AC fields are applied. The enhanced treatment efficacy of the SP-BE might be due to both the previously described increased permeability of the membranes under the AC component and the apparent improved diffusion of the amine labeled antibiotics under the DC component. The intensity of the SP electric field utilized here was well below the electrolysis potential of the biological fluid. Hence, we envision applications of this technique that would minimize generating harmful radicals due to media electrolysis. Based on these enhanced biofilm inhibition efficacies as well as low intensity of electric field, the treatment method can be applied for further toward clinical applications, such as in-vivo biofilm infection treatment.

3.2 Electrolysis of the Bioelectric Effect

3.2.1 Overview of the Experiment

Biofilm treatment was performed by applying an electrical signal with antibiotics based on the principles of the bioelectric effect as described section 3.1. The key consideration of the bioelectric effect in this work was utilizing the method with a biocompatible electrical signal that is below the threshold potential of media electrolysis (0.82 V at 25 °C in pH 7)[65]. The electric voltage is characterized with 0.5 V for the conventional cuvette setup that is lower than the threshold of medium electrolysis.

Even if the voltage was below the threshold, quantitative studies of the electrolysis effect of each electric field (AC, DC and SP fields) were conducted by measuring pH changes using a pH indicator (#36828, Fluka Analytical) which actively reacts at pH 4 – 10. Optical density characterization of the indicator was performed with 1 mL of phosphate buffer (pH 5, 7, 8) and measured the absorbance spectrum from 500 nm to 700 nm by a spectrophotometer (Evolution 60, Thermo Scientific Inc.). In this work, the cuvette setup was utilized to apply for electric fields as well as measure OD values directly as shown in figure 3.13.
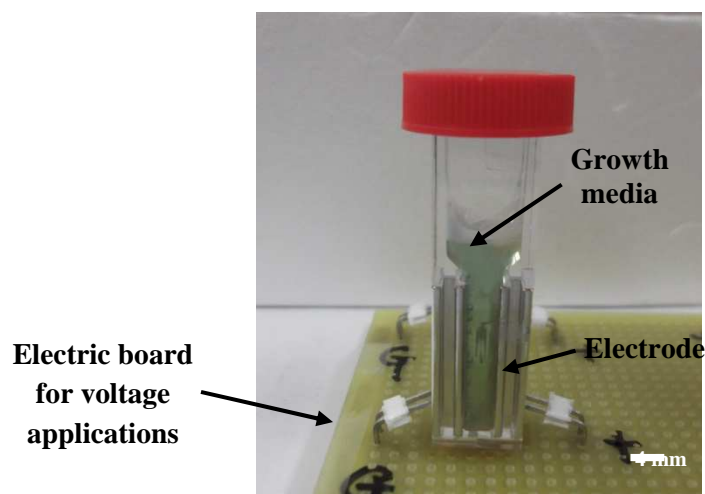
Figure 3.13: A photo of the cuvette setup for electrolysis quantification. The electric field was applied for 24 hours continuously to the bacterial growth media (LB). Changes of pH were quantified by a pH indicator.

A 1 mL of bacterial growth media (LB) was placed in sterilized cuvettes and applied either 0.5 V amplitude sinusoidal signal at 10 MHz (AC), 0.5 V DC, or SP-field (AC+DC) for the media by a function generator and DC power supply for 24 hours. Then, the pH indicator was added to the solution and measured a specific wavelength optical densities (OD_{616}) based on the initial wavelength scan result (figure 3.14 and 3.15). Each experiment was repeated three times and presented an average value with their standard deviations (figure 3.16).

3.2.2 Electrolysis Quantification Results

Since electrolysis of the media involves hydrogen gas generation resulting in decreased concentration of hydrogen ions, the pH of the medium was expected to become slightly

basic due to the electrolysis. Using a pH 8 buffer solution, a strong absorbance peak was shown at a wavelength of 616 nm (OD_{616}) (figure 3.15). Thus, the electrolysis effect was quantified by measuring the OD_{616} after applying electric fields. After applied each field to the media, the OD_{616} data are presented in figure 5.7.

Figure 3.14: Demonstration of color changes of the pH indicator in known pH solutions using a phosphate buffer solution. The pH 8 color was referred to quantify electrolysis effects.

Figure 3.15: Representative OD_{616} spectrum between 500 nm and 700 nm by a spectrophotometer (Evolution 60, Thermo Scientific Inc.). Since the peak value from pH 8 buffer solution using a pH indicator was observed at 616 nm wavelength, OD_{616} was selected to quantify the electrolysis effect from different field applications. Only the 820 mV applied potential showed significantly higher OD compared to other fields.

Figure 3.16: OD_{616} values in each experiment. The AC electrical signal was 0.5 V amplitude of sinusoidal signal at 10 MHz and the DC was 0.5 V magnitude. The SP-field was combination of the AC and DC fields. A 0.82 V of DC was also applied separated as a control experiment of the electrolysis threshold to the media. The experiments were repeated three times, the averages and standard deviations are presented. We conclude that SP field is not due to electrolysis of the growth media.

The results show the SP field was not induced significant electrolysis due to the electrical energy supply. Compared to the threshold of the electrolysis (820 mV DC), the SP-field was shown a minimal pH change (less than 0.05 changes of pH). Therefore, this concludes that the SP-field does not induce massive electrochemical condition changes in biofilm growth media.

3.2.3 Discussion

Biocidal effect of radicals due to electrolysis is significant side-effect to apply bioelectric effect to clinical fields. In this thesis work, by superpositioning AC and DC field, the required voltage was reduced below the threshold of the biological media electrolysis. Moreover, the treatment efficacy in both traditional cuvette setup and microfluidic environment was significant compared to the only antibiotic treatment. With this quantification of the pH changes in the field application, the biocidal effect of the SP field was studied and demonstrated that it does not induce major media electrochemical decomposition. Based on this result, significantly improved biofilm treatment efficacies as shown in the previous work (section 1.4.4) were possibly due to the simultaneous introduction of the AC and DC field rather than enhancement of electrochemical environmental modifications. The AC field can induce local molecular vibration of the partially charged cell proteins[67, 114] and DC field can improve electrophoresis of the biofilm based on the consistent electrostatic force[64, 114]. When these two mechanisms are applied in parallel, the biofilm treatment can be significantly improved. Perhaps more importantly, it is believed that this result encourages to apply this method for clinical biofilm management since this method does not cause massive harmful radical generation.

However, this quantification of electrolysis is focused on evaluating the bulk impacts of the electrolysis rather than local investigation. Even if a major electrolysis was not observed by the SP field application, local electrolyte distribution of the media can be varied due to the electrostatic energy supply from the SP field. This spatiotemporal critical electrolyte investigation when the field was applied can provide for fundamental

scientific information of the bacterial metabolic reactions in the condition as well as potential mechanisms of the bioelectric effect that are still under investigation[114].

3.3 On-Chip Demonstration of the Bioelectric Effect

Integration of bioelectric effect with a microdevice makes the concept of biofilm treatment enable to apply for biomedical applications. Although the bioelectric effect has been demonstrated by many groups[62, 63, 64, 66, 114], on-chip validation of the effect has never been investigated. Scaling of the SP-BE to the micro-scale is a critical requirement in realizing the SP-BE for in-vivo and in-vitro biofilm infection management, as the scaling of the treatment to smaller dimensions enables the SP-BE to utilize further biocompatible parameters, including voltage requirements.

Based on advantages of the microfluidic platform (i.e. small volume of samples, consistent environmental control, multi-parallel experiments, and compatible to the integration with other MEMS devices)[149, 150], a bioelectric effect integrated microfluidic device has been developed. The intensity of the electric field and concentration of gentamicin are the same as the previous superpositioned bioelectric effect studies.

Finally, I would like to acknowledge Mr. Matthew Mosteller in collaboration of this specific work that he contributed to developing the system significantly.

3.3.1 Principles of Operation

Here, optical density (OD) based microfluidic system was developed based on the advantages of low sample and precisely controlled environment for biofilms. The OD values are directly correlated with the total biomass[141]. For real-time OD measurement, linearly integrated charge-coupled-devices (CCDs) are aligned under the microfluidic platform. The schematic of operation is shown in figure 3.17.

111
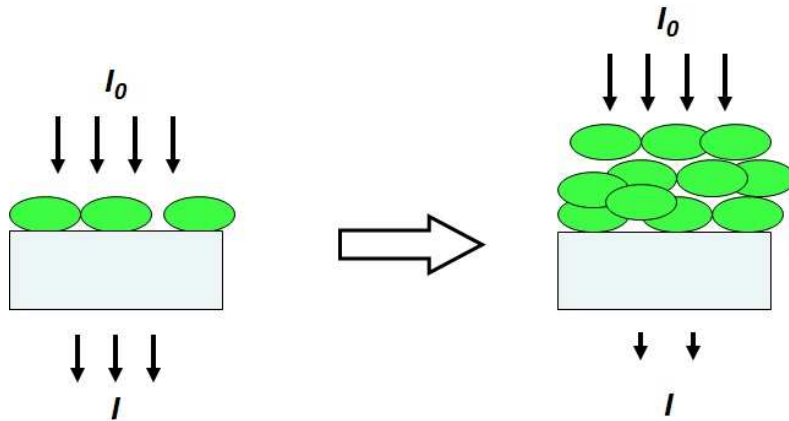
Figure 3.17: Schematic of the optical density measurement of the biofilms.

$$\text{Optical absorbance [AU]} = -\log_{10}\left(\frac{I}{I_0}\right)$$

As biofilms are grown thicker and thicker, the transmitted light intensity is changed corresponding to the total biomass changes. In the microsystem development, a light-emitting diode (LED) light is introduced over the platform continuously which provides nearly uniform illumination intensity over the whole platform. Transmitted light through the channel is monitored by optical absorbance in the CCDs.

3.3.2 Planar Electrodes for the Bioelectric Effect

To integrate the bioelectric effect to a microsystem, fabrication of electrodes is required. However, a planar electrode induces spatial non-uniformly distributed electric

field based on changes of the electrostatic force (Columb's law) as the distance is changed between the charge location and measured position inside of the reactor. Investigation of the non-uniformity of the field is critical since this spatial gradient of the field creates a dielectrophoretic force to charged molecules. For instance, in this work the antibiotic gentamicin is positively charged along with diverse electrolytes in the growth media. Therefore, distribution of the antibiotic can be varied due to the induced dielectrophoretic force. The non-uniform antimicrobial agent to biofilms is also known as a biocidal effect[151]. This additional condition can be challenged to analysis the efficacies of the bioelectric effect. Based on this consideration, numerical analysis of the electric field distribution in a relevant microfluidic reactor was performed focusing on the quantification of the dielectrophoretic force via the thin planar electrodes.

The calculation was focused on the variation of the intensity of the field from the bottom to the top layers of the microfluidic channel. Since the electrode was assumed as a submicron thickness of electrodes, non-uniform electric field distribution was expected since the intensity of electrostatic force is depended on the distance from the charge to the position of the observation point as shown an example in figure 3.18.
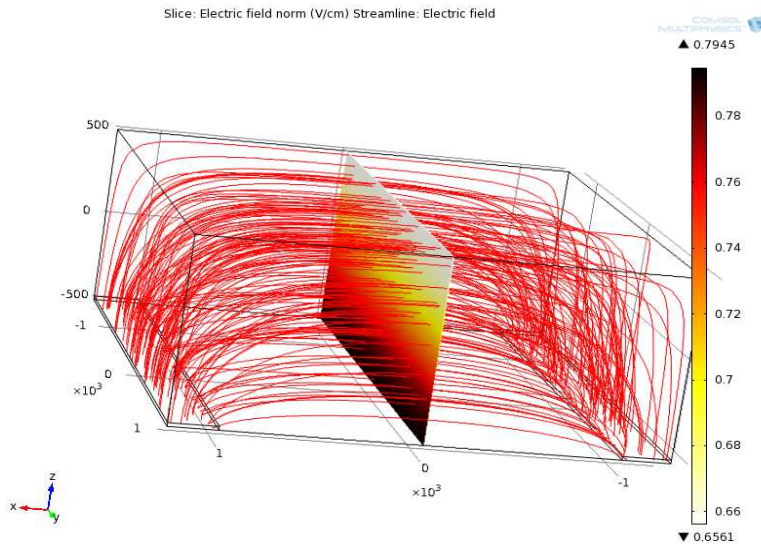
Figure 3.18: An example of non-uniform electric field distribution demonstrated via COMSOL simulation.

This spatial non-uniformity of the electric field induces a dielectrophoretic force that can create a gradient of charged molecules and non-uniform distribution of electrolytes along the direction of the force[152]. Since some antibiotics including gentamicin have partial charges[153], this dielectrophoretic force induction can cause changes of drug distribution over biofilm growth reactor that can affect to treatment efficacy of the method due to the local antibiotic concentration differences[143]. The dielectrophoretic force was proportional to the value of differentiated square of the electric field. The numerical analysis result is presented in figure 3.19.
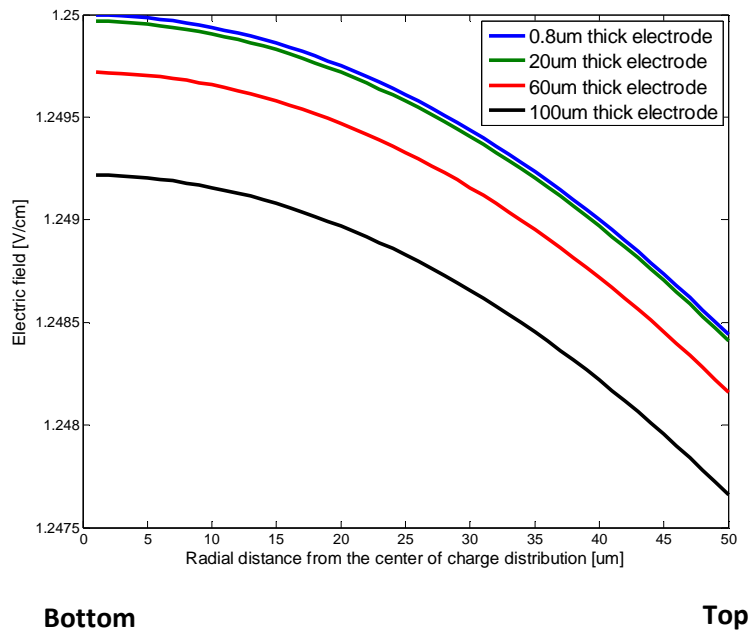
Bottom   **Top**

Figure 3.19: The intensity changes from the bottom to top of the microfluidic channel. The difference of the electric field was within 0.001 V/cm ranges which is not induced significant dielectrophoretic force.

As shown in the result, the variation of the intensity was not significant along the z-axis channel. The maximum difference between the top and bottom was approximately 0.001 V/cm which corresponds to ~ 10^{-24} N dielectrophoretic force[143]. This is not a significant force induction that enables local changes of the antibiotic gentamicin considering its density.

Based on this numerical analysis, it was concluded that the planar thin electrodes to supply electric field in the microfluidic chamber for biofilm treatments was not induced significant non-uniformity of the electric field. The calculated non-uniformity of the field expected to create a minimal dielectrophoretic force. Therefore, a conventional thin metal layer (Au: 200 nm) was chosen to integrate the SAW sensor with the bioelectric effect.

The parallel electrodes for the bioelectric effect were patterned on either side of the SAW sensing area (schematic is shown in figure 3.21). After the sensor fabrication presented in section 3.1.1, electrodes to apply for electric fields was patterned by photolithography. Cr/Au (15 nm / 200 nm) was deposited by an evaporation and lift-off as demonstrated in the previous on-chip bioelectric effect experiments (in section 2.6.1). The width of electrode was 2 mm for electric contacts of the power source.

3.3.3 Design and Fabrication of the Microfluidic System

The platform is consisting of electronics with linear array charge-coupled devices (CCD) and supporting electrical components, a microfabricated patterned base, and molded microfluidics. CCDs (TSL202R, Texas Advanced Optoelectronic Solutions) used for optical density (OD) detection are integrated on a custom printed circuit board (PCB, Advanced Circuits) to enable six parallel experiments on a single chip measuring 9.5 cm × 8.1 cm. The CCDs feature 128×1 linear photopixel arrays[154].

A 500 µm-thick Pyrex^{TM} wafer serves as a transparent substrate for the patterned base. Gold electrodes patterned on the substrate provide electric fields required to induce the SP-BE, while simultaneously limiting peripheral light from entering the CCD components. The electrodes (Cr/Au 15 nm / 200 nm), fabricated by physical vapor deposition on top of photoresist (AZ-5214, MicroChemicals GmbH) followed by liftoff, feature 2 mm spacing within the microchannels.

Molded microfluidic structures are fabricated through a standard polydimethylsiloxane (PDMS) process. Reversible bonding of the PDMS channel to the

patterned substrate is achieved by applying methanol to the PDMS, then aligning and placing it onto the Pyrex™ chip. The resulting microfluidic chambers measure 100 µm deep, 2 mm wide, and 1.75 cm long for a total chamber volume of 3.5 µL. The microfluidic chamber is integrated with an external syringe pump (Cole Parmer 74900) operating in withdrawal mode to minimize device leakage.

Actuation of the CCD devices in the Micro-BOAT platform requires a power source, drive clock, and serial input bit provided by an external power supply (Agilent E3631A) and accompanying function generators (BK Precision 4040). Signal readout from the CCDs is achieved using a data acquisition device (NI USB-6221, National Instruments). All external electrical signals are integrated with the Micro-BOAT platform via wire-to-board connectors (Molex Connector Corporation) and BNC cables (L-Com Global Connectivity). Illumination of the Micro-BOAT system for OD measurement is achieved using a diffusive edge-lit LED light panel to provide uniform illumination of the system (Luminous Film USA). Light emission is tuned to a wavelength spectrum centered at 630 nm by a polycarbonate lighting gel film (Roscolux #120, Rosco Laboratories) in order to match the peak sensitivity of the CCD components. The entire assembly is placed within an incubator (I5110, Labnet International, Inc.) at 37 °C[154].
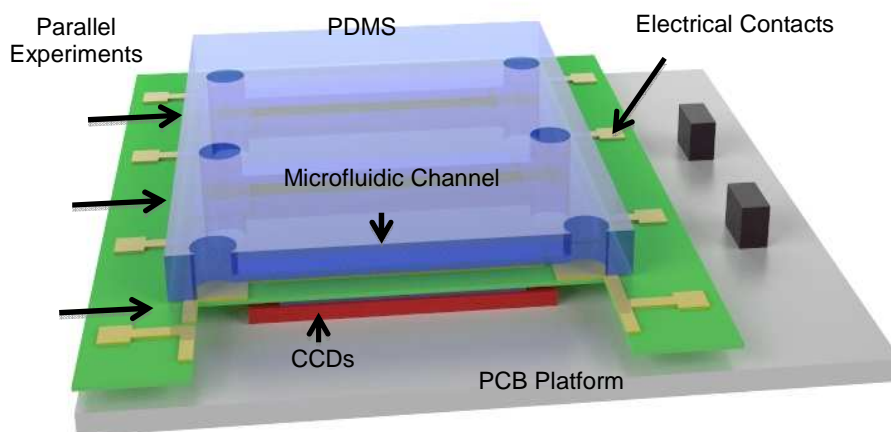
Figure 3.20: Schematic of the microfluidic biofilm observation, analysis and treatment (Micro-BOAT) platform used for the demonstration of the superpositioned bioelectric effect (SP-BE). Microfluidic channels serving as biofilm growth reactors are fabricated from polydimethylsiloxane (PDMS) and bonded on a transparent Pyrex^{TM} substrate to enable optical density (OD) measurement. The platform is capable of performing 6 experiments in parallel on a single chip. Real-time biofilm monitoring is achieved via the measurement of biofilm OD using charge-coupled devices (CCD) and a tuned light emitting diode (LED) source (not shown)[30].
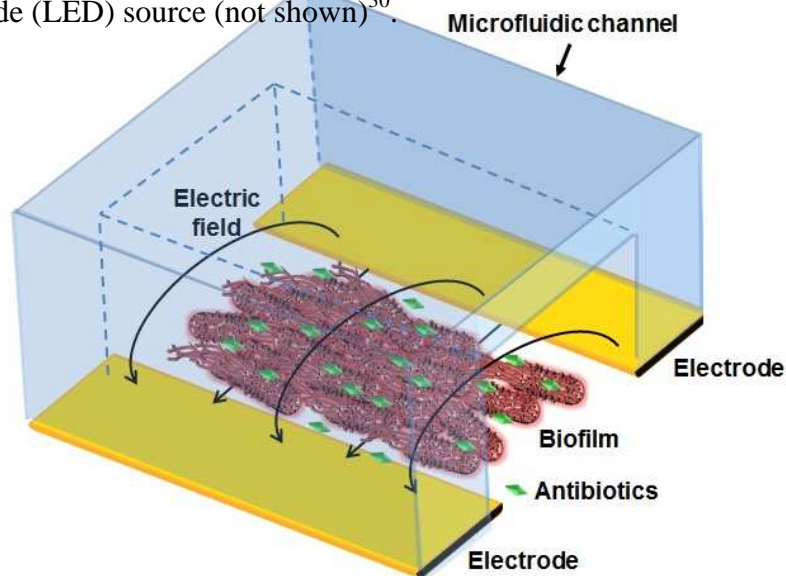
Figure 3.21: Schematic of the SP-BE biofilm treatment, which uses 200 nm thick planar electrodes spaced 2 mm across the 100 µm deep microfluidic channel to emit a SP electric field comprising a 10 MHz AC signal at 1.25 V/cm (corresponding to 0.25 V for 2 mm electrode spacing) with a 1.25 V/cm DC offset. Electrodes are exposed by 0.25 mm on each side of the microfluidic channels to expose the electrodes directly to the microfluidic channel. AC electric fields increase biofilm permeability, allowing for

greater antibiotic penetration into biofilms, while a DC electric field component induces localized non-uniform electrolyte distributions. The combination of the SP electric field with antibiotics (10 µg/mL of gentamicin) demonstrates significantly improved biofilm treatment efficacy due to the synergistic effect of the AC and DC BE.

3.3.4 Experimental Procedures

The demonstration of the superpositioned bioelectric effect in a micro-scale device has been achieved using the Micro-BOAT platform. Bacterial cultures of *Escherichia coli* BL21 pGFP are grown in Lysogeny Broth (LB) media to an OD_{600} of 0.25 AU. Testing is performed by initially inoculating a microfluidic chamber with bacterial suspension for 2 hours at 37°C with no flow to allow microbial attachment to occur on the channel substrate. LB media is then flowed continuously through the channel for 24 hours at 20µL/h by a syringe pump (Cole-Parmer Instrument Company, USA) to replenish nutrients and foster biofilm growth. For the channel dimensions presented here, this equates to an effective flow velocity of 30µm/s and has been optimized to provide an environment conducive to biofilm growth. Following the 24 hour growth period, four treatments are performed on the mature biofilms: control (no antibiotic or electric field applied), only superpositioned electric field, only gentamicin, and the enhanced bioelectric effect (superpositioned electric field with gentamicin). Control biofilms are continuously provided LB media at the same flow rate in order to determine steady-state biofilm growth. Biofilms treated with gentamicin, both in antibiotic-only experiments and those featuring the enhanced bioelectric effect, are done so with a 10 µg/mL concentration of the drug. The electric field featured in the biofilm experiments was introduced by a function generator (Agilent Inc., USA). Each of the four biofilm treatments is conducted with 3 experiment samples to demonstrate repeatability of the

various assays.

Optical density measurements are taken non-invasively in real-time with respect to both average OD change as well as localized morphology. Measurements are obtained every 8 minutes from the CCD devices to monitor the spatiotemporal development of the bacterial biofilms beginning after the initial two-hour inoculation period. Additionally, bacterial cell viability staining and fluorescence microscopy is used to provide end-point analyses of cell viability within the biofilms to verify treatment efficacy. Since the strain of bacteria used (BL21 pGFP) fluoresces green when the bacteria are metabolically active, only propidium iodide (PI) (Invitrogen Inc., USA) is needed to stain dead bacteria allowing them to fluoresce red. Following biofilm treatments, the microfluidic chamber is initially rinsed with phosphate buffered saline (PBS) solution at a rate of 200 μL/h for one hour to quantify only adherent bacteria. The stain is then supplied at a concentration of 1.5μL PI per 1000μL PBS at a flow rate of 200 μL/h for an additional 2 hours and unabsorbed stain rinsed from the microchannel using PBS at the same flow rate for an additional one hour. The ratios of live bacteria surface coverage with respect to the total biomass surface coverage for different treatments are analyzed using the software package ImageJ (Image J 1.44, USA). For each experiment, both optical density and viability analyses are performed to confirm the OD method for biofilm monitoring

3.3.5 Results and Discussion

Four separate experiments are performed simultaneously: control (no electric field or antibiotic), only superimposed electric field, only gentamicin and superpositioned bioelectric effect (gentamicin with the superimposed electric field). The overall biomass monitoring is achieved by the CCDs. In addition, the density of viable bacterial cells is investigated using live/dead cell staining at the end of the treatment.

Changes of OD during treatments are presented in figure 3.22. The results show more decrease OD in the superpositioned bioelectric effect than that in other treatments. It is for the first time the superpositioned bioelectric effect demonstrates effective treatment of biofilm compared to the only antibiotic treatment in a microfluidic device. At the end, biofilms treated by the superpositioned bioelectric effect showed a 40% decrease in OD respect to the beginning of treatments which implied substantial biomass decrease[155], while the control case demonstrated a 260% increase in OD as shown in figure 3.23.
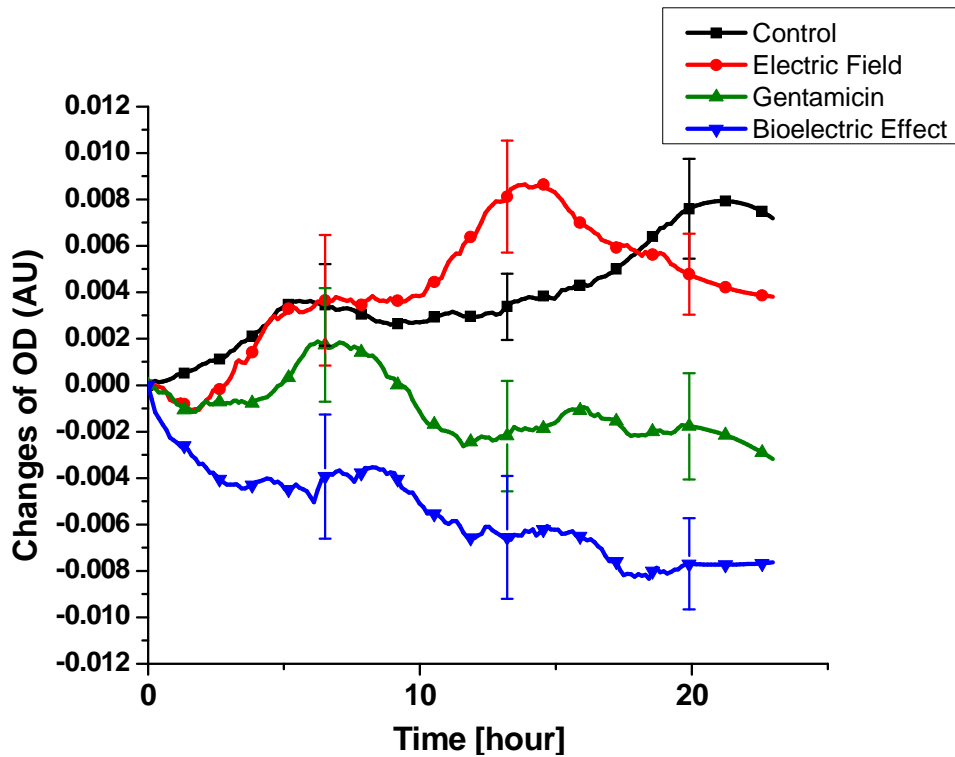
Figure 3.22: Measured changes in OD during biofilm treatment using the microfluidic optical platform. Each curve represents the average OD change for three samples with standard deviations shown at representative time points[30].

After treatment, the biofilm in the microfluidic channel is stained using live/dead fluorescent dye (Invitrogen Inc., USA) to investigate the treatment efficacy of the bioelectric effect. Using a fluorescent microscope (Olympus BX60), biofilm images are obtained (figure 3.24). The optical coverage of the images is evaluated using an image processing program (Image J) respect to the live and dead cell fluorescence surface coverage. The quantified viability of bacterial cell density is presented in figure 3.25.
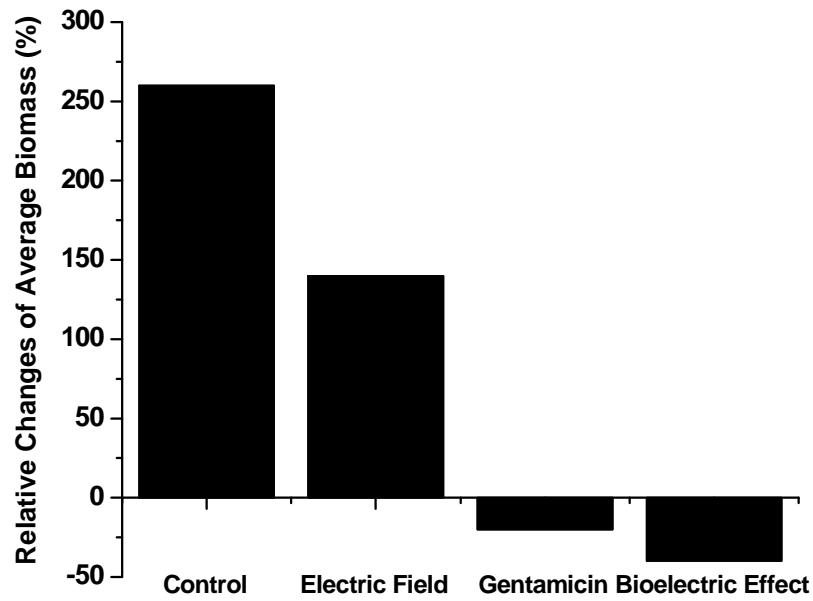
Figure 3.23: Relative changes of biomass after treatments in the microfluidic channel. Bioelectric effect treated biofilm revealed approximately 40% decrease overall biomass[30].
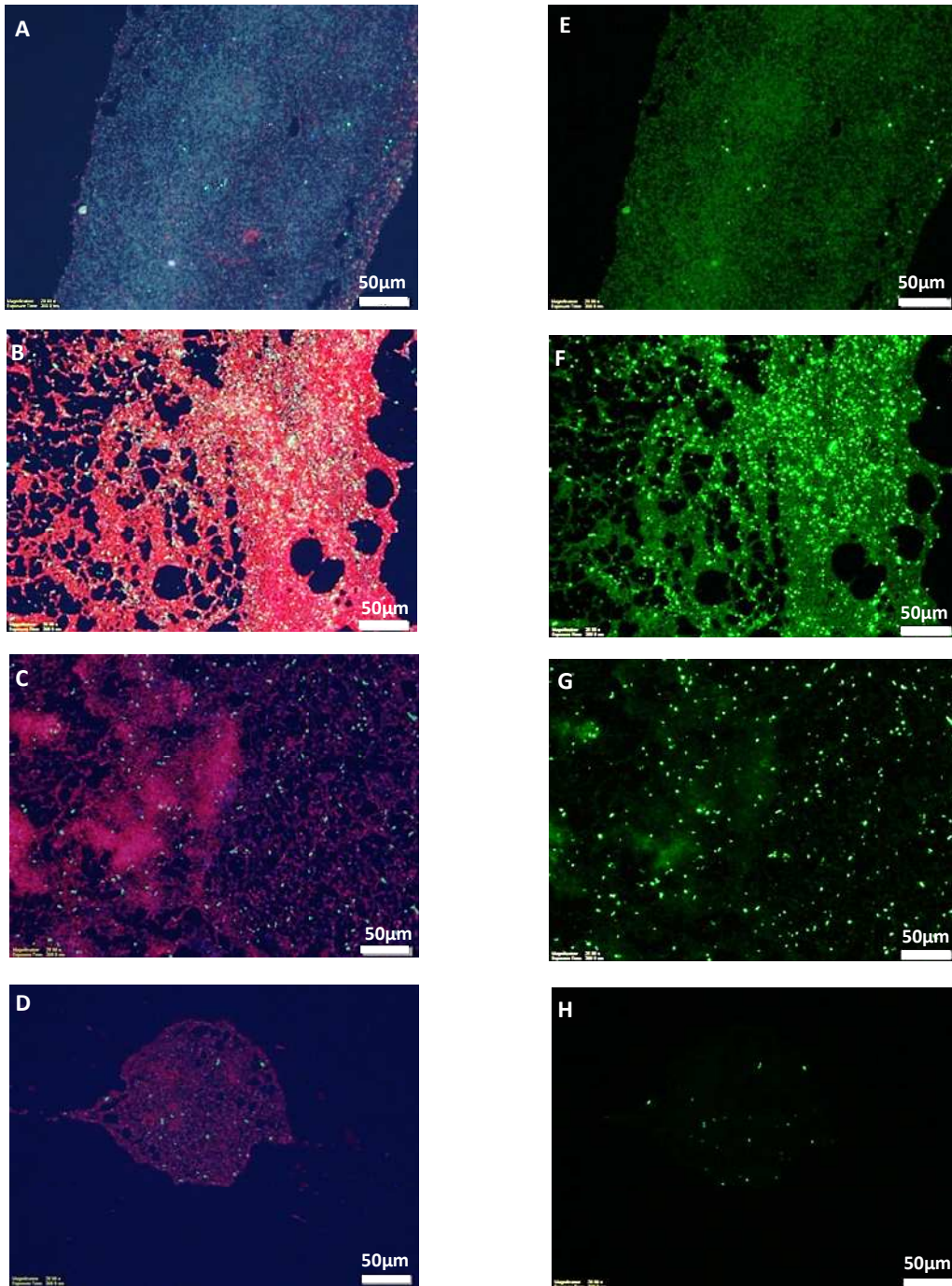
Figure 3.24: Representative fluorescence microscopy images of biofilms in the Micro-BOAT channels following maturation and treatment. The total biomass fluorescence images (left column) and viable biomass fluorescence (right column) of biofilms show control (A and E), SP electric field (B and F), traditional antibiotic (C and G), and SP-BE (D and H) treated biofilms. Biofilms treated with the SP-BE showed reduced biomass (D) as well as low viable bacterial cell density (H). Seven fluorescence images were taken for each of the four treatment methods (N=7), with the images presented here representing

regions of high biofilm density[30].
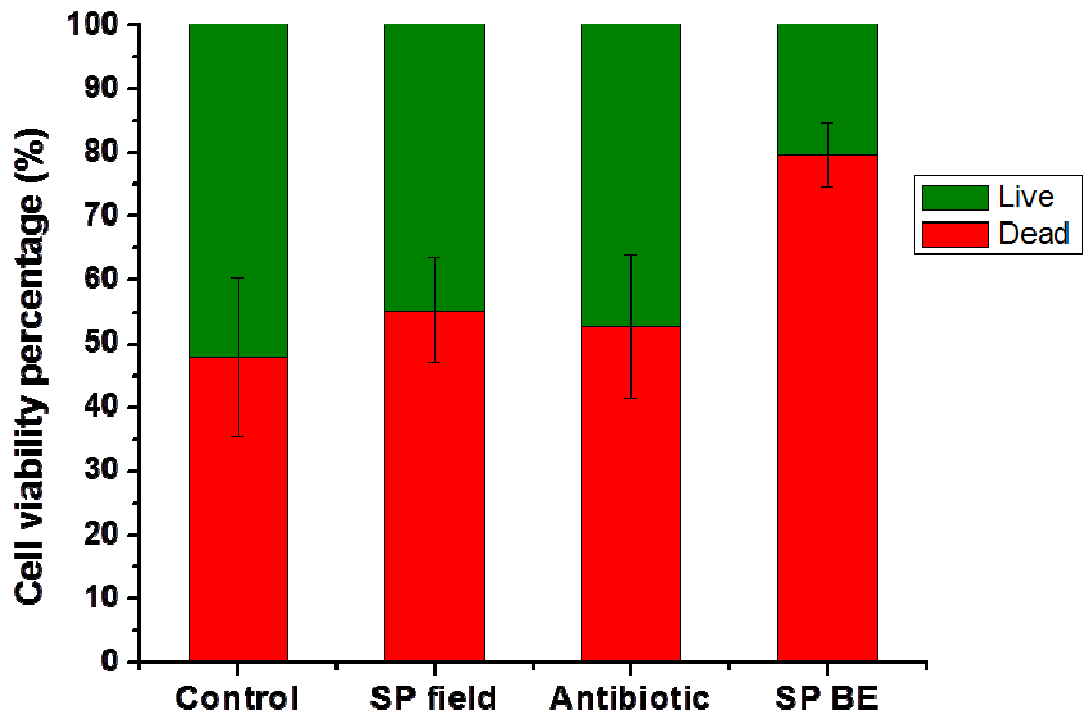
Figure 3.25: The percentage of viable biofilm bacteria with respect to total biomass after each treatment is calculated using image processing software (Image J 1.44). The results include the average of seven image analyses (N=7) for each of the four treatment methods. Viable cell percentages and standard deviations are obtained with respect to total fluorescent mass surface coverage using a binary image conversion (see the Methods). The density of non-viable cells in biofilms treated by the SP-BE is shown to increase 56% in comparison to treatments using antibiotics independently (P = 0.019)[30].

The biofilm treated with the superpositioned bioelectric effect shows a 56% decrease in bacterial viability compared to antibiotic treatment alone.

As shown in data, the superpositioned bioelectric effect has been demonstrated for the first time in a microfluidic platform. The on-chip bioelectric effect showed a 40%

decrease in overall biomass as well as 56% improved treatment efficacy compared to only antibiotic treatment based on the cell viability studies.

Validation of the SP-BE using thin-film planar electrodes in a micro-scale environment represents a critical step in the development of SP-BE treatments for future clinical applications. The reported levels of efficacy are statistically significant ($P < 0.05$, figure 3.25) and support the use of thin planar electrodes to induce the SP-BE, with the current Micro-BOAT system demonstrating efficient treatment in a microfluidic system that is 500 times deeper than the thickness of the electrodes (0.2 µm thin-film gold electrodes in a 100 µm deep channel) . The use of thin-film electrodes to induce SP electric fields enables the scaling of treatment systems utilizing the SP-BE to sub-micron thicknesses while maintaining broad effective treatment areas. Such a method provides a potential approach for localized infection treatments that require reduced antibiotic dosages compared to current therapies.

3.4 Summary

In this chapter, a new effective biofilm treatment technique was presented by combining a superpositioned electric field with antibiotic gentamicin. The method is utilized electric potential required even below the threshold of electrolysis of the biological fluid. This is critical to apply the bioelectric effect to clinical applications since generation of hazard radical ion can be minimized. More importantly, the superpositioned bioelectric effect (SP-BE) demonstrated significantly enhanced biofilm

reduction compared to the only antibiotic treated samples. The SP-BE was further demonstrated in a micro-scale device. Based on the low voltage requirement and significant biofilm inhibition in a microdevice, this technology can be further developed as an integrated system with the biofilm sensor.

Chapter 4: Integration of the Sensors with the Bioelectric Effect

4.1   Design of the System

Since the acoustic waves are induced by an electrical actuation on the piezoelectric material, the integration of the electric field for the biofilm treatment can cause attenuation of the wave propagation due to the proximity of the applied field for biofilm treatment to the SAWs. In addition to the potential electric field interference between the sensor and bioelectric effect, the microfluidic flow can affect to the SAW propagation since the flow induces surface friction that may result in changes of the SAW velocity. The initial speed shift of the waves will result in a decrease of the sensitivity and require calibration each time which can impact to the reliability of the sensor operations.

4.1.1 Electric Interference between the Sensor and Bioelectric Effect

The investigation of the electrical signal interference to the SAWs was conducted with a device geometry shown in figure 2.37. The Al_2O_3 film deposited on the ZnO layer and the electrodes for the bioelectric effect were fabricated with air gap in each side. The induced field intensity on the ZnO layer due to the voltage (0.25 V of DC + 0.25 V sinusoidal signal at 10 MHz) applied for the biofilm treatment was calculated based on the electromagnetic theory (Maxwell's equation)[156]. The derived equation for the ZnO layer is presented in equation 15.

The dielectric constant of each layer indicates the characteristics of the polarity of the medium that directly corresponds to the induced electric field intensity. Using Maxwell's equation, the induced electric field in the ZnO layer is derived.
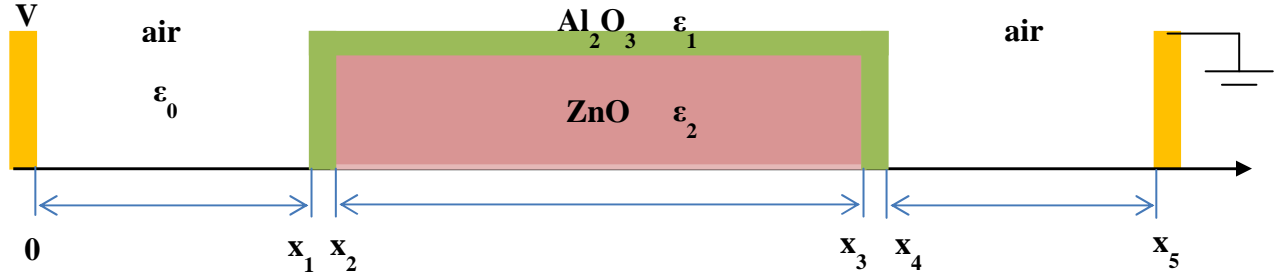
Figure 4.1: Schematic of the device cross-section for electric field distribution analysis. The ZnO can affected by the voltage applied for the bioelectric effect during the biofilm treatment. The simulation was focused on the ZnO layer from X_2 to X_3 locations. $\square$ represents a dielectric constant of the each medium.

$$x_2 < x < x_3 \quad \therefore E_x = \frac{Q}{2A\varepsilon_2} \approx \frac{Q}{2A \cdot (100\varepsilon_0)} \approx \frac{C_{total}V_0}{200A\varepsilon_0}\left[\frac{V}{m}\right]$$

(15)

where Q is total charge on the metal electrode (at position 0), A is the surface area of the electrode, C_{total} is overall capacity of the system, V_0 is the magnitude of the applied voltage (0.25 V) and $\square_0$ is the dielectric constant of air (vacuum). Using the current device design parameters, such as thickness and width of ZnO, Al_2O_3, electrode and air gap distance, the intensity of the electric field was calculated.

$$E_x \approx \frac{C_{total}V_0}{200A\varepsilon_0} = \frac{V_0}{200} \cdot \frac{1}{10.1\times10^{-4}} = \frac{0.25}{20.2\times10^{-2}}\left[\frac{V}{m}\right] = 1.238\left[\frac{V}{m}\right]$$

(16)

Based on the obtained value, the induced displacement of ZnO was estimated based on its piezoelectric coefficient, which was obtainedfrom literature [157]. The derivation is presented below in detail:

$$S = d \cdot E$$

S: *strain due to the applied E-field*
d: *piezoelectric strain coefficient (C/N)*
E: *electric field (V/m)*

$$d_{33} = 12.4 \times 10^{-12} \ [C/N]$$
$$E = 1.238 \ [V/m]$$

$$\therefore S = (12.4 \times 10^{-12}) \cdot (1.238) \left[\frac{C \cdot V}{N \cdot m} \right] = 15.4 \times 10^{-12}$$

$$S = \frac{\Delta L}{L}, \quad \Delta L = LS = (1mm) \cdot (15.4 \times 10^{-12}) = 15.4 \ fm$$

Through the calculation, the induced displacement is in thefemto-meter scale. Considering the wavelength (12 µm: twice of the displacement of the acoustic wave), the induced attenuation of the SAW is six orders of magnitude smaller than the wavelength displacement. Therefore, a potential cross-talk between the SAW and the bioelectric effect was not significant.

4.1.2 Shear Stress of the Flow on the SAW Sensor

The microfluidic flow shear effect to the SAW propagation was investigated based on the physics of the laminar microfluidic flow conditions. The schematic of the condition is shown in figure 2.38.
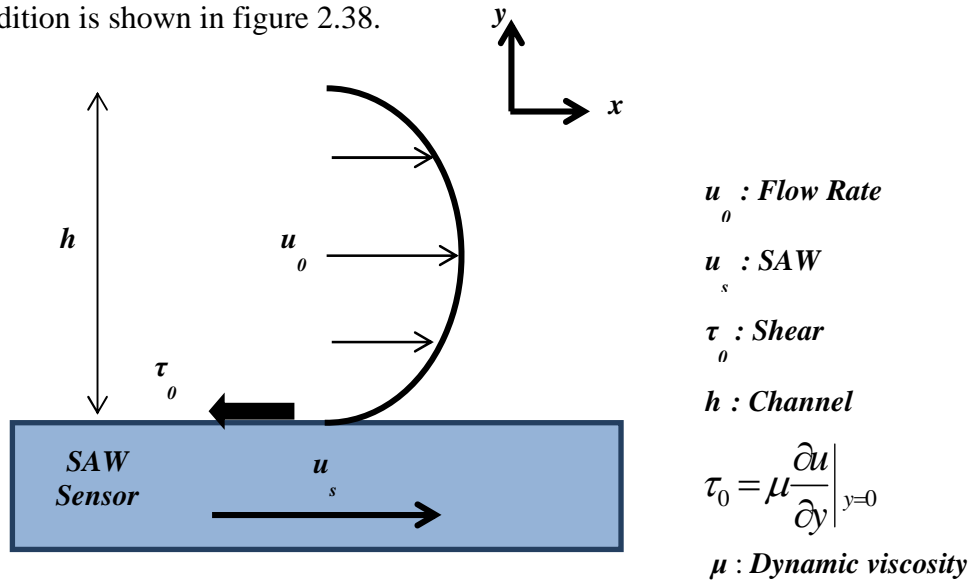
u_0 : *Flow Rate*

u_s : *SAW*

τ_0 : *Shear*

h : *Channel*

$$\tau_0 = \mu \frac{\partial u}{\partial y}\bigg|_{y=0}$$

μ : *Dynamic viscosity*

Figure 4.2: Schematic of the laminar flow on the SAW. The theoretical analysis was focused on the impact of the SAW speed changes due to the flow.

First, the Reynolds number was calculated to ensure that the flow in the channel is laminar. The dimension of the microchannel was taken from the previous microfluidic bioelectric effect demonstration device (100µm height, 2mm width and 2cm length). The Reynolds number[158] was found to be ~ 4.2 which is less than the threshold of laminar flow (10^5). Thus, in the given channel, laminar flow is induced[159].
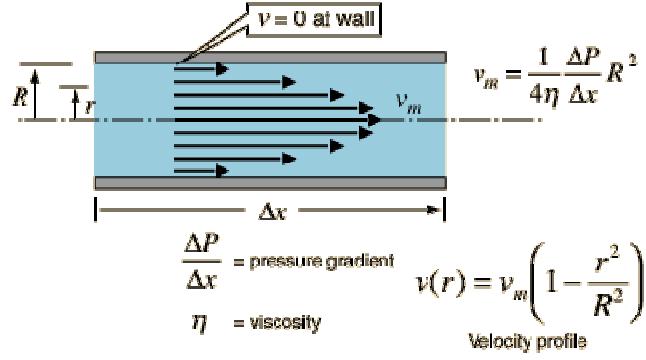
Figure 4.3: Schematic of the laminar flow at the microchannel. The velocity profile is related with the geometry of the channel (i.e. height)[133].

$$\frac{dv}{dr} = v_m(-\frac{2r}{R^2})$$

$$\frac{dv}{dr}\Big|_{r=R} = v_m(-\frac{2}{R}) = -\frac{v_m}{\frac{1}{2}R} \qquad (17)$$

$$\frac{\partial u}{\partial y}\Big|_{y=0} = \frac{\Delta u}{\Delta y}\Big|_{y=0} = \frac{u_0 - 0}{\frac{1}{2}h} = \frac{2u_0}{h} \qquad (18)$$

$$\tau_0 = \mu\frac{2u_0}{h} \qquad (19)$$

The shear surface tension on the substrate is known to be proportional to the velocity profile of the laminar flow. The derived velocity slope is shown in equation (18). In addition, the surface tension on the SAW is calculated based on the changes of SAW speed and density of the ZnO and the microfluidic flow rate (equation 19).

$$\tau_0 = \left(\frac{\rho_{ZnO} \Delta v}{\Delta t} \right) d_{ZnO} \Rightarrow \quad \Delta v = \frac{\tau_0 \cdot \Delta t}{\rho_{ZnO} \cdot d_{ZnO}} \tag{20}$$

Δt: time to propagate a wavelength (1/f)
d_{ZnO}: thickness of ZnO

Combining equations (19) and (20), the change in SAW velocityis derived below:

$$\Delta v = \mu \frac{2u_0}{h} \cdot \frac{\lambda}{u_s} \cdot \frac{1}{\rho_{ZnO} \cdot d_{ZnO}}$$

μ: dynamic viscosity of water
$\quad$ (1.002 x 10^{-3} N·S/m^2)
u_0: maximum flow rate (2 x 4.2 x 10^{-2} m/s)
h: height of channel (100 μm)
λ: wavelength of SAW (12 μm)
u_s: speed of SAW (4812m/s)
ρ_{ZnO}: density of ZnO (5.61 g/cm^3)
d_{ZnO}: thickness of ZnO (400 nm)

$$\Delta v = 9.34 \times 10^{-7} m/s$$
$$\Delta f = \frac{\Delta v}{\lambda} = \frac{9.34 \times 10^{-7} m/s}{12 \times 10^{-6} m} = 0.078 Hz$$

With relevant values of the parameters, the changes in the speed of the SAW due to the fluidic flow were approximately 10^{-7} m/s which corresponds to a 0.078 Hz resonant frequency shift. Since the resolution of the network analyzer (HP8510B) for monitoring of the SAW sensor when biofilms are treated or grown is 0.1 Hz, it is concluded that the microfluidic flow does not cause significant impact to SAW resonant frequency monitoring.

Through the numerical analysis to investigate potential integration challenges, the SAW sensor is expected to work properly in an integrated system with the bioelectric effect as an independent sensor demonstrated previously.

4.1.3 Overview of the Integrated System

The integrated microsystem was designed for real-time biofilm detection as well as effective treatment with low doses of antibiotics. The integration of the biofilm sensor with a treatment method is critical to manage biofilm associated infectious diseases systematically. The sensor provides a means to measure the total amount of the biofilms which acts as a feedback signal to the system to determine treatment methods. Moreover, the progress of the biofilm treatment is also monitored by the sensor. Through this systematic approach, biofilm management can be significantly more effective as the system detects the on-set of biofilm formation and subsequently provides the intensified inhibition of the biofilms. The integrated microsystem is composed of the SAW sensor for real-time biofilm detection and the superpositioned bioelectric effect.

The bioelectric effect has a unique capability for integration with a micro-scale device. To induce the effect, an electric field has to be applied through an electric potential between separated electrodes. The electric field (E) between two uniformly separated electrodes is defined by equation (21)[127],

$$E=V/d \qquad\qquad (21)$$

where V is the applied electric potential, d is the distance between the two electrodes, and E is the intensity of the electric field. Based on equation 1, a key requirement for

integration of the bioelectric effect with a microsystem is the induction of electric potential. Since the distance between the two electrodes *(d)* can be in the micro-scale in a microfabricated device, the electric potential can be significantly decreased. For example, a voltage of 1 V over a 1cm distance between electrodes is required to induce an 1 V/cm electric field intensity. However, when the distance between the electrodes is 10 µm, the electric potential is decreased to 1 mV which is more biocompatible than the intensity of the electric potential in a macro-scale device. By decreasing the intensity, the electric field for bioelectric effect can be implemented for future in-vivo applications. Therefore, the bioelectric effect integrated with a micro-scale device has a significant advantage over macro-scale devices in improving the antibiotic treatment efficacy on biofilms. Furthermore, by decreasing the magnitude of the electric field in the microsystem, the bioelectric effect can be used for clinical applications.

The schematic of the SAW sensor and bioelectric effect integrated microsystem is shown in figure 4.4. The SAW sensor is fabricated on a silicon wafer with a deposited thin layer of piezoelectric ZnO. The dimensions of the sensor are approximately 1mm by 3mm with a thickness of 0.5 mm. The electrodes for inducing the bioelectric effect are fabricated by metal evaporation after photolithography. The electrodes can also be extended to cover a wide area for biofilm treatment while maintaining the intensity of the electric field. Finally, a polydimethylsiloxane (PDMS) chamber is integrated over the microsystem to introduce growth media and antibiotics.
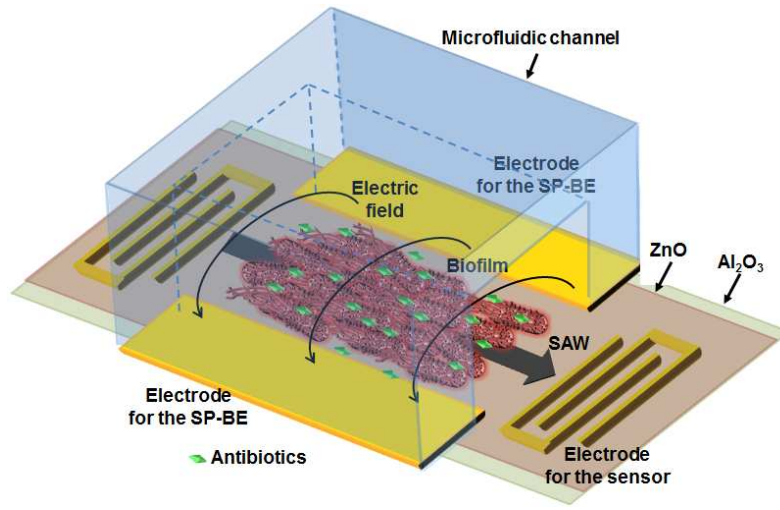
Figure 4.4: Schematic of the integrated microsystem of the SAW sensor and electrodes for induction of the bioelectric effect. A microfluidic chamber is integrated over the system to introduce bacterial growth media and antibiotics[32].

4.1.4 Summary

In the design of the integrated microsystem for both continuous biofilm detection and enhanced biofilm treatment, clinical applications for biofilm management were significantly considered. The SAW sensor was designed based on the biocompatibility of the material and minimizing the sensitivity loss when the sensor is passivated by a thin film to prevent degradation of the key material of the ZnO layer. Through theoretical modeling of the sensitivity, an appropriate material for the passivation film was chosen. The Love mode of SAW was designed to achieve a highly sensitive biosensor. The overall dimension of the sensor was compatible for future in-vivo applications (3 mm of width, 1 mm of length and 0.5 mm of the thickness). The treatment method was developed based on the bioelectric effect which increases biofilm treatment efficacy as combined electrical signals with antibiotics. To reduce the high voltage requirement that is limited by the electrolysis potential (0.82 V), a superposition of the AC and DC fields is designed. The intensity of the field is required a lower voltage than the threshold. Fabrication of two electrodes along with the SAW sensor allows to impose electrical signals to the biofilm. Biofilm growth is localized as a microchannel fabricated by PDMS is assembled over the system. This system is expected to provide the total presence of biofilms by the sensor as well as enable to apply a new treatment method for effective biofilm reduction.

4.2 Fabrication

In the fabrication of the integrated device, two processes are particularly critical to achieve highly sensitive and reliable operation of the system. These are the pulsed laser deposition (PLD) for the ZnO film growth and atomic layer deposition (ALD) for Al_2O_3 film fabrication. PLD provides the highest ZnO quality with extremely low concentration of impurities. The process is relatively simple and the orientation of the ZnO is well controlled due to the high stochastic correlation with the crystal structure of target material[160]. Based on the high quality and single crystal film fabrication advantages, the PLD was chosen to deposit the piezoelectric ZnO film (500 nm) for this system development. ALD can control the thickness of the film from a single to thousand atomic layers of the material which is critical to fabricate precise and robust microelectronic systems at a low temperature (~ 150 ℃). The ALD was utilized in this work for fabrication of a passivation layer for long term reliable operation of the device in bacterial growth media[13].

A 60 nm silicon dioxide (SiO_2) layer was deposited on (100) Si substrates by low pressure chemical vapor deposition (LPCVD) to prevent acoustic wave loss to silicon substrate. The IDT was patterned using traditional photolithography before depositing the ZnO film. Cr/Au (15 nm / 200 nm) as the IDT material was deposited on the wafer by electron-beam evaporation, followed by lift-off. The wafer was diced and crystalline (001) orientation ZnO (c-axis oriented ZnO) films on SiO_2/(100)Si substrates were grown by PLD. The laser deposition system used a KrF excimer laser at a wavelength of 248 nm with pulse duration of 25 ns to ablate a high purity (99.999 %) ZnO ceramic target. The ZnO layer was grown at 300 ℃ with an ambient oxygen partial pressure of ~1.0×10^{-4}

Torr. After ZnO film deposition, the ZnO was patterned using a solution that consisted of phosphoric acid, acetic acid, and deionized water (1:1:30) with photoresist mask. The device was annealed at 800 °C for one hour to increase the resistivity of the ZnO[161]. Finally, the ZnO surface of the SAW sensor was coated by depositing a 100 nm thickness Al_2O_3 film using atomic layer deposition (ALD) at 150 °C[162].

A polydimethylsiloxane (PDMS) chamber was assembled to the fabricated chip to provide a constant supply of fresh bacterial growth media and the antibiotic. The PDMS has advantages for biofilm research based on the air permeability, low-cost and ease fabrication process[163]. A mold of the microfluidic structures was fabricated by patterning 100 μm–thick KMPR-1050 on a silicon substrate using contact photolithography. PDMS (Sylgard 184, Dow Corning) in a 10:1 ratio was then poured over the mold and cured in a furnace for 20 minutes at 80 °C[16]. After cooling, the PDMS was removed from the mold and cut to fit the fabricated device. The bonding between the microfluidic channel and the device was reversible using methanol to treat the PDMS layer. A schematic of the overall process flow is shown in figure 4.5.
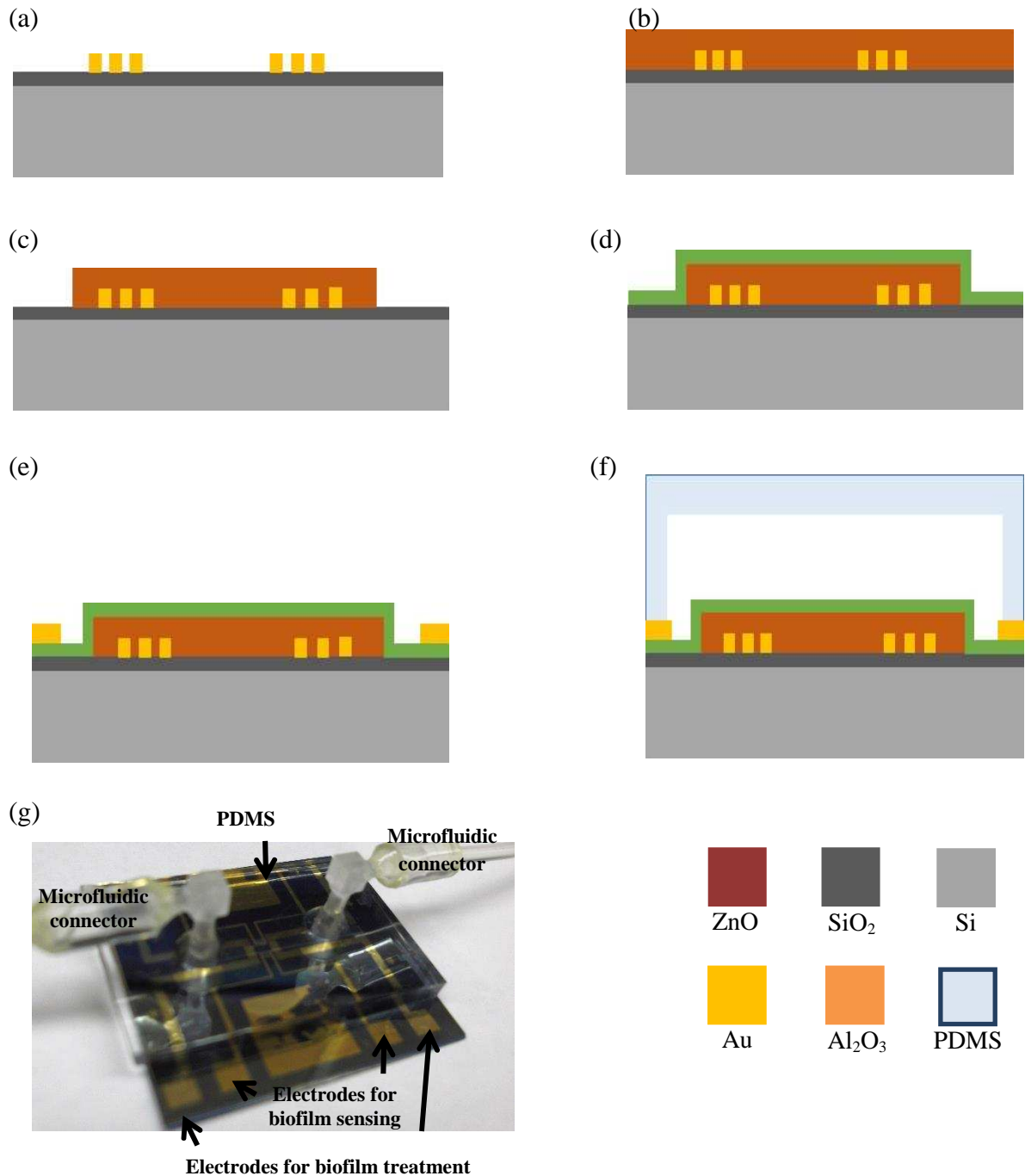
Figure 4.5: Overall schematic process flow. (a) 60 nm PECVD SiO_2 deposition and interdigitated electrode pattern and deposition (Au) by an electron beam evaporation, (b) 500 nm ZnO deposition using pulsed laser deposition, (c) ZnO patterning using weak acid etchant (1:1:30 ratio of acetic acid: phosphoric acid: deionized water), (d) 100 nm thickness of ALD Al_2O_3 deposition at 150 C, (e) Electrode patterning and fabrication via Au evaporation (Cr/Au, 15 nm/200 nm) and (f) PDMS microchannel assemble. (g) Photo of assembled device with the PDMS reactor.
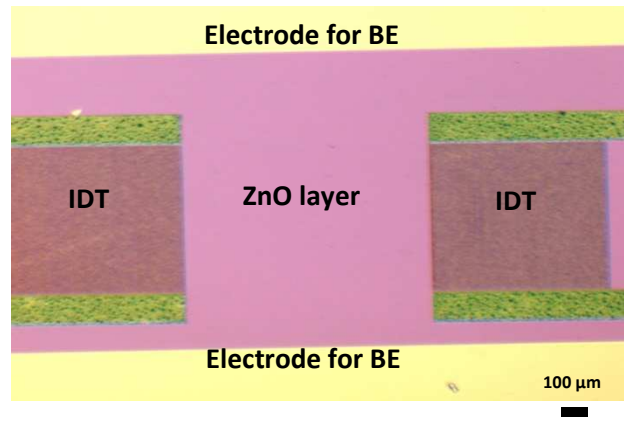
Figure 4.6: Optical microscopy image of the fabricated integrated microchip.

4.3 Testing Setup

Design of a parallel experimental setup is critical to achieve the high throughput that is needed to investigate the variation of biofilm growth with statistical significance[164]. Moreover, since bacterial biofilms growth is stochastic, conducting experiments in parallel with the same condition is critical to reduce statistical variations in each experiment. A multiplex logic circuit was implemented to conduct four parallel biofilm experiments simultaneously to overcome a single channel network analyzer to monitor resonant frequency of the system. Depending on the multiplexing bits, it is possible to expand the numbers of experiments from one to 16 or 32 experiments.
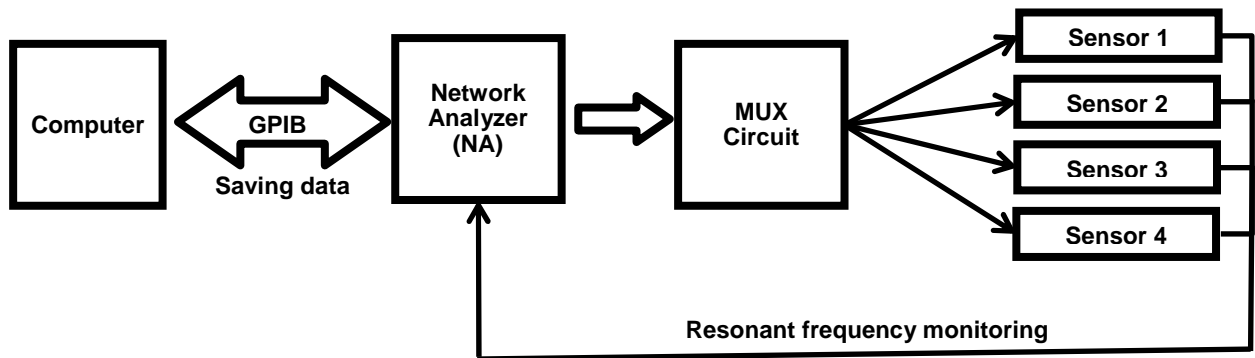
Figure 4.7: Flow chart of the switching setup. With this circuit integration, four sensors were tested at the same time for biofilm growth and treatment experiments.

In this setup development, a 4 bit multiplexer is used to perform four parallel experiments: control, electric field only, antibiotic only, and combination of the antibiotic with the electric field. The temperature was controlled to be 37 °C by a hotplate[27]. To localize the biofilm growth in the biofilm sensing area where the SAWs propagates between input

and output of the IDT, a microfluidic channel was assembled over the device. In addition, fresh bacterial growth media and antibiotics were provided to the microchannel by an external syringe pump with a constant flow rate (20 µL/h). The resonant frequency of the SAW sensor was continuously monitored by a network analyzer and recorded by the computer through the general purpose interface bus (GPIB) communication. For application of electric field to the biofilms, an external power source (Agilent Inc., 3320A) was connected to the setup for 24 hours. Finally, electric contacts between the device and external equipment were properly achieved by a spring loaded pin on each contact. The overall electric data flow chart is shown in figure 4.7.

The multiplexer (MC74HC4052N, Motorola Inc.) was switched by 4 bit counter (DM74LS161A, Fairchild Semiconductor Inc.). Each bit corresponds to one of sensors.

Binary Number	Sensor
00	Sensor 1
01	Sensor 2
10	Sensor 3
11	Sensor4

Table 4.1: Binary code of the counter for each sensor

Figure 4.8 shows the designed electronic board for the parallel experiments. The electric contacts between the board and the device are achieved by using spring loaded pins as shown in figure 4.9. Operation of the setup was confirmed by applying an input DC voltage (5 V) and measured output using an oscilloscope. The results showed a successful input signal switching following the designed frequency (1 Hz) as shown in figure 4.10.
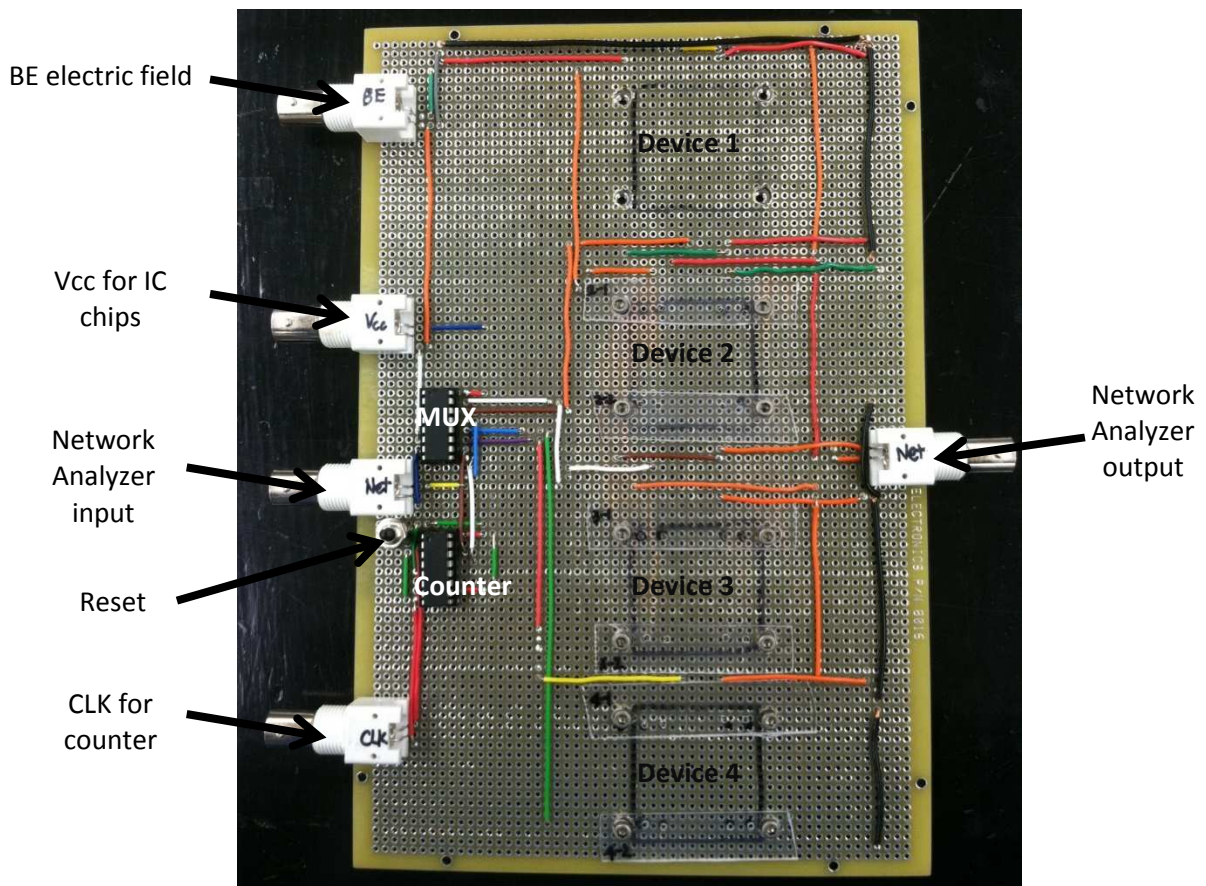
Figure 4.8: Photo of the custom designed multiplexing testing electronic board. The counter controls switching rate of the multiplexer. The reset can initiate the switching from device 1.
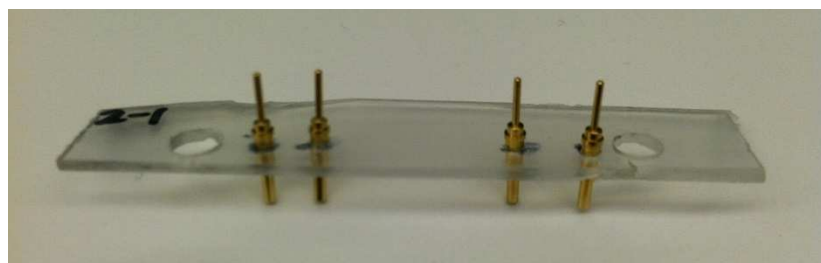
Figure 4.9: Spring loaded electrodes for the contact with the chip.
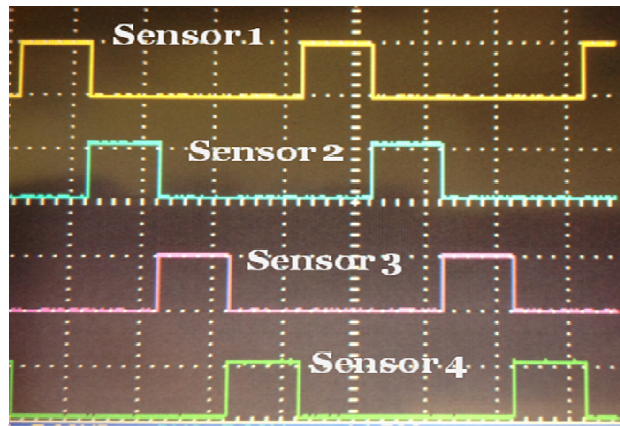
Figure 4.10: Sensors are sequentially addressed every second

In biofilm growth experiments, four chips were operated in parallel with 4 minutes switching time which is sufficient to monitor biofilm changes.

The biofilm growth area is designed as 1.2 mm length by 1 mm width to optimize generation of SAWs with a specific wavelength (12 µm)[27]. The biofilm treatment by an electric field for the bioelectric effect is imposed by additional electrodes along with the biofilm active area. Evaluation of total biomass changes in the chip is confined to the biofilm active area. Therefore, there is a need to confine biofilm growth on the area to investigate the device performance. A microfluidic biofilm reactor was assembled on the chip to achieve the restricted biofilm growth. Microfluidic biofilm reactors have been widely used for biological applications since the microchannel can provide more precise environment control over a macroscale setup as well as small volume requirement[31]. The fabrication of the channel is relatively simple compared to the traditional microfabrication methods. Typically the channel fabricated by PDMS can be disposable due to the low cost of process[165].

To have sufficient area for reversible boning between the PDMS microchannel and the chip, the overall dimension of the device was designed as 2.5 cm width by 2.5 cm length. The bonding was achieved by methanol[30]. The PDMS was soaked in methanol for 2 minutes and place on the chip overnight. Due to the methanol evaporation through the PDMS, reversible bonding was achieved based on Van der Waals forces. Through the channel, fresh growth media or antibiotics were continuously supplied by a syringe pump in withdrawal mode. Overview of the assembled system is shown in figure 4.11.
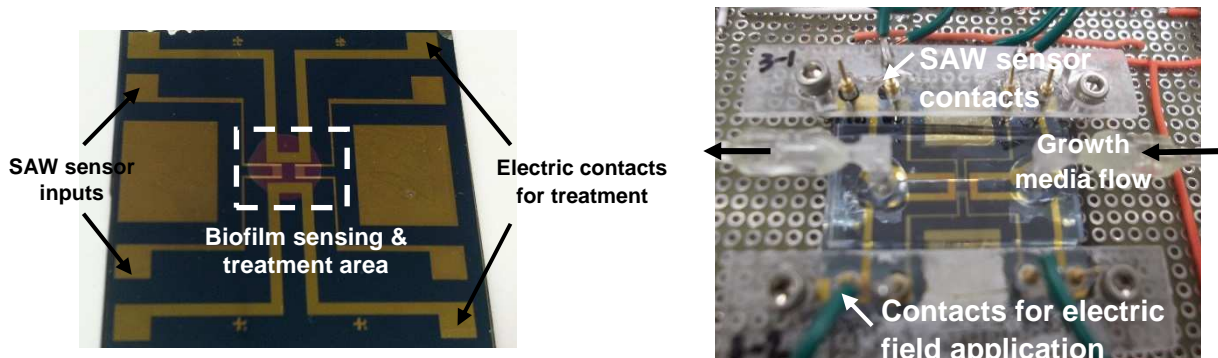
Figure 4.11: (a) Photo of the fabricated device. Electric pads are extended to have an effective contact with external instruments (e.g. network analyzer, power source). (b) Microfluidic reactor assembled chip with connections of growth media supply microtubes[32].

4.4 Experimental Procedures

Luria Broth (LB) bacterial growth media has become an industrial standard for *E. coli* cultivation far back in 1950's and it is the most common media used in molecular microbiology applications. Biofilm growth in the microfluidic channel with the integrated device was performed with a flow of the growth media. Continuous LB media supply

fostered biofilm growth that resulted in increase of total biomass.. LB media is mainly composed of yeast, NaCl, and amino acids. Amino acids, such as tryptophan, are the source for the protein synthesis needed for bacterial growth. NaCl produces an osmotic pressure balance of the bacteria in the media. Therefore, LB media provided favorable environment for *E. coli* as well as *P. aeruginosa* biofilm growth[166].   To prepare bacteria for the biofilm tests, a 20 μL frozen culture of *E. coli* K12 W3110 (wild type) was transferred into 5 mL of LB media in a cell culture tube. Then, the bacteria were cultured overnight in the 250 rpm shake incubator at 37 °C for 16 hours. The optical density (OD$_{600}$) was measured after the overnight culture growth, and the OD was typically in the 4.20 - 4.50 range. 1 mL of the overnight cultured bacteria was diluted 20 times by adding LB media to achieve the initial bacterial concentration to be OD$_{600}$ ≈ 0.21 - 0.23. For *Pseudomona aeruginosa* PAO1, a standard strain of the bacteria, preparation procedures are identical to the processes of *E. coli*.

Testing is performed by initially disinfecting the microfluidic channels of the integrated chip using 70 % ethyl alcohol under flow by the syringe pump. After rinsing with deionized water, bacterial suspensions, prepared as above, are inoculated without flow for 2 hours to allow for bacterial attachment to the substrate[30]. LB media is then continuously supplied to the channel for 24 hours at 20 µL/h, an effective flow velocity of 30 µm/s for the given channel dimensions (100 µm height, 2 mm width, and 2 cm length), to replenish nutrients and foster biofilm growth. Treatments are started after 24 hours of growth and continued for an additional 24 hours. To achieve an exchange of fluid sources during experiments with minimal disturbance, flow is stopped and the inlet tubing is transferred to the new source of media before reinitializing flow.

After biofilm growth, diverse treatment methods including control (no treatment), electric field only, bioelectric effect and antibiotic therapies were applied. Finally, at the end of the experiments, the total biofilm was quantified by a traditional method, such as a live/dead biofilm staining. During the entire biofilm experiments, the SAW sensor monitors the total biomass changes continuously by measuring its frequency changes.

Procedure	Details
1. Promote bacterial adhesion on the channel	Supply bacterial suspension for two hours (no flow)
2. Biofilm growth	Provide bacterial growth media for 24 hours
3. Biofilm treatment	Introduce difference treatments (no treatment, antibiotic, electric field and bioelectric effect for 24 hours)
4. Biofilm evaluation	Stain biofilm with live/dead dyes
5. Microscopy imaging work	Fluorescent microscope inspection

Table 4.2: Details of experimental procedures

4.5 Characterization of the Integrated System

4.5.1   Detection Limit of the SAW Sensor

Prior to biofilm tests, the mass detection limit of the SAW sensor was characterized. The SAW sensor sensitivity (frequency changes per unit mass; [Hz/g]) of the integrated device was characterized by measuring a resonant frequency shift due to a known mass loading. Based on the resolution of the SAW sensor resonant frequency measurement equipment (network analyzer, 0.1 Hz resolution), the detection limit [g] was calculated as shown in below.

$$Sensitivity = \frac{frequency\ shift}{loaded\ mass}[Hz/g]$$

$$Detection\ \lim it = \frac{resolution}{sensitivity}[g]$$

The known mass was loaded on the SAW propagating area of the sensor between input and output IDTs by filling the microfluidic channel with DI water (207 µg). The frequency changes were recorded by the network analyzer (HP8510B). Depending on the thickness of the passivation layer, different frequency shifts due to the initial mass loading by the passivation layer were expected. As the passivation thickness was increased, the detection limit of the sensor was decreased since more initial mass loading due to the thicker film reduced the mass sensitivity. The Al_2O_3 film layer was deposited 55 nm, 100 nm and 110 nm to prevent ZnO damages from the long term growth media exposure. The sensitivity of the different SAW sensor was presented in table 4.3.

	Sensor #1	**Sensor #2**	**Sensor #3**	**Sensor #4**
ZnO	~ 500 nm	~ 500 nm	~ 500 nm	~ 500 nm
Al_2O_3	55 nm	100 nm	100 nm	110 nm
Δf	1.22 MHz	271 KHz	341 KHz	125 KHz
Detection Limit	17 pg	76 pg	61 pg	166 pg

Table 4.3: Summary of the SAW sensor characterization

The detection limit characterized by experiments was decreased from 17 pg to 166 pg as the thickness of Al_2O_3 film was increased from 55 nm to 110 nm. This is expected since the passivation film causes attenuation of acoustic wave propagation as well as energy loss from the ZnO to the Al_2O_3 film where biofilms are actually grown. This energy loss is due to the mechanical property mismatch including shear modulus and density. As a result, minimum detectable mass by the sensor was approximately in tens or hundreds pico-gram ranges that are 6 orders decrease of the sensitivity compared to the state of art SAW sensor[72]. However, this is still applicable sensitivity for biofilm detection considering a bacterium mass is ~ 1 pg[27] and biofilms are comprised of typically more than millions of bacteria[6].

4.5.2 Discussion

Since the SAW sensor is required to have a passivation film to prevent ZnO degradation due to the growth media contact, the sensitivity loss compared to the non-passivated sensor was taken as a trade-off between a highly sensitive sensor and reliable operation of the system. Theoretical work to analyze the loss of detection limit was conducted concentrated on the effect of different materials to the sensitivity loss of the system. The analysis was focused on the mechanical acoustic wave energy loss in multilayer composition of the structure. Based on the model, a specific material for the passivation film was chosen from the candidate material. In the derived equation, attenuation of the SAWs was related with the shear modulus, density, thickness of the passivation layer on the ZnO.

The characterization of the sensor was performed on the only Al_2O_3 passivated SAW sensor with different thicknesses of the film. Thus, it may not be appropriate to compare the model to the test results (table 1). However, through this comparison, it was expected to see the limitations of the current model that would be critical to have further sophisticated theory development for future work. To compare the experimental characterization results with the model calculation, the raw data was normalized respected to the non-passivated SAW sensor and the results from different thickness of the Al_2O_3 film are shown in figure 4.12.
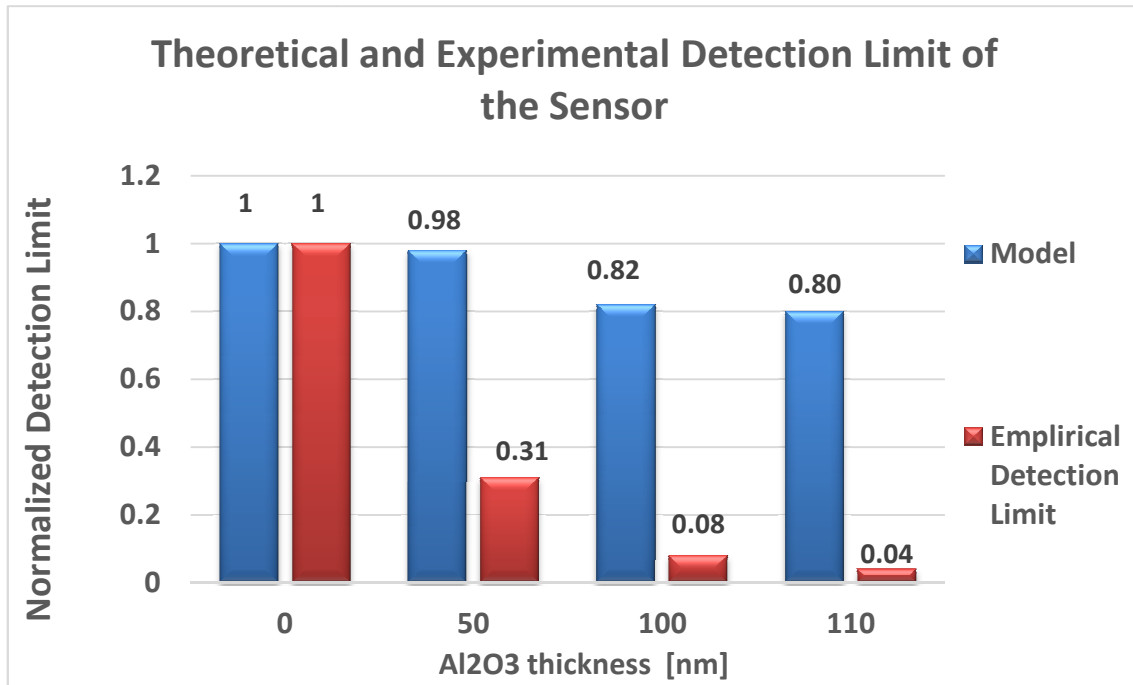
Figure 4.12: Normalized sensitivity of the equation (9) in chapter 2 and experimental results from table 4.3. The sensitivity was normalized respected to the sensitivity of non-passivated SAW sensor.

As shown in figure 4.12, the results are not exactly matched since there are assumptions to simplify the calculations in the model, such as the speed of the SAW at the bottom and top regions of the ZnO layer are identical (no dispersion). Intensities of the mechanical displacement (acoustic wave) induced at the piezoelectric layer are maximized where the electric potential is applied (interdigitated electrode transducer, IDT). Typically, groups of acoustic waves are induced since the piezoelectricity of the film is not a completely homogeneous[167]. The majority of the SAW is determined by the electrode distance of the IDT (section 2.1.1). As the acoustic wave propagated further toward the bulk substrate from the IDT patterned area, the velocity of partial waves can be changed due to energy loss in energy conversion between mechanical and electrical energy domains as well as

interference among the groups of the SAWs resulting in dispersion of the wave propagation[146]. This dispersion can be more dominant in the inverted SAW sensor than the traditional structure where molecules of interest react at the IDT patterned surface. However, in the model, it was assumed that no dispersion in the ZnO layer can be contributed to the calculation error compared to the experimental results. The adhesion between the ZnO and passivation film is also assumed to be ideal in the analysis, which may not be perfect compared to the single layer film versus multilayer structure.

The experimental data for the sensitivity was shown to be four times lower than the theoretical values. In the modeling, the total effective shear modulus of the multilayers of dielectric material on the piezoelectric layer was assumed as a series connection to transfer the mechanical energy between the layers[27]. However, in real energy transfer between the layers, the induced mechanical displacement energy on the piezoelectric film by an electrical signal cannot be transferred to the non-piezoelectric layer completely as a series connection, since there is significant energy loss or reflection at the boundary of the two layers[168].
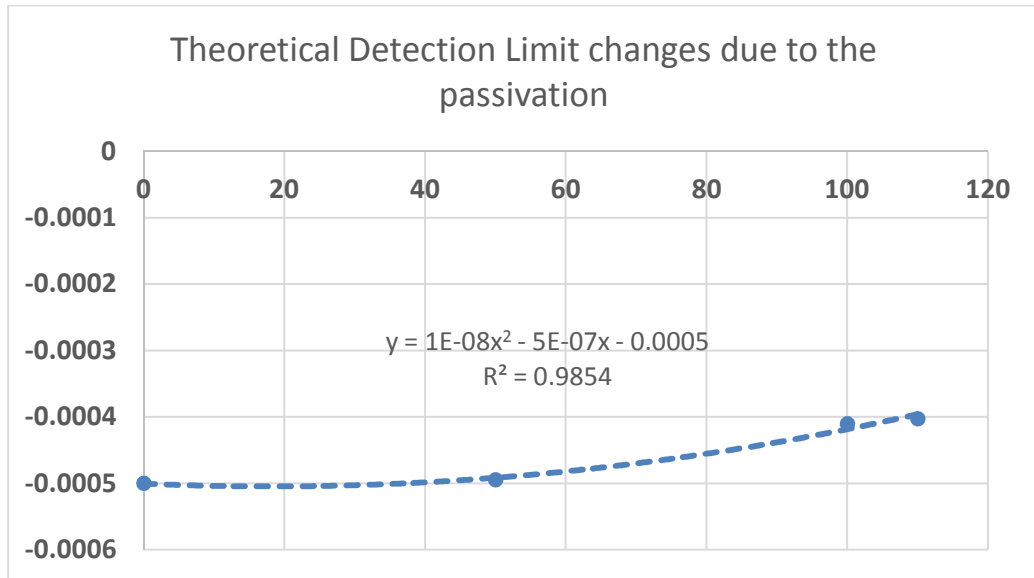
Figure 4.13: Theoretical sensitivity changes in different passivation thicknesses.
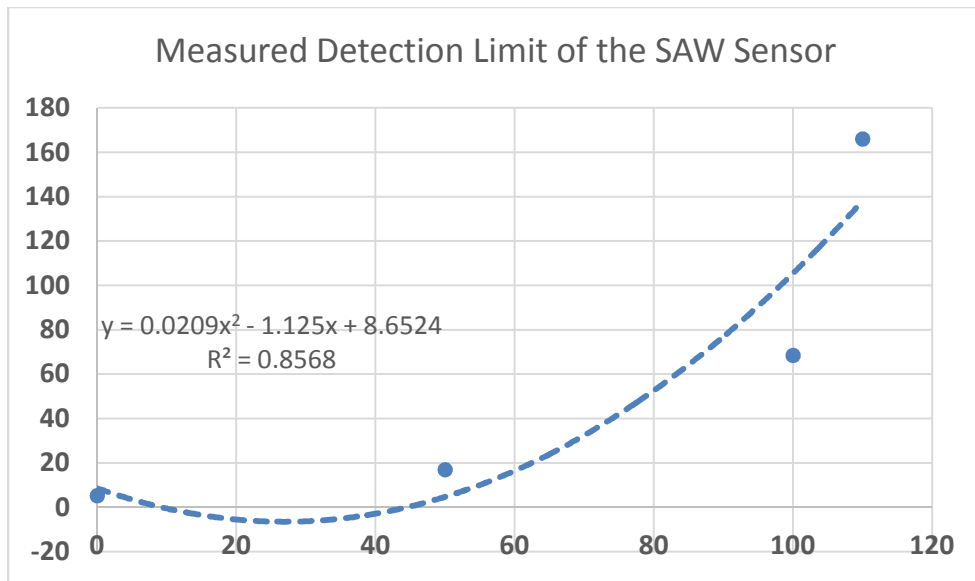
Figure 4.14: Experimental data of the normalized sensitivity of the SAW sensor. Its trend also approximate to polynomial (2 orders) of relation between the thickness of the passivation film and the sensitivity.

However, the trend of sensitivity changes of the theoretical and experimental data can be closely related as shown in figure 4.13 and 4.14. The orders of magnitude of the trend line were approximately in the second order polynomial for both the theoretical and experimental results. Considering the purposes of the modeling that was focused on investigating the impact of different materials to the sensitivity as well as the applied assumptions, this approximation can be validated.

Typical measured sensitivity of the SAW sensor was in the hundreds of pico-gram even for 110 nm passivated sensors. Thisis extremely sensitive for biofilms, (approximately three orders of magnitude) which are usually more than hundreds of nano-gram total biomass. With this experimental characterization of the SAW sensor, it has been demonstrated that a highly sensitive detection limit for bacterial biofilm applications can be achieved. Although the model contributed to select appropriate materials as passivation layers among other candidates, the theory can be further developed to analyze mechanical energy transfer in multilayer structures that are comprised of piezoelectric and dielectric films.

4.6 Biofilm Monitoring of the Integrated System

4.6.1 *Escherichia coli* Biofilm

E. coli (wild type: K-12 W3110) is tested with the integrated system as a model biofilm[169] (figure 5.8). The bacteria was introduced to the microfluidic channel (100 µm height, 2 mm width and 2 cm length) after inoculation of the frozen sample. The increase of total biomass was monitored by the SAW sensor based on the speed decrease of the wave. The recorded frequency changes are presented in figure 4.15.
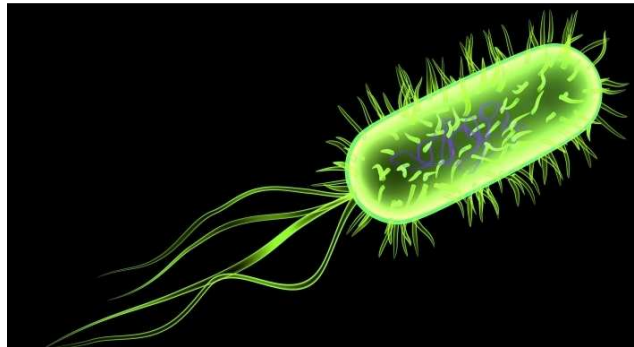
Figure 4.15: Schematic of *Escherichia coli* (Gram negative bacteria)[170]

The resonant frequency of the sensor decreased by approximately 2 MHz due to the significant total mass increase in the biofilm growth after 24 hours. In all experiments, *E. coli* biofilm was established quickly over 10 hours with a continuous supply of fresh bacterial growth media. Once biofilms matured, the total biomass was not changed significantly due to the limit of nutrient diffusion into the biofilms. After the biofilms were treated by different methods (no treatment, only antibiotic, only SP field, and SP-field with the antibiotic), the SP-BE showed approximately a 1.6 MHz resonant frequency increase from the start of treatment which corresponds to the reduction of total

biomass, while antibiotic or electric field treatment only do not show any frequency changes (no biofilm reduction).
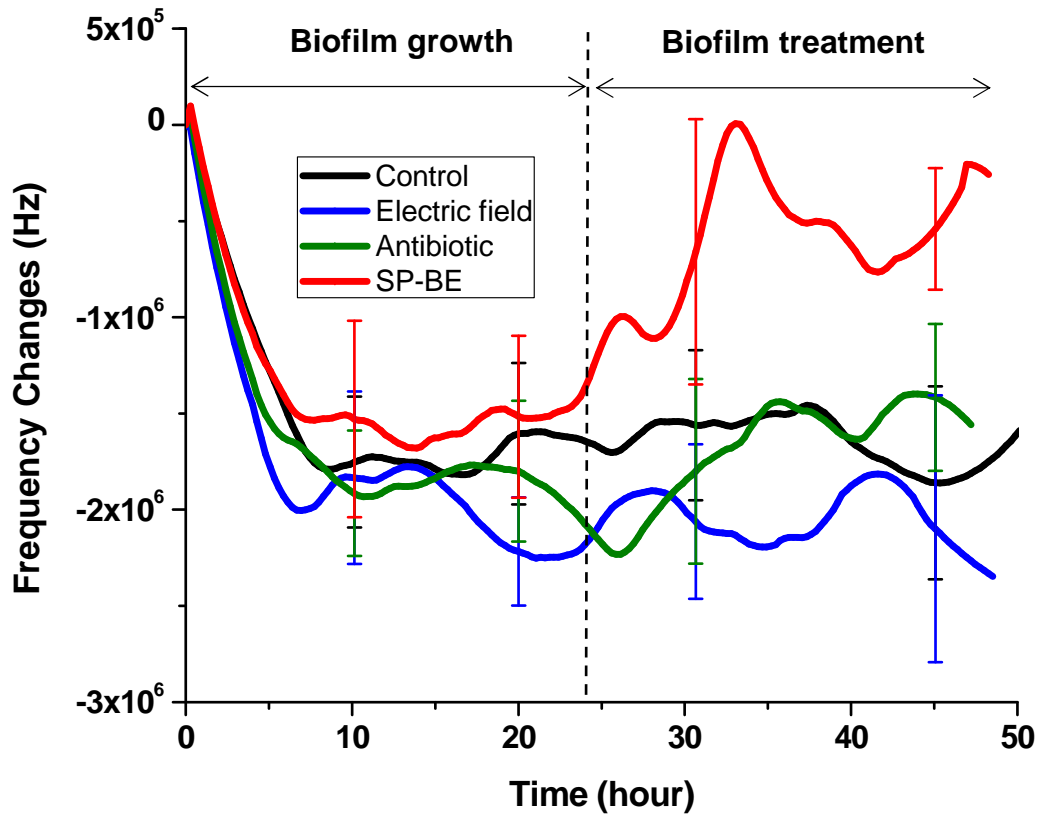
Figure 4.16: Graph showing the resonant frequency of the SAW sensor tracking the changes in biomass due to four different biofilm treatments initiated after 24 hours of biofilm growth. Only the SP-BE demonstrates significant biomass reduction (80% reduction of total biomass)[32].

Since biofilm treatment typically requires one thousand times more antibiotic than treatment of suspended bacteria (~ 5 µg/mL of gentamicin), antibiotic treatment only (10 µg/mL of gentamicin) administered by itself does not show effective biofilm reduction. This is mainly due to the extracellular matrix of biofilms that prevent drug penetration

through the matrix. The biofilm treated with electric field only is not effectively inhibited since intensity of the electric signal (0.25 V) lower than the threshold of electrolysis (0.82 V) is not sufficient to impose biocidal effects on the biofilm as suggested in previous literature[112]. The SP-BE treatment that combines the SP field with the antibiotic demonstrated 80% more biomass reduction than antibiotic treatment alone. This result shows the increased biofilm reduction based on the principles of the bioelectric effect. The combination of the AC and DC electric field may induce a synergy between AC and DC bioelectric effect mechanisms, including increase in permeability of the biofilms due to the AC component and non-uniform distribution of electrolytes due to the DC component. In addition, it is demonstrated that antibiotics has to be applied simultaneously with an electric field to induce enhanced biofilm treatment from the comparison between the SP-field and SP-BE results.

As biofilms are grown, the sensitivity of the SAW sensor also decreases due to the additional mass loading compared to the initial pristine sensor. The non-linearity between the mass loading and SAW velocity changes has already been studied (section 2.1.1). Thus, the frequency changes of the sensor can be directly converted to the biomass based on the empirically characterized sensitivity of the system.

After biofilm experiments are completed, the biofilms were stained by a live/dead (green/red) fluorescent dye to visualize viable bacteria in biofilms. Representative images of each treatment are shown in figure 4.17. No treatment applied biofilm (control) shows significant green bacteria in biofilms that correspond to low biofilm treating efficacy. Either solely antibiotic or electric field treated biofilms show much more green stained

bacterial surface coverage than the SP-BE applied biofilm (figure 4.17d). These results

are in parallel to the total biomass changes monitored by the SAW sensor.

Control (no treatment)   Antibiotic (Gentamicin 10µg/mL)

SP field (AC + DC fields)   SP-BE (SP field +

Gentamicin)
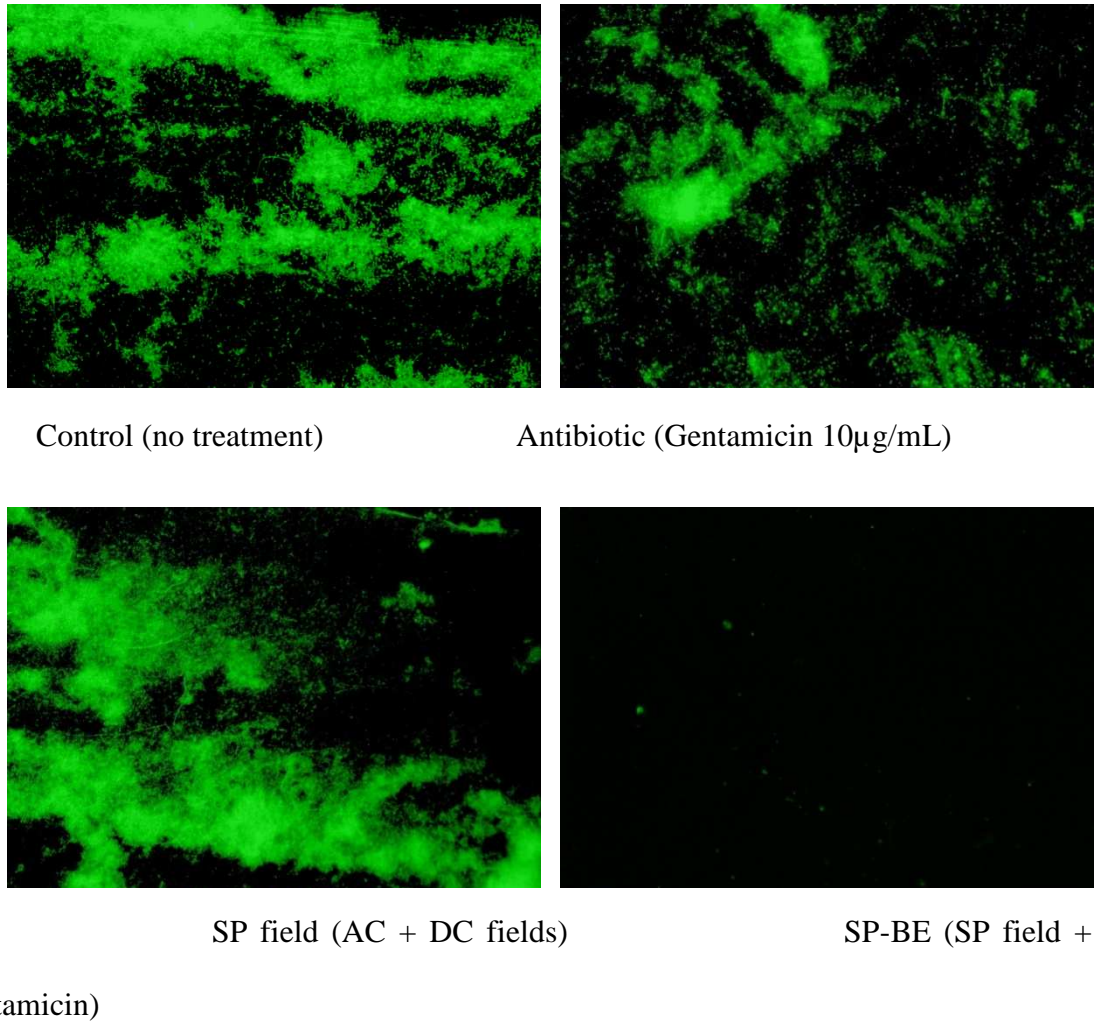
Figure 4.17: Representative fluorescence microscopy images after different biofilm
treatment. The green bacteria indicate live cells in biofilm. The SP-BE treated *E. coli*
biofilm show significantly reduced live cells in biofilm compared to the traditional
antibiotic therapy[32].

4.6.2 *Pseudomonas aeruginosa* Biofilm

Pseudomonas aeruginosa is one of the major bacterial strains that cause severe hospital infections[171]. *P. aeruginosa* are categorized as gram negative bacteria that comprise double layers of cell membrane. Since both *E. coli* and *P. aeruginosa* are gram negative bacteria, cell membrane structures are expected to be closely related which is critical to the principles of activity mode of the bioelectric effect. Either AC or DC electric field impacts \ the membrane based on partial charges from the protein and lipid bilayer compositions of the cell membrane[172]. Based on the previous *E. coli* biofilm treatment demonstration in this thesis work in addition to other literature[173], it is expected *P. aeruginosa* biofilm can also be treated by the bioelectric effect.
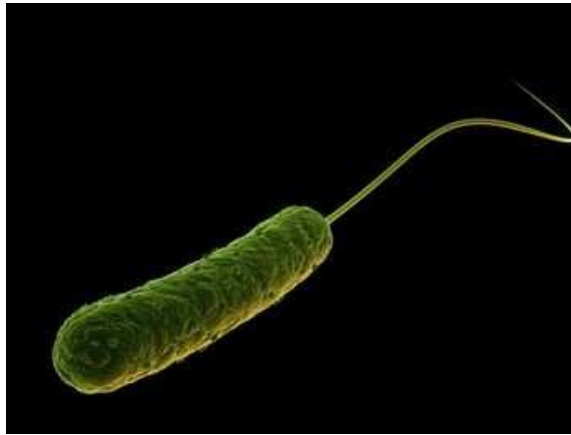
Figure 4.18: Schematic of *Pseudomonas aeruginosa* (Gram negative bacteria)[174]

The experimental procedures are identical to the previous *E. coli* biofilm tests. *P. aeruginosa* PAO1 biofilm was matured in the microchannel for 24 hours and followed by four different treatments: (1) control (no treatment), (2) only SP field (1.25 V/cm

amplitude sinusoidal signal with 1.25 V/cm DC offset), (3) only gentamicin (10 µg/mL) and (4) SP-BE (SP field with the gentamicin). The frequency shifts result from the SAW sensor during the biofilm experiments are shown in figure 4.19.
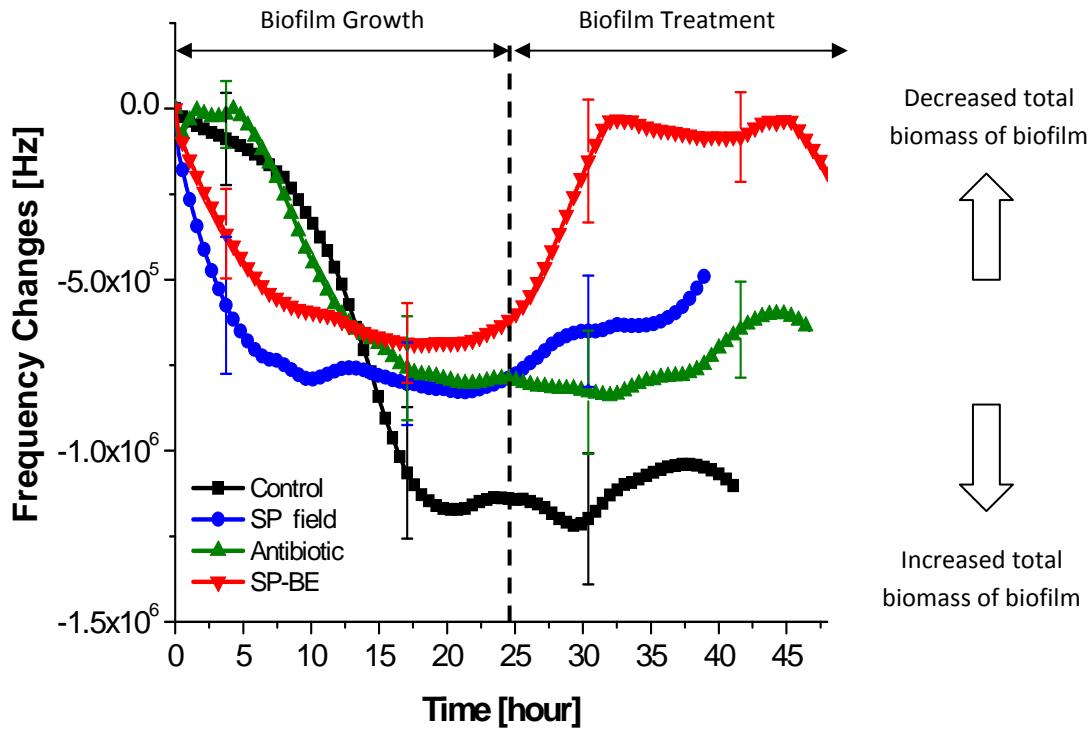
Figure 4.19: Changes of the resonant frequency of the SAW sensor in *P. aeruginosa* biofilm experiments. The results also showed significant biofilm reduction by the SP-BE compared to the other treatments.

As shown in the results, the *P. aeruginosa* biofilms are established within 20 hours during the growth stage. After maturation, the biofilms are in a saturation phase since fresh nutrient diffusion is limited by the extracellular matrix of the biofilm. In biofilm treatments, significantly reduced biofilms were measured when the SP field was

combined with the antibiotics (SP-BE). This result is also in parallel to the previous *E. coli* biofilm tests.

After the experiment, biofilms are stained by the live/dead (green/red) dye and investigated by a fluorescent microscope. Representative images of each treatment are shown in figure 4.20. The results also support that significant *P. aeruginosa* biofilm reduction by the SP-BE has been demonstrated.
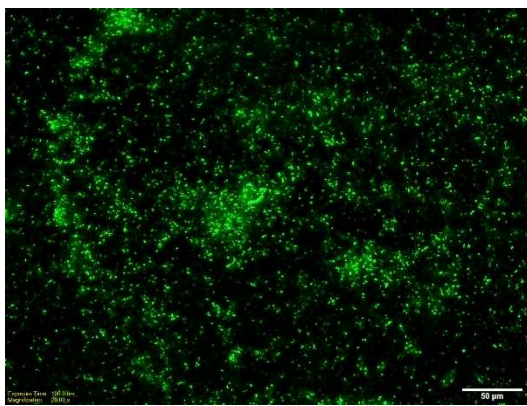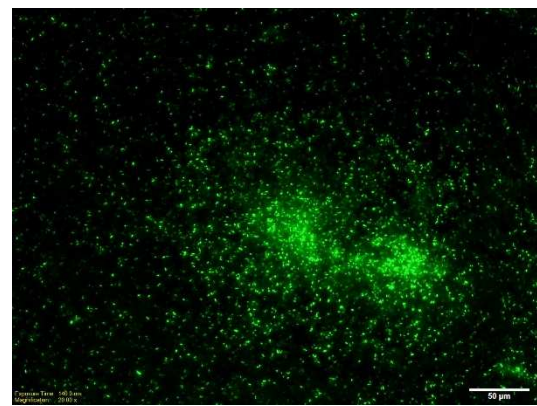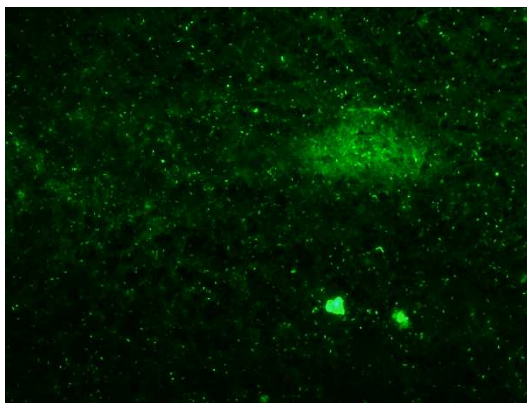
Control (no treatment)	Antibiotic (Gentamicin 10 µg/mL)
SP electric field	SP-BE (SP field + Gentamicin)

Figure 4.20: Representative fluorescence microscopy images after four different biofilm treatment. The green fluorescence indicates live cells in biofilm. *P. aeruginosa* biofilm treated by the SP-BE shows significantly reduced live cells in biofilm compared to the traditional antibiotic therapy.

4.6.3 Discussion

The integrated system of the SAW sensor and bioelectric effect successfully demonstrated the biofilm detection and treatment in both *E. coli* and *P. aeruginosa* biofilm experiments. Two different strains of biofilm are expected to induce enhanced biofilm treatment efficacy by the bioelectric effect based on the membrane structure of bacteria (gram negative bacteria)[175] and literature[152]. Since the established hypothesis for the mechanisms of bioelectric effect is focused on bacterial cell membrane effect by external electric field applications[112], the same membrane structure between *P. aeruginosa* and *E. coli* was a critical substance to expect significant biofilm reduction due to the bioelectric effect. The membrane is comprised of double layer of phospholipid bilayer as shown in figure 5.14. There are a lot of partial charges in the membrane that can be distorted by an external electrostatic force. With this induced bacterial membrane attenuation due to the electric field, biofilm treatment efficacy can be dramatically enhanced with small doses of antibiotics[176]. Comprehensive studies with diverse strains of bacteria have been conducted in the literature[65] and demonstrated enhanced biofilm reduction when electric fields were applied with antibiotics simultaneously[65]. Therefore, results from this integrated system also correspond to the suggested mechanisms of the bioelectric effect to both *E. coli* and *P. aeruginosa* biofilms.
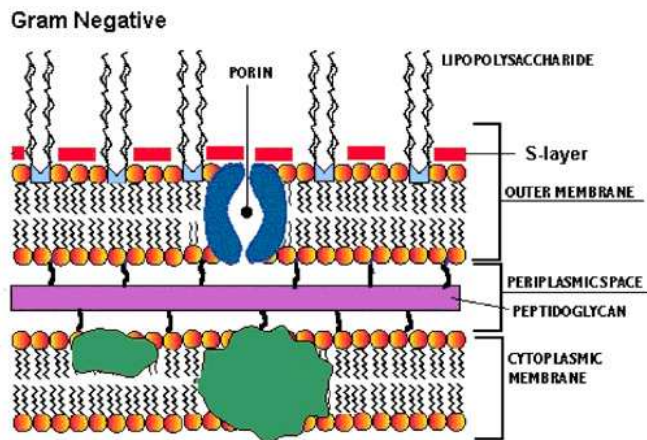
Figure 4.21: Schematic of gram negative bacteria. It shows double layers of membrane opposed to gram positive bacteria which have only a single layer of cell membrane. Both *E. coli* and *P. aeruginosa* bacteria are categorized in the gram negative bacteria[177].

In the SAW sensor results of two bacterial biofilms, the improved efficacy of the biofilm reduction was closely correlated in terms of total biomass changes. In *E. coli* experiments, 80% reduction of biofilm was approximately observed compared to other treatments. *P. aeruginosa* biofilm similarly showed 70% total biofilm decrease. Since the noise level of the resonant frequency monitoring was not able to distinguish within 1% level of biomass changes, it was not appropriate to analyze the biofilm differences in detail. These noise effects mainly originated from the setup which can contribute to include non-uniform distribution of nutrients[178], electric interference between the samples due to the proximity of each sample[179], possible inadequate electric contact via spring loaded pins and slight thermal local non-uniformity in the growth chamber[180]. For more sophisticated investigations of biofilm changes, electrical isolation between external power supply and each device is necessary although the current setup is able to detect the biofilm changes successfully.

165

The device was reused typically five times in consecutive biofilm experiments based on the ZnO film passivation by the ALD Al_2O_3 film. A 500 nm of ZnO layer was completely dissolved within 3 hours without the Al_2O_3 film coating due to the high chemical reactivity of the Zn compared to the hydrogen ion (see section 2.1.3). ALD provided a conformal and high density film compared to other physical vapor deposition methods including sputtering and evaporation. Thus, the ALD was an enabling technology to protect the piezoelectric ZnO layer from the growth media diffusion. This effective passivation resulted in significantly extended life time of the device from three hours to about a week. However, after the chip has been used more than five times , the ZnO layer was still damaged due to extended growth media exposure. The surface of the sensor was inspected via an optical microscope (figure 4.22) that showed ZnO damage.
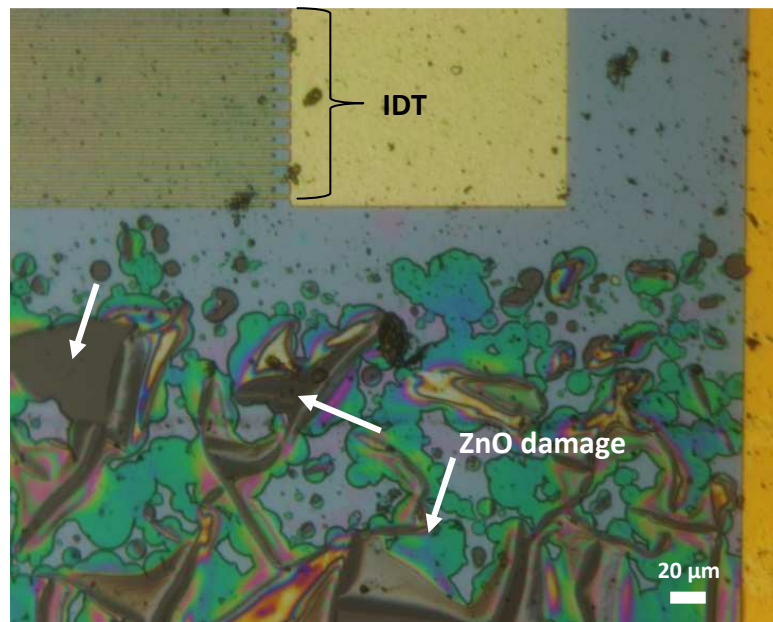
Figure 4.22: Optical microscopy image of the ZnO layer after five times of consecutive biofilm growth experiments. ZnO layer was damaged due to the growth media exposure through the passivation layer (arrows indicate ZnO damages).
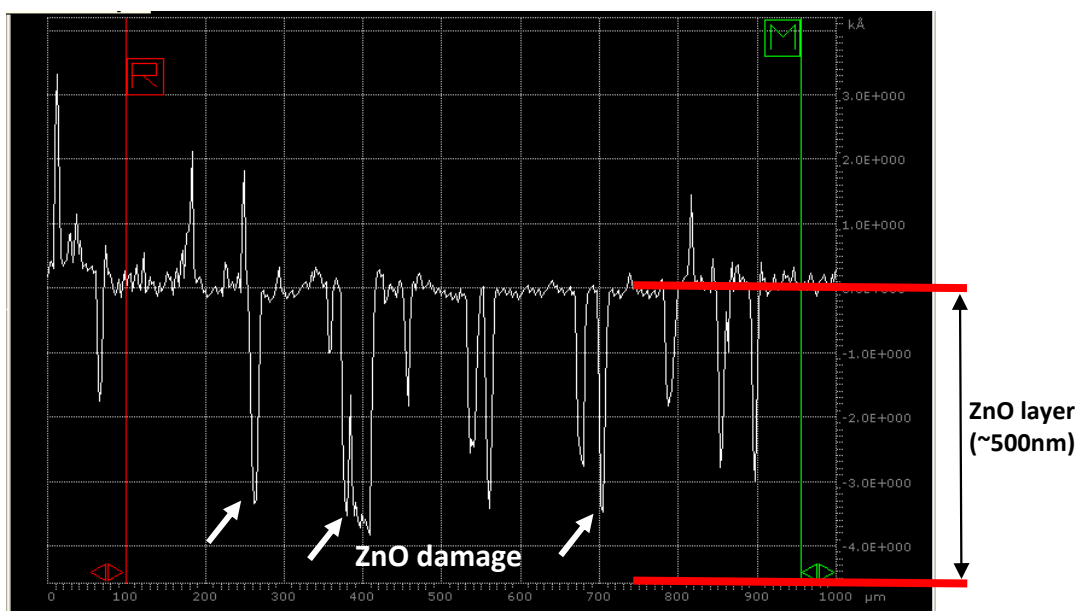
Figure 4.23: Profile of the ZnO damaged surface after five times consecutive uses of the device for biofilms. The depth of surface damaged points (arrows indicates damaged surface) are around 400 nm which is close to the ZnO thickness.

The surface profile of the damaged ZnO layer was investigated using a contact profiler (Veeco Dektak 6M Surface Profiler) as shown in figure 5.16. The depth of surface damaged area is close to the thickness of the ZnO (500 nm) that indicates bacterial growth media penetrated into the ZnO through the Al_2O_3 film. Once the piezoelectric layer is degraded, acoustic waves cannot be induced resulting in failure of biomass detection. Even if the single ALD Al_2O_3 film improved the device life time significantly, the reliable operation of the device can be further prolonged using multilayer thin film deposition[181]. For instance, multilayer thin film fabrication by ALD for gas diffusion barrier was demonstrated[182]. However, the sensitivity degradation due to the multilayer of dielectric films should be investigated via sophisticated numerical models as well as experimental studies as a future work.

4.7 Summary

The sensing component of the system was characterized focused on the detection limit with a known mass loading and showed extremely high sensitivity for biofilms detections. Quantitative electrolysis analysis when an electric field was applied to the growth media was conducted using a pH indicator. The result concluded that the SP field does not induce major electrolysis compared to the threshold voltage applied samples. This result suggests that the potential mechanisms of the enhanced biofilm inhibition due to the SP field can be due to the superposisition of the AC and DC methods rather than creating electrochemical radical ions by electrolysis.

The integrated microsystem successfully demonstrated real-time biofilm detection as well as effective inhibition. Both *E. coli* and *P. aeruginosa* biofilms were tested with the system. With matured biofilms, the electric field provided by the planar electrodes with small doses of the antibiotic gentamicin showed significant total biomass reduction in both bacterial biofilms. The continuous biofilm monitoring was demonstrated by measuring resonant frequency shifts of the SAW sensor. At the end of the biofilm experiment, biofilms were stained by a live/dead fluorescence dye to confirm the biofilm surface coverage reduction through the traditional method. The fluorescence images were in good agreement with the resonant frequency results from the device. This systematic integration of the biofilm sensor with the treatment method as a single platform will advance in managing biofilm associated problems based on the small dimension and low electric power consumption. Furthermore, this platform can be applied for fundamental chemical and biological research, such as for drug discovery studies.

Chapter 5: Conclusions

5.1 Summary of Accomplishments

Biofilms are extremely difficult to eradicate when they are established due to their complex structures. As a result, bacterial biofilms cause severe clinical infections. Revisional surgery and care cost in excess of $500,000 per patient, amounting to more than $2 billion annually in the United States. Therefore, it is crucial to alert patients at the early stage of biofilm growth to prevent maturation into severe biofilm infections. In addition, a highly effective non-invasive biofilm treatment method is desirable to prevent additional surgeries for the treatment.

In this dissertation work, a microsystem for effective bacterial biofilm management through real time biofilm detection and integrated enhanced treatment method was successfully designed, fabricated and demonstrated as a single platform. In the biofilm sensor development, a numerical analysis model suggested focusing on the evaluation of the sensitivity of the sensor with different passivation films. Through the model, a passivation material was selected. The key parameters of the derived equation are density, thickness and shear modulus of the passivation material that can be varied in other similar multilayer analysis which involves the elastic modulus. The sensor was shown to have highly sensitive and reliable biofilm detection performance. The sensor was reusable based on the effective passivation film preparation deposited by the atomic layer deposition. Based on these theoretical analysis and fabrication process developments to extend life time of the device, real time biofilm monitoring was successfully achieved which is significant for effective biofilm managements.

Since biofilm treatment typically requires 500-5000 times of antibiotics, an enhanced biofilm treatment method has been developed in a traditional millimeter-scale cuvette setup and transferred the new technology into a micro-scale device as parts of the thesis work. Vastly improved treatment of biofilms was demonstrated by employing a superpositioned (SP) electric field in conjunction with an antibiotic. The SP bioelectric effect (SP-BE) was greater than the sum of the bioelectric effects of the DC and AC fields independently. Thus, it is suggested that the SP field enables a synergistic effect that yields more bacteriocidal activity when both DC and AC fields are applied. This newly developed method can be highlighted that the intensity of the SP electric field utilized here was well below the electrolysis potential of the biological fluid. Hence, we envision applications of this technique that would minimize generating harmful radicals due to media electrolysis. Perhaps most importantly, these findings suggest that this method is aptly suited for deployment in clinical applications.

Finally, the biofilm sensor and bioelectric treatment were successfully integrated as a single platform via microfabrication technologies. Integration of the biofilm detection with effective treatment is crucial to realize effective managements of biofilm infections through bidirectional biofilm information exchanges from the sensor and treatment. As the sensing component provides the early detection of biofilm growth, the biofilm treatment via the SP-BE can be more effective before establishing their structures. In addition, when biofilms are treated by the bioelectric effect, this integrated chip allows to monitor changes of biofilms in real time without requiring additional external bulk equipment. The integrated chip was also shown successful operations with two different strains of biofilm (i.e. *E. coli* and *P. aeruginosa*). These results suggested that the

integrated system can be used for diverse biofilms. The utilization of the system to more clinically relevant bacterial biofilms is significant for realizing this device approaches to the clinical biofilm infection managements.

This work can be used as a platform for other biological/clinical fundamental researches, such as bacterial metabolism with in different drug treatments and investigation of the mechanisms of action of new bacterial treatment methods including the bioelectric effect[112].

5.2 Future Work

The integrated system can be further developed with a wireless system as a signal read out as well as operational power supply methods. The SAW sensor requires only micro-watts of electrical energy[183]. In addition, the bioelectric effect is needed to supply nano-watt of electrical energy which can be delivered by a traditional radio-frequency (RF) inductive coupling[184]. A RF coil can be microfabricated with a specific resonant frequency[185]. The coil will be tuned to maximize the electric energy coupling for the SAW sensor from an external power supply. This wireless system development is critical to realize a non-invasive biofilm management and significantly advance point of care and further implantable microsystem developments based on the batteryless operation.

Investigation of the life time of the system in an in-vivo environment is required future work toward an implantable system development. Considering variable conditions of in-vivo fluidic, such as pH, temperature, compositions of electrolytes, immune reaction from the host and water concentration or viscosity of blood, the passivation film characterization during extensive blood or serum exposure is required. Based on the studies in in-vivo conditions, new passivation material/fabrication techniques including multilayers ALD thin films fabrication[158, 159] need to be developed for long term reliable operations.

Finally, once the reliability of the device is investigated, animal tests are required to study biocompatibilities as well as performance evaluation of the system in in-vivo conditions. As the immune system can react with the device including specific and non-specific responses, biofouling of the implanted system[186] can cause massive signal

attenuations and challenges of the output readout especially through a wireless interface. In addition, broad immune reaction studies with electrolysis effect due to the biofilm treatment should be performed.

Appendix A

Network analyzer data save program (S$_{11}$)

```c
/*
 * Include the WINDOWS.H and DECL-32.H files. The standard Windows
 * header file, WINDOWS.H, contains definitions used by DECL-32.H and
 * DECL-32.H contains prototypes for the GPIB routines and constants.
 */

#include "stdafx.h"
#include <stdio.h>
#include <time.h>

#define ARRAYSIZE 100          // Size of read buffer

int  Dev;                      // Device handle
char ReadBuffer[ARRAYSIZE + 1]; // Read data buffer
char ErrorMnemonic[21][5] = {"EDVR", "ECIC", "ENOL", "EADR", "EARG",
                "ESAC", "EABO", "ENEB", "EDMA", "",
                "EOIP", "ECAP", "EFSO", "", "EBUS",
                "ESTB", "ESRQ", "", "", "", "ETAB"};


void GPIBCleanup(int Dev, char* ErrorMsg);


int _cdecl main(void)  {

/*
 *
 ================================================================
 =========
 *
 * INITIALIZATION SECTION
 *
 *
 ================================================================
 =========
 */

/*
 * Assign a unique identifier to the device and store in the variable
 * Dev.  If the ERR bit is set in ibsta, call GPIBCleanup with an
 * error message. Otherwise, the device handle, Dev, is returned and
 * is used in all subsequent calls to the device.
```

```c
 */
#define BDINDEX            0     // Board Index
#define PRIMARY_ADDR_OF_DMM  16    // Primary address of device
#define NO_SECONDARY_ADDR    0    // Secondary address of device
#define TIMEOUT           T10s  // Timeout value = 10 seconds
#define EOTMODE           1     // Enable the END message
#define EOSMODE           0     // Disable the EOS mode

  Dev = ibdev (BDINDEX, PRIMARY_ADDR_OF_DMM,
NO_SECONDARY_ADDR,
          TIMEOUT, EOTMODE, EOSMODE);
  if (ibsta & ERR)
  {
    GPIBCleanup(Dev, "Unable to open device");
    return 1;
  }

/*
 * Clear the internal or device functions of the device.  If the error
 * bit ERR is set in ibsta, call GPIBCleanup with an error message.
 */

  ibclr (Dev);
  if (ibsta & ERR)
  {
    GPIBCleanup(Dev, "Unable to clear device");
    return 1;
  }

/*
 *
=================================================================
=========
 *
 * MAIN BODY SECTION
 *
 * In this application, the Main Body communicates with the instrument
 * by writing a command to it and reading its response. This would be
 * the right place to put other instrument communication.
 *
 *
=================================================================
=========
 */

/*
```

```
 *  Request the identification code by sending the instruction '*IDN?'.
 *  If the error bit ERR is set in ibsta, call GPIBCleanup with an error
 *  message.
 */



        ibwrt (Dev, "MARKMINI;OUTPACTI", 17L);
   if (ibsta & ERR)
   {
     GPIBCleanup(Dev, "Unable to write to device");
     return 1;
   }

/*
 *  Read the identification code by calling ibrd. If the ERR bit is
 *  set in ibsta, call GPIBCleanup with an error message.
 */

   ibrd (Dev, ReadBuffer, ARRAYSIZE);
   if (ibsta & ERR)
   {
     GPIBCleanup(Dev, "Unable to read data from device");
     return 1;
   }

/*
 *  Assume that the returned string contains ASCII data. NULL terminate
 *  the string using the value in ibcntl which is the number of bytes
 *  read in. Use printf to display the string.
 */
/* time example */


   ReadBuffer[ibcntl] = '\0';
   printf("Returned string:  %s\n", ReadBuffer);

        //Create a file to write to
   FILE *OutFile = fopen("S21freq.txt","a");
   //Send data to file
   fprintf(OutFile,"%s\n",ReadBuffer);
   //Close the file
   fclose(OutFile);

ibwrt (Dev, "OUTPMARK;MARKMINI", 17L);
   if (ibsta & ERR)
```

```c
    {
      GPIBCleanup(Dev, "Unable to write to device");
      return 1;
    }

/*
 *  Read the identification code by calling ibrd. If the ERR bit is
 *  set in ibsta, call GPIBCleanup with an error message.
 */

    ibrd (Dev, ReadBuffer, ARRAYSIZE);
    if (ibsta & ERR)
    {
      GPIBCleanup(Dev, "Unable to read data from device");
      return 1;
    }

/*
 *  Assume that the returned string contains ASCII data. NULL terminate
 *  the string using the value in ibcntl which is the number of bytes
 *  read in. Use printf to display the string.
 */

    ReadBuffer[ibcntl] = '\0';
    printf("Returned string:  %s\n", ReadBuffer);

        //Create a file to write to
    FILE *OutFile1 = fopen("S11intensity.txt","a");
    //Send data to file
    fprintf(OutFile1,"%s\n",ReadBuffer);
    //Close the file
    fclose(OutFile1);


/*
 *
 ================================================================
 =========
 *
 * CLEANUP SECTION
 *
 *
 ================================================================
 =========
 */
```

```c
/*  Take the device offline.                                    */

    ibonl (Dev, 0);

    return 0;

}


/*
 *  After each GPIB call, the application checks whether the call
 *  succeeded. If an NI-488.2 call fails, the GPIB driver sets the
 *  corresponding bit in the global status variable. If the call
 *  failed, this procedure prints an error message, takes the
 *  device offline and exits.
 */
void GPIBCleanup(int ud, char* ErrorMsg)
{
  printf("Error : %s\nibsta = 0x%x iberr = %d (%s)\n",
        ErrorMsg, ibsta, iberr, ErrorMnemonic[iberr]);
  if (ud != -1)
  {
    printf("Cleanup: Taking device offline\n");
    ibonl (ud, 0);
  }
}
```

Network analyzer data save program (S$_{21}$)

```c
/*
 *  Include the WINDOWS.H and DECL-32.H files. The standard Windows
 *  header file, WINDOWS.H, contains definitions used by DECL-32.H and
 *  DECL-32.H contains prototypes for the GPIB routines and constants.
 */

#include "stdafx.h"
#include <stdio.h>
#include <time.h>

#define ARRAYSIZE 100          // Size of read buffer

int  Dev;                      // Device handle
char ReadBuffer[ARRAYSIZE + 1]; // Read data buffer
char ErrorMnemonic[21][5] = {"EDVR", "ECIC", "ENOL", "EADR", "EARG",
                "ESAC", "EABO", "ENEB", "EDMA", "",
                "EOIP", "ECAP", "EFSO", "", "EBUS",
                "ESTB", "ESRQ", "", "", "", "ETAB"};


void GPIBCleanup(int Dev, char* ErrorMsg);


int _cdecl main(void)  {

/*
 *
 ==============================================================
 =========
 *
 * INITIALIZATION SECTION
 *
 *
 ==============================================================
 =========
 */

/*
```

```
 *  Assign a unique identifier to the device and store in the variable
 *  Dev.  If the ERR bit is set in ibsta, call GPIBCleanup with an
 *  error message. Otherwise, the device handle, Dev, is returned and
 *  is used in all subsequent calls to the device.
 */
#define BDINDEX              0    // Board Index
#define PRIMARY_ADDR_OF_DMM  16    // Primary address of device
#define NO_SECONDARY_ADDR    0    // Secondary address of device
#define TIMEOUT             T10s  // Timeout value = 10 seconds
#define EOTMODE              1    // Enable the END message
#define EOSMODE              0    // Disable the EOS mode

   Dev = ibdev (BDINDEX, PRIMARY_ADDR_OF_DMM,
NO_SECONDARY_ADDR,
           TIMEOUT, EOTMODE, EOSMODE);
   if (ibsta & ERR)
   {
     GPIBCleanup(Dev, "Unable to open device");
     return 1;
   }

/*
 *  Clear the internal or device functions of the device.  If the error
 *  bit ERR is set in ibsta, call GPIBCleanup with an error message.
 */

   ibclr (Dev);
   if (ibsta & ERR)
   {
     GPIBCleanup(Dev, "Unable to clear device");
     return 1;
   }

/*
 *
 ====================================================================
 =========
 *
 *  MAIN BODY SECTION
 *
 *  In this application, the Main Body communicates with the instrument
 *  by writing a command to it and reading its response. This would be
 *  the right place to put other instrument communication.
 *
```

```
 *
 ==============================================================
 =========
 */


/*
 * Request the identification code by sending the instruction '*IDN?'.
 * If the error bit ERR is set in ibsta, call GPIBCleanup with an error
 * message.
 */



        ibwrt (Dev, "MARKMAXI;OUTPACTI", 17L);
    if (ibsta & ERR)
    {
      GPIBCleanup(Dev, "Unable to write to device");
      return 1;
    }


/*
 * Read the identification code by calling ibrd. If the ERR bit is
 * set in ibsta, call GPIBCleanup with an error message.
 */

    ibrd (Dev, ReadBuffer, ARRAYSIZE);
    if (ibsta & ERR)
    {
      GPIBCleanup(Dev, "Unable to read data from device");
      return 1;
    }

/*
 * Assume that the returned string contains ASCII data. NULL terminate
 * the string using the value in ibcntl which is the number of bytes
 * read in. Use printf to display the string.
 */
/* time example */


    ReadBuffer[ibcntl] = '\0';
    printf("Returned string:  %s\n", ReadBuffer);

        //Create a file to write to
    FILE *OutFile = fopen("S21freq.txt","a");
    //Send data to file
```

```c
    fprintf(OutFile,"%s\n",ReadBuffer);
    //Close the file
    fclose(OutFile);

ibwrt (Dev, "OUTPMARK;MARKMAXI", 17L);
    if (ibsta & ERR)
    {
      GPIBCleanup(Dev, "Unable to write to device");
      return 1;
    }

/*
 * Read the identification code by calling ibrd. If the ERR bit is
 * set in ibsta, call GPIBCleanup with an error message.
 */

    ibrd (Dev, ReadBuffer, ARRAYSIZE);
    if (ibsta & ERR)
    {
      GPIBCleanup(Dev, "Unable to read data from device");
      return 1;
    }

/*
 * Assume that the returned string contains ASCII data. NULL terminate
 * the string using the value in ibcntl which is the number of bytes
 * read in. Use printf to display the string.
 */

    ReadBuffer[ibcntl] = '\0';
    printf("Returned string:  %s\n", ReadBuffer);

        //Create a file to write to
    FILE *OutFile1 = fopen("S21intensity.txt","a");
    //Send data to file
    fprintf(OutFile1,"%s\n",ReadBuffer);
    //Close the file
    fclose(OutFile1);


/*
 *
 ==============================================================
 =========
 *
 * CLEANUP SECTION
```

```
 *
 *
 ================================================================
 =========
 */

/*  Take the device offline.                                 */

   ibonl (Dev, 0);

   return 0;

}


/*
 *  After each GPIB call, the application checks whether the call
 *  succeeded. If an NI-488.2 call fails, the GPIB driver sets the
 *  corresponding bit in the global status variable. If the call
 *  failed, this procedure prints an error message, takes the
 *  device offline and exits.
 */
void GPIBCleanup(int ud, char* ErrorMsg)
{
   printf("Error : %s\nibsta = 0x%x iberr = %d (%s)\n",
         ErrorMsg, ibsta, iberr, ErrorMnemonic[iberr]);
   if (ud != -1)
   {
     printf("Cleanup: Taking device offline\n");
     ibonl (ud, 0);
   }
}
```

Appendix B: MATLAB Code for Data Analysis

Data filtering program

```
% Data smooth filter program
% final plot is time vs negative frequency shift

a = 1; % constant for filtering function
m = 3; % number of average points, you can change it.
b=zeros(1,m);
for l=1:1:m
    b(1,l)=1/m;
end

% raw data %
x=[

% Copy here raw data
];

X=filter(b,a,x);
[z,w]=size(X);
X1=zeros(z+1-m,1);
X2=zeros(z+1-m,1);

for n=1:1:(z+1-m)
  X2(n,1)=X(n+m-1,1);
   X1(n,1)=-X(m)+X2(n,1);
end


t=1:1:n;
T=t*16/60;   % time [hour]
plot(T, X1)  % negative frequency shift plot
```

References

[1] http://en.wikipedia.org/wiki/File:Microplates.jpg

[2] http://en.wikipedia.org/wiki/File:ELISA-sandwich.svg

[3] Garth D. Ehrlich, "Intelligent Implants to Battle Biofilms", ASM News, 2004, p.127-133.

[4] Darouiche, R. O., "Treatment of infection associated with surgical implants". N. Engl. J. Med., 2004, p. 1422-1429.

[5] J. W. Costerton, Philip S. Stewart, E. P. Greenberg, "Bacterial Biofilms: A Common Cause of Persistent Infections", Science, Vol. 284, 21 May 1999, p. 1318-1322,

[6] Sutherland, I. W. "Bacterial exopolysaccharides – their nature and production", Surface Carbohydrates of the Prokaryotic Cell, London, academic, 1977, p. 27-96

[7] J. W. Costerton, Z. Lewandowski, D.E Caldwell, D.R. Corber, H.M. Lappin-Scott, Annu. Rev. Microbiol, 41, 1987, 435

[8] H. Flemming, T. R. Neu, D. J. Wozniak, "The EPS Matrix: The"House of Biofilm Cells"", Journal of Bacteriology, Nov. 2007, p.7945-7947.

[9] J. William Costerton, B. Ellis, K. Lam, F. Johnson, and A. E. Khoury, "Mechaisom of Electical Enhancement of Efficacy of Antibiotics in Killing Biofilm Bacteria", Antimicrob. Agents Chemother.Vol.38, No.12, 1994, p.2803-2809

[10] C. McKenzie, "Antibiotic dosing in critical illness", J. Antimicrob. Chemother, 66, 2011, ii25-ii31

[11] Pilaski et al., "Microsystems and Nanoscience for Biomedical Applications: A view to the future", Bulletin of Science, Technology & Society, Vol. 24, No. 1, February 2004, p.40-45

[12] G. B. SAlleb-Beugelaar, G. Simons, A. Arira, A. Philippi, A. Manz, "Latest Developments in Microfluidic Cell Biology and Analysis Systems", Anal. Chem., 82, 2010, p.4848-4864.

[13] C. B. Rohde, F. Zeng, R. Gonzalez-Rubio, M. Angel, M. F. Yanik, "Microfluidic system for on-chip high-throughput whole-animal sorting and screening at subcellular resolution", Proceedings of the National Academy of Sciences of the United States of America, vol. 104, no. 35, August 2007, p. 13891-13895.

[14] H. Moon, A. R. Wheeler, R. L. Garrell, J. A. Loo, C. J. Kim, "An integrated digital microfluidic chip for multiplexed proteomic sample preparation and analysis by MALDI-MS", Lab on a Chip, 2006, 6, p. 1213-1219.

[15] L. G. Carrascosa, M. Moreno, M. Alvarez, L. M. Lechuga, "Nanomechanical biosensors: a new sensing tool", Trends in Analytical Chemistry, Vol. 25, No. 3, 206, p. 196-206.

[16] M. Li, H. X. Tang, M. L. Roukes, "Ultra-sensitive NEMS-based cantilever for sensing, scanned probe and very high-frequency applications", Nature Nanotechnology, vol. 2, 2007, p. 114-120.

[17] A. Khademhosseini, R. Langer, J. Borenstein, J. P. Vacanti, "Microscale technologies for tissue engineering and biology", PNAS, February 2006, vol. 103, no. 8, p.2480-2487.

[18] N. M. Elman, H. L. Ho Duc, M. J. Cima, "An implantable MEMS drug delivery device for rapid delivery in ambulatory emergency care", Biomed. Microdevices, 2009, 11: 625-631.

[19] N. Verma, A. Shoeb, J. Bohorquez, J. Dawson, J. Guttag, A. P. Chandrakasan, "A micro-power EEG acquisition SoC with integrated feature extraction processor for a chronic seizure detection system", IEEE Journal of Solid-State Circuits, Vol. 45, No. 4, 2010, p. 804-816.

[20] P. Cong, W. H. Ko, D. J. Young, "Integrated Electronic System Design for an Implantable Wireless Batteryless Blood Pressure Sensing Microsystem", IEEE Communications Magazine, April 2010, p.98-104.

[21] I. Clausen, S. T. Moe, L. G. W Tvedt, A. Vogl, D. T. Wang, "A miniaturized pressure sensor with inherent biofouling protection designed for in vivo applications", 33rd Annual Internation Conference of the IEEE EMBS, Boston, August 2011, p. 1880-1883.

[22] S. Ingebrandt et al., "Label-free detection of single nucleotide polymorphisms utilizing the differential transfer function of field-effect transistors", Biosensors and Bioelectronics, 22, (2007), p.2834-2840

[23] http://www.cardiomems.com/index.asp

[24] David L Arruda et al., "Microelectrical sensors as emerging platforms for protein biomarker detection in point-of-care diagnostics", Expert Rev. Mol. Diagn. 9(7), (2009), 749 - 755

[25] Mohammad Mahdi Ahmadi, "A Wireless-Implantable Microsystem for Continuous Blood Glucose Monitoring", IEEE Transactions on Biomedical Circuit and Systems, VOL.3, NO.3, June 2009, p.169-180

[26] Patricia M. Nieva, "New Trends on MEMS Sensor Technology for Harsh Environment Applications", Sensors & Transducers Journal, Special Issue, October 2007, p. 10-20

[27] J. A. Otter, "Hospital infection control in 2012: new solution for old and resurgent problems", Journal of Healthcare-associated Infection 2012, 5, p.68-72.

[28] B. S. Stevenson, H. S. Drilling, P. A. Lawson, K. E. Duncan, V. A. Parisi, J. M. Sulflita, "Microbial communities in bulk fluids and biofilms of an oil facility similar composition but different structure", Environmental Microbiology, 2011, 13(4), p. 1078-1090.

[29] Y.W. Kim, S. E. Sardari, A. A. Iliadis, M. T. Meyer, H. C. Wu, W. E. Bentley, R. Ghodssi, "An ALD aluminum oxide passivated surface acoustic wave sensor for early biofilm detection", Sensors and Actuators B-Chemical, Vol. 163, 2012, p. 136-145.

[30] Young Wook Kim, Saeed E. Sardari, Agis A. Iliadis, Reza Ghodssi, "Atomic Layer Deposition of Aluminum Oxide for Effective Surface Passivation of a MEMS Biosensor", 11th International Conference on Atomic Layer Deposition (AVS-ALD 2011), Cambridge, MA, USA, June 26 – 29.

[31] Y.W. Kim, H. Ben-Yoav, H.C. Wu, D. Quan, K. Carter, M.T. Meyer, W.E. Bentley, and R. Ghodssi, "An Enhanced Bacterial Biofilm Treatment Using Superpositioned Electric Field", The 7th International Conference on Microtechnologies in Medicine and Biology (MMB 2013), Marina del Rey, CA, USA, April 10-12, p. 102-103.

[32] Young Wook Kim, Matt P. Mosteller, Mariana T. Meyer, Hadar Ben-Yoav, William E. Bentley, Reza Ghodssi, "MICROFLUIDIC BIOFILM OBSERVATION, ANALYSIS AND TREATMENT (Micro-BOAT) PLATFORM", A Solid-State Sensors, Actuators and Microsystems Workshop (Hilton Head Workshop 2012), Hilton Head, SC, USA, June 3-7, p. 233-236.

[33] V. Lecault, A. K. White, A. Singhal, C. L. Hansen, "Microfluidic single cell analysis: from promise to practice", Current Opinion in Chemical Biology, 2012, 16: 381-390.

[34] Young Wook Kim, Mariana T. Meyer, Andrew Berkovich, Agis A. Iliadis, William E. Bentley, and Reza Ghodssi, "An Integrated Microsystem for Biofilm Detection and Treatment", The 17th International Conference on Miniaturized Systems for Chemistry and Life Sciences (MicroTAS 2013), Freiburg, Germany, 27-31 October 2013.

[35] http://en.wikipedia.org/wiki/File:Microplates.jpg

[36] Ryo Maeyama, Yoshimitsu Mizunoe, James M. Anderson, Masao Tanaka, Takehisa Matsuda, "Confocal imaging of biofilm formation process using fluoroprobed *Escherichia coli* and fluoro-stained exopolysaccharide", Journal of Biomedical Materials Research Part A, Vol 70A, Issue 2, (2004), p. 274-282.

[37] Salman et al., "Quantitative PCR analysis of genes expressed during bioilm development of methicillin resistant *Staphylococcus aureus* (MRSA)", Infection, Genetics and Evolution 18, (2013), p.106-112.

[38] Joon Myong Song, Mustafa Culha, Paul M. Kasili, Guy D. Griffin, Tuan Vo-Dinh, "A compact CMOS biochip immunosensor towards the detection of a single bacteria", Biosensors and Bioelectronics 20, pp. 2203-2209, 2005.

[39] E. Heyduk, T. Heyduk, "Fluorescent homogeneous immunosensors for detecting pathogenic bacteria", Anal. Biochem. 396, pp. 298-303, 2010

[40] Steven A. Soper et. al., "Pont of care biosensor systems for cancer diagnostics/prognostics", Biosensors and Bioelectronics, 21, pp.1932-1942, 2006

[41] http://en.wikipedia.org/wiki/File:ELISA-sandwich.svg

[42] V. Roy, M. T. Meyer, J. A. I. Smith, S. Gamby, H. O. Sintim, R. Ghodssi, and W. E. Bentley, "AI-2 analogs and antibiotics: a synergistic approach to reduce bacterial biofilms," *Applied Microbiology and Biotechnology*, vol. 97, pp. 2627-2638, March 2013.

[43] Derek E. Moormeier et al., "Use of Microfluidic Technology to analyze gene expression during Staphylococcus aureus biofilm formation reveals distinct physiological niches", Applied and Environmental Microbiology, Vol. 79, No. 11, (2013), p.3413-3424.

[44] Jeongyun Kim, Manjunath Hegde, Sun Ho Kim, Thomas K. Wood, and Arul Jayaraman, "Microfluidic Device for High Throughput Bacterial Biofilm Studies", *LabChip*, 12(2012), pp.1157-1163.

[45] P. W. Butterfield et al., "Modified enzyme activity assay to determine biofilm biomass", J. Microbiol Methods, 50 (1), 2002, p. 23-21

[46] Somashekar Bangalore Prakash, "On-chip capacitance sensing for cell monitoring applications", IEEE Sensors Journal, VOL.7, NO. 3, (2007), p.440-447

[47] E.S. McLamore, D.M. Porterfield, M.K. Banks, "Non-invasive self-referencing electrochemical sensors for quantifying real-time biofilm analyte flux", Biotechnology and Bioengineering, 15;102(3), 2009, p. 791-799

[48] M. Fischer et al., "Design and field application of a UV-LED based optical fiber biofilm sensor", Biosensors and Bioelectronics, (2012), doi:10.1016/j.bios.2011.12.048

[49] H. Helle et al., "Monitoring of biofilm growth with thickness-shear mode quartz resonators in different flow and nutrition conditions", Sensors and Actuators B: Chemical, Vol. 71, (2000), p.47-54

[50] M. Reeslev, M. Miller and K.F. Nielsen, "Quantifying mold biomass on gypsum board:comparison of ergosterol and beta-N-acetylhexosaminidase as mold biomass parameters", Applied and Environmental Microbiology, vol. 69, no.7, (2003), p.3996-3998

[51] R. Hadi, K. Vickery, A. Deva, T. Charlton, "Biofilm removal by medical device cleaners: comparion of two bioreactor detection assays", Journal of Hospital Infection, 2010, 74, p. 160-167.

[52] Z. Xie, A. Thompson, H. Kashieva, A. Dongari-Bagtzoglou, "A quantitative real-time RT-PCR assay for mature C. albicans biofilms", BMC Microbiology 2011,11:93.

[53] X. Tang et al., "A new interdigitated array microelectrode-oxide-silicon sensor with label-free, high sensitivity and specificity for fast bacteria detection", Sensors and Actuators B: Chemical, Vol 156, Issue 2, (2011), p.578-587

[54] A. Qureshi, Y. Gurbuz, S. Kallempudi, J. H. Niazi, "Label-Free capacitive E. coli biochip for determining chemicals that induce cellular toxicity", Procedia Engineering, Vol. 25, (2011), p.928-931

[55] E. Ghafar-Zadeh, M. Sawan, V.P. Chodavarapu, T. Hosseini-Nia, "Bacterial growth monitoring through a differential CMOS capacitive sensor", IEEE Transactions on Biomedical Circuits and Systems, Issue 4, (2010), p.232 – 238.

[56] E. Spiller et al., "A microsystem for growth inhibition test of *Enterococcus faecalis* based on impedance measurement", Sensors and Actuators B: Chemical, Vol. 118, Issue 1-2, (2006), p.182-191.

[57] H. Ben-Yoav, A. Freeman, M. Sternheim, Y. Shacham-Diamond, "An electrochemical impedance model for integrated bacterial biofilms", Electrochimica Acta, 56, 2011, p.7780-7786.

[58] K. Hermans et al., "Gene expression analysis of monospecies *Salmonella Typhimurium* biofilms using differential fluorescence induction", Journal of Microbiological Methods, Vol. 84, Issue 3, (2011), p. 467-478.

[59] E. Heyduk, T. Heyduk, "Fluorescent homogeneous immunosensors for detecting pathogenic bacteria", Anal. Biochem. 396, pp. 298-303, 2010.

[60] http://www.assaymetrics.com/fluorescence_lifetime.htm

[61] R. Srivastava and A. Maningh, "Surface acoustic wave transduction in the ZnO-SiO2-Si structure", J. Phys. D: Appl. Phys. 21 (1988), p.1535-1536.

[62] Sai Liu et al., "Detection of explosive vapors by surface acoustic wave sensors containing novel siloxane based coatings", Journal of Macromolecular Science, Part A: Pure and Applied Chemistry (2010) 47, p. 1172-1175.

[63] M. Bisoffi et al., "Detection of viral bioagents using a shear horizontal surface acoustic wave biosensor", Biosensors and Bioelectronics 23, (2008), p.1397-1403.

[64] Soumya Krishnamoorthy, Agis A. Iliadis, "Properties of high sensitivity ZnO surface acoustic wave sensors on SiO_2/(100) Si substrates", Solid-State Electron., 52, pp. 1710-1716, 2008.

[65] J-M Friedt, C. Droit, G. Martin, and S. Ballandras, "A wireless interrogation system exploiting narrowband acoustic resonator for remote physical quantity measurement", Review of Scientific Instruments, 81, 014701-014709, 2010.

[66] A. Springer, R. Weigel, A. Pohl, F. Seifert, "Wireless identification and sensing using surface acoustic wave devices", IEEE ASME Trans Mechatron, 9, pp. 745-756, 1999.

[67] Werner Zimmerli, "Prosthetic-joint-associated intections", Best Practice & Research Clinical Rheumatology, Vol.20, No.6, p. 1045 – 1063, 2006.

[68] Guillaume Cottarel and Jamey Wierzbowski, "Combination drugs, an emerging option for antibacterial therapy", TRENDS in Biotechnology, Vol. 25, No.12, p.547-555, 2007.

[69] M. A. Kohanski et al., "A common mechanism of cellular death induced by bactericidal antibiotics", Cell 130, p.797-810, 2007.

[70] C. L. Smith, M. Kubo, and F. Imamoto, "Promoter-specific inhibition of transcription by antibiotics which act on DNA gyrase", Nature 275, p.420-423, (1978).

[71] L. R. Hoffman et al., "Aminoglycoside antibiotics induce bacterial biofilm formation", Nature 436, (2005), p.1171-1175.

[72] Daryl Efron er al., "Side effects of methylphenidate and dexamphetamine in children with attention deficit hyperactivity disorder: A double-blind, crossover trial", Pediatrics Vol. 100, No. 4, (1997), p.662-666.

[73] Gines Sanz and Valentin Fuster, "Fixed-dose combination therapy and secondary cardiovascular prevention: rationale, selection of drugs and target population", Nature Clinical Practice Cardiovascular Medicine, Vol 6, No2, p.101-110, (2009).

[74] M. Giladi et al., "Microbial Growth Inhibition by Alternating Electric Fields in Mice with Pseudomonas aeruginosa Lung Infection", Antimicrob. Agents Chemother.Vol. 54, No. 8, p.3212 – 3218, (2010).

[75] J. L. Del POZO et al., "The Electricial Effect: Reduction of *Staphylococcus* and *Pseudomonas* Biofilms by Prolonged Exposure to Low-Intensity Electrical Current", Antimicrob. Agents Chemother. Vol.53, No.1, p. 41-45, (2009).

[76] J. W. Costerton, "Mechanism of Electrical Enhancement of Efficacy of Antibiotics in Killing Biofilm Bacterial", Antimicrobial Agents and Chemotherapy, Dec. 1994, p. 2803-2809.

[77] J.O'M. Bockris, K.N. Reddy, *Modern Electrochemistry* (Kluwer Academic / Plenum Publishers, New York, 2000), pp.1903-1980 [second edition].

[78] J. L. Del Pozo et al., "Effect of Electrical Current on the Activities of Antimicrobial Agents against *Pseudomonas aeruginosa*, *Staphylococcus aureus*, and *Staphylococcus epidermidis* Biofilms", Antimicrob. Agents Chemother.Vol.53, No.1, p. 35-40, (2009).

[79] R. Caubet et al., "A Radio Frequency Electric Current Enhances Antibiotic Efficacy against Bacterial Biofilms", Antimicrob. Agents Chemother.Vol. 48, No.12, p.4662-4664, (2004).

[80] M. Nakayama, H. Nakano, H. Hamada, N. Itami, R. Nakazawa, "A novel bioactive haemodialysis system using dissolved dihydrogen (H2) produced by water electrolysis: a clinical trial", Nephrology Dialysis Transplantation, 2010, 25:3026-3033.

[81] Heh-Nan Lin, Sy-hann chen, Shu-Te ho and Ping-Ren Chen, I-Nan Lin, "Comparative measurements of the piezoelectric coefficient of a lead zirconate titanate film by piezoresponse force microscopy using electrically characterized tips", J. Vac. Sci. Technol. B 21(2), p. 916-918, (2003).

[82] http://en.wikipedia.org/wiki/Rayleigh_wave

[83] J. Du, G.L. Harding, J.A. Ogilvy, P.R. Dencher, M. Lake, "A study of Love-wave acoustic sensors", SENSOR ACTUAT A, 56, pp. 211-215, 1996.

[84] S. Krishnamoorthy, A.A. Iliadis, "Properties of high sensitivity ZnO surface acoustic wave sensors on SiO2/(100) Si substrates", Solid-State Electron., 52, pp. 1710-1716, 2008.

[85] Kourosh Kalantar-Zadeh, David A. Powell, Wojtek Wlodarski, Samuel Ippolito, Kosmas Galatsis, "Comparison of layered based SAW sensors", SENSOR ACTUAT B, 91, pp. 303-308, 2003

[86] Chengtao Yang, Jiahe Dong, Heping Xie, Jianxiong Li, and Shuren Zhang, "Calculation of the dispersion properties of Rayleigh wave on ZnO/Metal/Diamond/Si-layered structure", INTEGR FERROELECTR, 84, pp. 39-48, 2006

[87] I. D. Avramov, A. Voigt and M. Rapp, "Rayleih SAW resonators using gold electrode structure for gas sensor applications in chemically reactive environments", Electronics Letters, 31st, Vol. 41, No.7, March 31st 2005

[88] http://en.wikipedia.org/wiki/Rayleigh_wave

[89] Nachappa Gopalsami, Ivan Osorio, Stanislav Kulikov, Sergey Buyko, Andrey Martynov, and ApostolosC. Raptis, "SAW Microsensor Brain Implant for prediction and Monitoring of Seizures", IEEE SENSORS JOURNAL, VOL. 7, NO.7, pp.977-982, July 2007

[90] Mattews H., Van de Vaart, "Observation of Love Wave Propagation at UHF Frequencies", Applied Physics Lettersm Volume 14, Issue 5, pp. 171-172, Mar 1969

[91] Sean Wu, Zhi-Xun Lin, Ruyen Ro, and Maw-Shung Lee, "Rayleigh and Shear Horizontal Surface Acoustic Properties of (100) ZnO Films on Silicon", IEEE T ULTRASON FERR, Vol.57, No.5, May 2010.

[92] Glen McHale, "Generalized concept of shear horizontal acoustic plate mode and Love wave sensors", Meas. Sci. Technol., 14, pp. 1847-1853, 2003.

[93] E. Gizeli, N.J. Goddard, C.R. Lowe and A.C. Stevenson, "A Love plate biosensor utilizing a polymer layer", SENSOR ACTUAT B-CHEM, 6 (1992), pp. 131-137.

[94] G. Kovacs, G.W. Lubking, M.J. Vellekoo, and A. Vennema, "A Love wave sensor for (bio) chemical sening in liquids", SENSOR ACTUAT A, 43 (1994), pp. 38 – 43.

[95] Soumya Krishnamoorthy, Agis A. Iliadis, Thaleia Bei, George P. Chrousos, "An interleukin-6 ZnO/SiO2/Si surface acoustic wave biosensor", Biosensors and Bioelectronics, 24, pp. 313-318, 2008.

[96] D.D. Stubbs, L.Sang-Hun and W.D. Hunt, "Molecular recognition for electronic noses using surface acoustic wave immunoassay sensors", *IEEE sensors*, vol. 2, no. 2, pp. 294-300, 2002.

[97] Heh-Nan Lin, Sy-hann chen, Shu-Te ho and Ping-Ren Chen, I-Nan Lin, "Comparative measurements of the piezoelectric coefficient of a lead zirconate titanate film by piezoresponse force microscopy using electrically characterized tips", J. Vac. Sci. Technol. B 21(2), pp 916-918, Mar/Apr 2003.

[98] M.C. Horrillo, M.J. Fernandez, J.L. Fontecha, I. Sayago, "Optimization of SAW sensors with a structure ZnO-SiO2-Si to detect volatile organic compounds", SENSOR ACTUAT B, 118 (2006), pp.356-361.

[99] Y.Q. Fu et al. "Recent developments on ZnO films for acoustic wave based bio-sensing and microfluidic applications: a review", SENSOR ACTUAT B, 143, pp. 606-619, 2010.

[100] Zhou Li, Rusen Yang, Min Yu, Fan Bai, Cheng Li, and Zhong Lin Wang, "Cellular Level Biocompatibility and Biosafety of ZnO Nanowires", Journal of Physical Chemistry C Letters, 112, pp.20114-20117, 2008.

[101] A Szczepanik et al. "ZnO nanostructures by Atomic Layer Deposition Method", Journal of Physics, conference Series 146, 012017, 2009.

[102] Lamia Znaidi, "Sol-gel-deposited ZnO thin films: A review", Material Science and Engineering:B, Volume 174, Issue 1-3, pp.18-30, 25 Oct 2010.

[103] Pappas David L. et al., "Pulsed laser deposition of diamond-like carbon films", Journal of Applied Physics, Volume 71, Issue 11, pp. 5675-5684, 1992.

[104] Chang-Feng Yu, Sy-Hann Chen, Shih-Jye Sun, and Chou, "Influence of the substrate temperature on the electrical and magnetic properties of ZnO: N thin films grown by pulse laser deposition", Journal of PhysicsD: Applied Physics, 42, 035001, 2009.

[105] Soumya Krishnamoorthy, and Agis A. Iliadis, "Development of ZnO/SiO2/Si Love Mode Surface Acoustic Wave Devices with High Sensitivity for Biosensor Applications", IEEE Sensors Applications Symposium, Houston, Texas, USA, 7-9 Feb 2006

[106] Y.Q.Fu, J.K. Luo, X.Y. Du, A.J. Flewitt, Y. Li, G.H. Markx, "Recent developments on ZnO films for acoustic wave bio-sensing and microfluidic applications: a review", Sens Actuators B Chem, 143, pp.606-619, 2010.

[107] X.Y. Du et al, "ZnO film for application in surface acoustic wave device", Journal of Physics: Conference Series 76, 012035, 2007.

[108] Axelevitch A, Gorenstein B, Darawshe H, Golan G, "Investigation of thin solid ZnO films preparaed by sputtering", THIN SOLID FILMS, Volume 518, Issue 16, pp.4520-4524, June 1 2010.

[109] Y.W. Kim, S. E. Sardari, A.A. Iliadis, and R. Ghodssi, "A Bacterial Biofilm Surface Acoustic Wave Sensor for Real Time Bacterial Growth Monitoring", IEEE Sensors 2010, November1-4, Hawaii, pp1568-1571.

[110] F. Herrmann, D. Hahn, S. Buttgenbach, „Separation of density and viscosity influence on liquid-loaded surface acoustic wave devices", Applied Physics Letters, Volume 74, Number 22, pp. 3410-3412, May 31st 1999.

[111] NIST Property Data Summaries, http://www.ceramics.nist.gov/srd/summary/emodox00.htm

[112] http://www.lenntech.com/teflon.htm, http://www.cctplastics.com/teflonall.html

[113] Biljana A. Cavic, Gordon L. Hayward, and Michael Thompson, "Acoustic Waves and the study of biochemical macromolecules and cells at the sensor-liquid interface", Analystm 124, pp. 1405-1420, 1999.

[114] A. Springer, R. Weigel, A. Pohl, F. Seifert, "Wireless identification and sensing using surface acoustic wave devices", IEEE ASME Trans Mechatron, 9, pp. 745-756, 1999.

[115] J-M Friedt, C. Droit, G. Martin, and S. Ballandras, "A wireless interrogation system exploiting narrowband acoustic resonator for remote physical quantity measurement", Review of Scientific Instruments, 81, 014701-014709, 2010.

[116] Peter A. Lieberzeit, Christian Palfinger, Franz L. Dickert, and Gerhard Fischerauer, "SAW RFID-Tags for Mass-Sensitive Detection of Humidity and Vapors", Sensors, 9, pp 9805-9815, 2009.

[117] Wu Ping, Cheng Jingzhi, "Theory of acoustic impedance matching of ultrasonic transducers", Proceedings of the Annual International Conference of the IEEE, Vol.3, pp 1281, 4-7 Nov 1988.

[118] Guigen Zhang, "Nanostructure-Enhanced surface acoustic waves biosensor and its computational modeling", journal of Sensors, Volume 2009, Article ID 215085, 2009.

[119] D. H. Lowndes, D. B. Geohegan, A. A. Puretzky, D. P. Norton, C. M. Rouleau, "SYNTHESIS OF NOVEL THIN-FILM MATERIALS BY PULSED LASER DEPOSITION", Science 16 August 1996: Vol. 273 no. 5277 pp. 898-903.

[120] Zerrouki C et al, "Shear Horizontal Surface Acoustic Waves Sensor for Label-Free DNA Detection", Sensor Letters, Volume 8, Issue 6, pp.813-817, Dec 2010.

[121] Chengtao Yang, Jiahe dong, Heping Xie, Jianxiong Li, and Shuren Zhang, "Calculation of the Dispersion Properties of Rayleigh Wave on ZnO/Metal/Diamond/Si-Layered Structure", Integrated Ferroelectrics, 84, pp. 39-48, 2006.

[122] Chengtao Yang, Jiahe dong, Heping Xie, Jianxiong Li, and Shuren Zhang, "Calculation of the Dispersion Properties of Rayleigh Wave on ZnO/Metal/Diamond/Si-Layered Structure", Integrated Ferroelectrics, 84, pp. 39-48, 2006.

[123] Irie RF, "Natural antibody in human serum to neoantigen in human cultureed cells grown in fetal bovine serum", J. Natl Cancer Inst, 52(4), (1974), p.1051-1058.

[124] Hang Ju Ko et. al., „Improvement of the quality of ZnO substrates by annealing", Journal of Crystal Growth, 269, p.493-498, 2004

[125] Mikko Ritala and Jaakkoo Niinisto, *Chemical Vapor Deposition*: Precursors, Processes and Applications: chapter 4 Atomic Layer Deposition, Edited by Anthony C. Jones and Michael L. Hitchman (Royal Society of Chemistry, 2009).

[126] K. Kalantar-Zadeh, Y. Y. Chen, B. N. Fry, A. Trinchi, W. Wlodarski, "A Novel Love Mode SAW Sensor with ZnO layer Operating in Gas and Liquid Media", IEEE Ultrasonic Symposium, 2001, p.353-356.

[127] R. Hong, H. Qi, J. Huang, H. He, Z. Fan, J. Shao, "Influence of oxygen partial pressure on the structure and photoluminescence of direct current reactive magnetron sputtering ZnO thin film", Thin Solid Film, Vol. 473, 1, 2005, p. 58-62.

[128] *Pulsed Laser Deposition of Thin Films,* by Douglas B. Chrisey (Editor), Graham K. Hubler (Editor), pp. 648. ISBN 0-471-59218-8. Wiley-VCH , May 2003.

[129] K. Vanheusden, C. H. Seager, W. L. Warren, D. R. Tallant, J. A. Voigt, :Correlation between photoluminescence and oxygen vacancies in ZnO phosphors", Applied Physic Letter, 68, 403 (1996).

[130] A. L. Ryland, "X-Ray Diffraction", Journal of Chemical Education, Vol. 35, No. 2, 1958, p. 80-83.

[131] T. M. Mayer, J. W. Elam, S. M. George, P. G. Kotula, R. S. Goeke, "Atomic-layer deposition of wear resistant coatings for microelectromechanical devices", Applied Physics Letters, vol. 82, 17, 2003, p.2883-2885.

[132] M. Semlitsch, M. Lehmann, H. Weber, E. Doerre, H. G. Willert, "New prospects for a prolonged functional life-span of artificial hip joints by using the material combination polyethylene/aluminium oxide ceramic/metal", Journal of Biomedical Materials Research, vol. 11, issue 4, p. 537-552, July 1977.

[133] http://cp.literature.agilent.com/litweb/pdf/5965-7707E.pdf

[134] W.A. Craig and S.C. Ebert, "Killing and regrowth of bacteria in vitro: a review", Scandinavian Journal of Infectious Diseases, 74, p. 63-70, (1990).

[135] J. W. Costerton, "Mechanism of Electrical Enhancement of Efficacy of Antibiotics in Killing Biofilm Bacterial", Antimicrobial Agents and Chemotherapy, Dec. 1994, p. 2803-2809.

[136] J. L. Del Pozo, M. S. Rouse, R. Patel, "Bioelectric effect and bacterial biofilms. A systematic review.", The International Journal of Artificial Organs, 2008, 31(9): 786-795.

[137] U. Zimmermann, J. Vienken, "Electric Field-Induced Cell-to-Cell Fusion", The Journal of Membrane Biology", 67, p.165-182, (1982).

[138] P. S. Stewart, W. Wattanakaroon, L. Goodrum, S. M. Fortun, B. R. McLeod, "Electrolytic Generation of Oxygen Partially Explains Electrical Enhancement of Tobramycin Efficacy against Pseudomonas aeruginosa Biofilm", Antimicrobial Agents and Chemotherapy, February 1999, vol. 43, no. 2, p.292-296.

[139] Z. Qian, R. D. Sagers, W. G. Pitt, "The Effect of Ultrasonic Frequency upon Enhanced Killing of P. aeruginosa Biofilms", Annals of Biomedical Engineeringm vol. 25, pp. 69-76, 1997.

[140] http://en.wikipedia.org/wiki/Gentamicin

[141] T. G. Dzherayan, I. V. Bykov, M. V. Kostitsyna, E. V. Shipulo, O. M. Petrukhin, A. A. Dunnaevam E.V. Vladimirova, "Study of a gentamicin-selective membrane polymer matrix by infrared spectroscopy", Journal of Analytical Chemistry, Vol. 65, Number7, p.726-731, 2010.

[142] L. G. Reimer, C. W. Stratton, L. B. Reller, Antimicrob. Agents Chemother.**19**, 1050-1055 (1981).

[143] Y. Wu, D. Sun, and W. Huang, "Force and motion analysis for automated cell transportation with optical tweezers", Proceeding of the 8th World Congress on Intelligent Control and Automation, June 21-25 2011, Taiwan, p. 839-843

[144] J. H. Merritt, D. E. Kadouri, and G. A.O'Toole, "Growing and Analyzing Static Biofilms", Current Protocols in Microbiology 1B.1.1-1B.1.18, August 2011, Wiley Online Library, DOI: 10.1002/9780471729259.mc01b01s22

[145] Kao JC, Geroski DH, Edelhauser HF. 2005. Transscleral Permeability of Fluorescent-Labeled Antibiotics. J. Ocul. Pharmacol. Th. 21 (1): 1-10.

[146] Amaral L, Trigenis B., Atkinson BA. 1982. The Radioactive Thymidine Incorporation Method for the Determination of Antibiotic Susceptibility of Gram-Negative Bacilli. Eur. J. Clin. Microbiol. 1(3): 149-154

[147] D. K. Cheng, *Field and Wave Electromagnetics* (Addison - Wesley, 1989) [second edition]

[148] Young Wook Kim, Hadar Ben-Yoav, Huan Chen Wu, David Quan, Karen Carter, Mariana T. Meyer, Konstantinos Geraspoulos, William E. Bentley, Reza Ghodssi, "Bacterial Biofilm Treatment via the Superpositioned Bioelectric Effect", submitted to Applied and Environmental Microbiology (AEM).

[149] George M. Whitesides, "The origins and the future of microfluidics", Nature 442, p.368-373, (2006)

[150] M. T. Meyer et al., "Development and validation of a microfluidic reactor for biofilm monitoring via optical methods", Journal of Micromechanics and Microengineering, Vol. 21, No.5, 054023

[151] Rohini Srinivasan, Phillip S. Stewart, Thomas Griebe, Ching-I Chen, Xiaoming Xu, "Biofilm parameters influencing biocide efficacy", Biotechnology & Bioengineering, Vol. 46, p.553-560, (1995).

[152] R. Pethig, G. H. Markx, "Applications of dielectrophoresis in biotechnology", Trends in Biotechnology, vol. 15, Issue 10, October 1997, p.426-432.

[153] M. P. Singh, J. Stefko, J. A. Lumpkin, J. Rosenblatt, "The Effect of Electrostatic Charge Interactions on Release Rates if Gentamicin from Collagen Matrices", Pharmaceutical Research, vol. 12, No. 8, 1995, p. 1205-1210.

[154] M. P. Mosteller, "AN OPTICAL DENSITY DETECTION PLATFORM WITH INTEGRATED MICROFLUIDICS FOR *IN SITU* GROWTH, MONITORING, AND TREATMENT OF BACTERIAL BIOFILMS," Master of Science, University of Maryland, College Park, MD, 2012.

[155] R. Bakke, R. Kommedal, S. Kalvenes, "Quantification of biofilm accumulation by an optical approach", Journal of Microbiological Methods, Vol. 44, Issue 1, (2001), p.13 -16

[156] D. K. Cheng, Field and Wave Electromagnetics (Addison - Wesley, 1989) [second edition]

[157] N. W. Emanetoglu, C. Gorla, Y. Liu, S. Liang, Y. Li, "Epitaxial ZnO piezoelectric thin films for saw filters", Materials Science in Semiconductor Processing, 2, (1999), p.247-252.

[158] E. M. Purcell, "Life at low Reynold number", AIP Conf. Proc. 28, 49 (1976).

[159] X. J. Wang, T. E. Milner, J. S. Nelson, "Characterization of fluid flow velocity by optical Doppler tomography", Optics Letter, Vol. 20, No. 11, June 1, 1995, p. 1337-1339.

[160] *Pulsed Laser Deposition of Thin Films,* by Douglas B. Chrisey (Editor), Graham K. Hubler (Editor), pp. 648. ISBN 0-471-59218-8. Wiley-VCH , May 2003.

[161] H. Ko, M. Han, Y. Park, Y. Yu, B. Kim, S. S. Kim, J. Kim, *J. Cryst. Growth*, 2004, 269, 493-498.

[162] Mikko Ritala and Jaakkoo Niinisto, *Chemical Vapor Deposition*: Precursors, Processes and Applications: chapter 4 Atomic Layer Deposition, Edited by Anthony C. Jones and Michael L. Hitchman (Royal Society of Chemistry, 2009).

[163] A. M. Christensen, D. A. Chang-Yen, B. K. Gale, *J. Micromech. Microeng.*, 2005, 15, 928-934.

[164] P. S. Stewart, M. J. Franklin, "Physiological heterogeneity in biofilms", Nature Review Microbiology, Vol. 6, March 2008, p.199-210.

[165] Q. Xiang, B. Xu, R. Fu, D. Li, "Real Time PCR on Disposable PDMS Chip with a Miniaturized Thermal Cycler", Biomedical Microdevices, 7:4, 273-279, 2005.

[166] G. Sezonov, D. Joseleau-Petit, R. D'Ari, "Escherichia coli Physiology in Luria-Bertani Broth", Journal of Bacteriology, 2007, 189(23):8746.

[167] C. Glorieux, W. Gao, S. E. Kyuger, K. Van de Rostyne, W. Lauriks, J. Thoen, "Surface acoustic wave depth profiling of elastically inhomogeneous materials", Journal of Applied Physics, 88, 4394 (2000).

[168] J. Du, G. L. Harding, "A multilayer structure for Love-mode acoustic sensors", Sensors and Actuators A: Physical, vol. 65, Issue 2-3, March 1998, p.152-159.

[169] A. F. Gonzales Barrios, R. Zuo, Y. Hashimoto, L. Yang, W. E. Bentley, T. K. Wookd, "Autoinducer 2 Control Biofilm Formation in Escherichia coli through a Novel Motility Quorum-Sensin Regulator (MqsR, B3022), Journal of Bacteriology, 2006,, vol. 188, no 1, p. 305-316.

[170] http://ishbytes.blogspot.com/2011/06/escherichia-coli-and-its-outbreak-in.html

[171] J. A. Driscoll, S. L. Brody, M. H. Kollef, "The epidemiology, pathogenesis and treatment of Pseudomonas aeruginosa infections", Drugs, February 2007, Vol. 67, Issue 3, pp. 351-368.

[172] T. Palmer, B. C. Berks, "Moving folded proteins across the bacterial cell membrane", Microbiology, (2003), 149, p. 547-556.

[173] P. Stoodley, D. deBeer, H. M. Lappin-Scott, "Influence of electric fields and pH on biofilm structure as related to the bioelectric effect", Antimicrobial Agents and Chemotherapy, September 1997, vol. 41, no. 9, p. 1876-1879.

[174] http://colloidalsilversecrets.blogspot.com/2011/01/colloidal-silver-and-pseudomonas.html

[175] A. S. Juncker, H. Willenbrock, G. Von Heijne, S. Brunak, H. Nielsen, A. Krogh, "Prediction of lipoprotein signal peptides in Gram-negative bacteria", Protein Science, (2003), 12:1652-1662.

[176] T. Teorell, "Membrane Electrophoresis in Relation to Bioelectrical Polarization Effects", Nature, 162, p. 961, December 1948.

[177] http://microbewiki.kenyon.edu/index.php/Proteobacteria

[178] L. Kim, Y. Toh, J. Voldman, H. Yu, "A practical guide to microfluidic perfusion culture of adherent mammalian cells", Lab on a Chip, 2007, 7, p.681-694.

[179] D. R. Kaplan, S. R. Forrest, "Electrical Crosstalk in p-i-n Arrays Part I: Theory", Journal of Lightwave Technology, Vol. LT-4, No. 10, October 1986, p. 1460-1469.

[180] L. Hall-Stoodley, J. W. Costerton, P. Stoodley, "Bacterial biofilms: from the Natural environment to infectious", Nature Review Microbiology, 2, p.95-108, February 2004.

[181] C. F. Herrmann, F. H. Fabreguette, D. S. Finch, R. Geiss, S. M. George, "Multilayer and functional coating on carbon nanotubes using atomic layer deposition", Applied Physics Letters, 87, 123110, (2005).

[182] A. A. Dameron, S. D. Davidson, B. B. Burton, P. F. Carcia, R. Scott Mclean, S. M. George, "Gas Diffusion Barriers on Polymers Using Multilayers Fabricated by Al2O3 and Rapid SiO2 Atomic Layer Deposition", Journal of Physical Chemistry C, 2008, 112(12), pp. 4573-4580.

[183] T. M.A. Gronewold, "Surface acoustic wave sensors in the bioanalytical field: Recent trend and challenges", Analytica Chimica Acta, Vol. 63, Issue 2, November 12 2007, pp. 119-128.

[184] J. A. Von Arx, K. Najafi, "On-Chip Coils With Integrated Cores For Remote Inductive Powering Of Integrated Microsystems", International Conference on Solid-State Sensors and Actuators (Transducers 97), Chicago, USA, 1997, p.999-1002.

[185] C. Massin, G. Boero, F. Vincent, J. Abenhaim, P.-A. Besse, R. S. Popovic, "High-Q factoer RF planar microcoils for micro-scale NMR spectroscopy", Sensors and Actuators A, 97-98, (2002), p. 280-288.

[186] W. Kenneth Ward, "A Review of the Foreign-body Responses to subcutaneously-implanted Devices: The Role of Macrophages and Cytokines in Biofouling and Fibrosis", Journal of diabetes science and technology, 2008 September: 2(5):768-777.